RICE UNIVERSITY

Monitoring Transport at Interfaces of Tunable Soft Surfaces

by

Charlisa Revé Daniels

A THESIS SUBMITTED
IN PARTIAL FULFILLMENT OF THE
REQUIREMENTS FOR THE DEGREE

Doctor of Philosophy

APPROVED, THESIS COMMITTEE

Christy Landes, Chair
Norman Hackerman-Welch
Young Investigator, Assistant Professor of
Chemistry

Sibani Lisa Biswal
Assistant Professor in Chemical and
Biomolecular Engineering

Jason Hafner
Associate Professor of Physics and
Astronomy and Chemistry

HOUSTON, TEXAS

April 2012

Abstract

Monitoring Transport at Interfaces of Tunable Soft Surfaces

by

Charlisa Revé Daniels

The present work utilizes single molecule methods and analysis to investigate soft and hard substrates. First, the effect of charged hard surfaces on charged probes were evaluated, as the soft surfaces were built upon such a structure. Then, selected polymers were selected according to their importance in smart surface technology. The extent of interaction of the selected probes with the array of soft surfaces gives insight to the potential tunability of these surfaces. The three distinct polymers range from ubiquitous usage to advancements in current technology. The studies presented here are needed to characterize, on the nanoscale, the Coulombic interactions of these polymers.

Acknowledgements

First, I would like to thank the author and finisher of my faith, whose patience is unbounded and favor undeserved.

I would like to thank my advisor, Dr. Christy F. Landes. Words, much less sentences, will not form easily as I try to write, edit, and re-edit this. She has been a culmination of nearly everything that motivates me and this phase of my life will serve as a marker for the type of drive that she represents. It has been great, exciting, terrifying, scary, and tough to carry out the research that makes us proud and showcases her talents as advisor and mentor.

Of course, the extended Landes (and Link) family, especially Carmen Reznik (!), Nick Taylor, Lydia Kisley; Stephan Link, Alexei Tcherniak, Sergio Dominguez-Medina, Liane Slaughter, David Solis, and Wei-Shun Chang.

I would like to thank my professors and colleagues who have helped me get to this point as well. My Scottie Profs: B. Lachele Foley, Ruth Riter, Lilia Harvey, T. Leon Veneble. My former research advisors: Rob Woods and Bill Acree.

I would like to thank and acknowledge my wonderful family, namely those who have had to hear no end to my rants: John, Barbara, and Julisa Daniels. I love you, family. Emotion will not allow me to go any further.

And of course, my friends who have had to deal with my strict time issues and exhaustion. First and foremost: Luz Martinez. Sister, we have been through some rough times, haven't we? During our own respective career shaping times, we

have fought together, giggled together, analyzed together, and decided together. You have to know what a part of the family you are and you are always welcome. To my other girls/editors/cheerleaders: Saralyn Hernandez (née McMorris), Claudia Calhoun, Maggie Nudelman (née Jennings), Kaleena Scoggins (née Dooley), Jennifer Bartell and Howard Williams . Thank You, Thank you, thank you for all of your support, understanding, and consoling. Thank you for helping me sort out what is important to me, letting me talk it out, and determine my path in life. Best. Friends. Ever!

Contents

List of Figures

List of Tables

List of Equations

Chapter 1

Introduction

1.1 Motivation

Learning the nuances of mass and charge transport in confined regions is important when trying to engineer structures for technological advancement. Study of transport at interfaces, even at the single molecule level, is a area of interest that continues to call for understanding.[1] Although there is much in the literature about metallic molecular electronics that have been developed to control electron transport,[2-4] organic thin films present an alternative for building nanostructures adequate for transport. An additional step would be to have fabrication control over these structures to further promote tunability, but such an advance requires a deeper understanding about the relationship between interfacial charge and structure and the resulting transport properties.

"Smart" materials are an increasingly interesting subject in the advancement of technology. These materials are of interest in a range of areas: electronics, biomedicine, diagnostics, agriculture, personal care and more.[5-13] In a 2008 market research study, the growth of nanotechnology applications was assessed and projected (Figure 1.1). Medicinal devices were projected to have the highest growth; within that category, nanostructured materials would have the second largest growth behind nanoparticles. Characterizing these surfaces on the nanoscale is therefore needed to assess their utility.

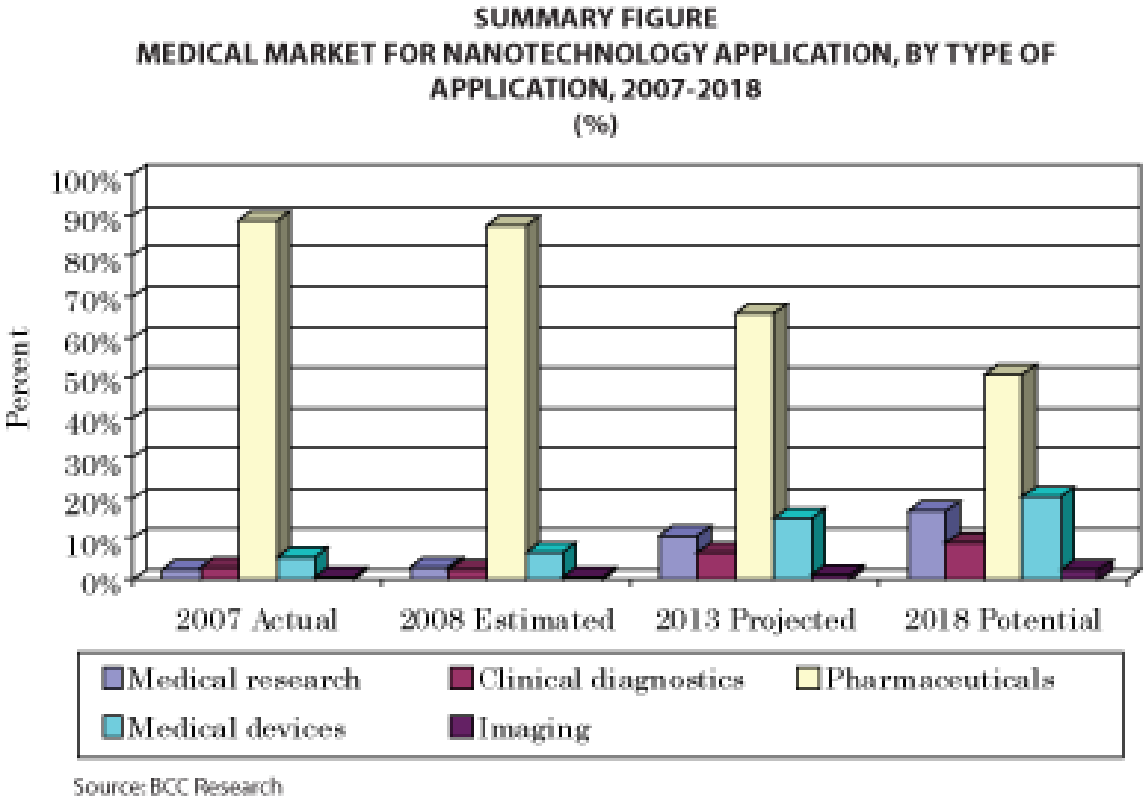

Figure 1.1: Projected market for nanotechnology applications from 2007 to 2018. Nanostructured devices are the second largest growth, behind nanoparticles, in the field of medical devices. *Data obtained from BCC Research Market Forecasting.*[14]

Biological and medicinal fields are starting to turn toward smart materials as a way to more accurately diagnose and treat conditions. If such materials can be tuned for specific associations and/or environmental conditions, the biomedicine field advances in diagnostic ability. In a separate study, the same market research company projected the world market for coating medical devices with polymers, alloys, nanoparticles, etc. (Figure 1.2).[14] The market for coating materials is expected to nearly double from 2009 to 2014.

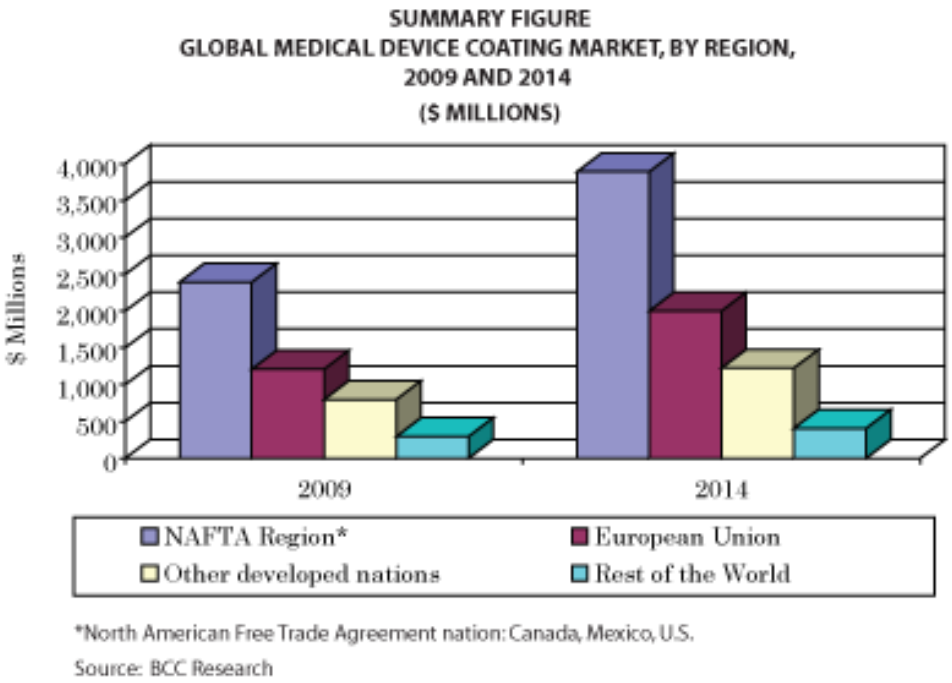

Figure 1.2: Projected world market for medical device coatings. *Data obtained from BCC Research Market Forecasting.*[14]

The usage for "smart", nanostructured materials proves imperative for diagnostic analyses. Functionalized surfaces, such as those presented in this work, will be part of the solution. Chapter 2 will provide a review of the current literature focusing on the specific advances in arenas of organic polymers and surface treatments. Methods for assessing transport within thin films will be presented and will show our contribution to advancing the comprehension of how finely engineered structures can be used to control transport within them.

1.2 Specific Aims

1.2.1 Aim 1

Utilize single molecule spectroscopy techniques and analysis, as well as Fluorescent Correlation Spectroscopy (FCS), to monitor the interaction of single fluorescent probes (dyes or dye-labeled species) with hard (e.g. glass) surfaces, and the distributions of these

residence times for multiple samples. These observations will reveal dynamic charge-dependent interactions of the probes with the surfaces in question. Consequently, through Specific Aim 2, these analyses will help characterize the tunability of more advanced engineered surface preparations.

1.2.2 Aim 2

Survey the effects of varying dendron or ligand density, ionic or pH strength, and the presence of competitors on transport at tunable soft interfaces. The necessary experimental procedures and analysis parameters for these single molecule experiments in charged and crowded environments will be explained.

1.3 Overview

Background information on the systems highlighted in this work is provided in Chapter 2. The advancement of smart surfaces is outlined as well as the wide usages for such materials. The importance of studying interfacial interactions is explained.

Chapter 3 explains the theory behind Fluorescence Correlation Spectroscopy, the principle experimental technique utilized in this work.

The contents of Chapter 4 were published in the *Langmuir* journal in 2010. It discusses the Coulombic effects of dye interactions at the glass/water interface. A comparison the diffusion behavior of oppositely charged dyes over the anionic glass surface is made. This is discussed as a function of distance from the surface as well as identity and pH of the aqueous environment. The strength and length of interaction was determined with dwell time and blip analyses.

The contents of Chapter 5 were published in the *Colloids and Surfaces B* journal in

2011. This work discusses the potential of using dendrons of PEG to tune surfaces to the size of protein anticipated. The interaction of a charged probe with an array of densities of neutral PEG was compared; this comparison was also made with dye-labeled protein. Additionally, the strength of interaction was determined with dwell time analysis.

Chapter 6 discusses the interaction between a cationic cluster-charged peptide-functionalized agarose surface and the dynamics of a protein diffusing near that surface. The surface was characterized using our optical setup, as well as our techniques and analysis. The observation of weak binding of the protein to the functionalized surface at the single molecule level was a welcome counterpart to previous ensemble observations. This work is under review at *Molecular Recognition*.

Chapter 7 discusses the tunability of a weak polycationic polymer that responds to external chemical stimuli. In this chapter, the polymer is manipulated by changing pH and transport of dyes is measured as a function of tunable brush chemistry and density, as well as how this tunability changes with brush thickness. This manuscript is in preparation and will be submitted to *Journal of Physical Chemistry C*.

Chapter 2

Background

The objective of this thesis is to contribute to the fundamental understanding of molecular ion transport in charged and crowded environments. The information garnered from this work can be applied to drug delivery, smart surfaces for diagnostics and other biomedical applications. As tunable, responsive, nanostructured materials are increasingly regarded in the fields of electronics, biomedicine, diagnostics, agriculture, and personal care,[5-13] the need for understanding the mechanisms behind the transport also increases. The objective of this thesis is to contribute to the fundamental understanding of transport in charged and crowded environments.

2.1 Biomedical Devices and Applications

Chapter 1 gives an overview of the interest in and market for advances in biomedical technology for diagnostics, drug delivery, and improved equipment. These improvements of tailoring surfaces for enhancing specific interactions are welcomed as the biomedical field looks for more sterile, accurate, and purposeful tools.

The "biointerface", the interface between man-manipulated materials and biological systems, requires extensive study and understanding to prevent mishaps with living systems as technology advances to make better interactions. Two challenges these surfaces face and strive to overcome are the tunability of the physical properties and/or functions and the robustness and reversibility of the surface. [15] Thus bio-scientists contribute knowledge of biomacromolecules (DNA, RNA, proteins, etc.) while materials scientists and

engineers develop materials that respond to pH, temperature, salt and other relevant chemical concentrations. Together, biomimetic systems are produced that can be applied to the biomedical arena.

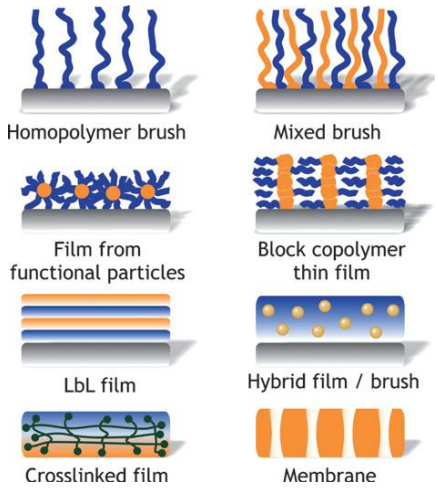

Figure 2.1: Cartoon the various polymer types[12]

Surfaces can be modified with homopolymer brushes,[16-19] mixed brushes,[20-21] block copolymer brushes,[22-28] cross-linked films[29-31] and many other types of engineered structures, as depicted in Figure 2.1. In the case of simple homopolymer brushes, density is the tuning property while the physical properties of the polymer remain the same.[17, 19, 32]Mixed brushes and copolymer brushes have the versatility of retaining the physical properties and environmental response of the constituent polymers, in addition to the density.[16, 21, 23-24, 33-34] Cross-linked films offer the ultimate density, in a mass of isotropy.[30, 35-37]

The range of physical properties offered by the multitude of synthetic and biopolymers presents the opportunity for nearly any type of surface imaginable. Response to pH,[5, 38] temperature,[39-44] electric field,[25, 45] ionic concentration,[46-48] and specific interactions[49-50] (e.g. antibody-antigen) are options for surface development.

These smart surfaces have applications as the foundation for gating materials,[51-53] which can selectively filter and separate species in response to external stimuli; substrates to control drug release[54-57]; organic/inorganic hybrid materials,[20, 58-60] which can improve

MRI imaging, magnetic drug targeting, and tumor ablation; and microfluidic devices,[61-63] which can control and direct transport. One example of this is a recent work by the Braun group.[61] They pattern a surface with a block copolymer in a maze-like fashion. They then use a small organic fluorescent molecule to show its interaction with the soft surface, and therefore its directed transport. The work herein strives offer basic understanding of similar soft surfaces as a step toward the engineering of devices that retain highly controllable properties.

2.2 Types of Surfaces Presented Herein

2.2.1 Functionalized Surfaces

The first portion of this work is concerned with surfaces that have the potential to be finely tuned for enhancing specific interactions or reducing nonspecific interactions. Stationary phases for separations,[64-66] coatings to eliminate nonspecific protein adsorption,[46, 67-70] and bio/immunoassays[50] all use functionalized surfaces in their utility. The spacing between the functional groups has an impact on the efficacy of the surface. In order to assess the effect of nanostructure on signal transduction pathways for hematopoietic blood stem cells, Altrock, et.al. studied the effects of ligand spacing and nanostructural properties of the extracellular matrix on fabricated biofunctionalized slides.[71] The extracellular matrix that surrounds these cells, as well as the lipid raft spacing, affects signal transduction as the cells begin to reproduce. Understanding the effects of these components is imperative to understanding optimum conditions for stem cell growth and sustainability.[71]

This example illustrates the continued need to study the effect of microenvironments using functionalized surfaces. This thesis will contribute understanding of probe interactions on similarly well-designed surfaces.

2.2.2 Responsive Surfaces

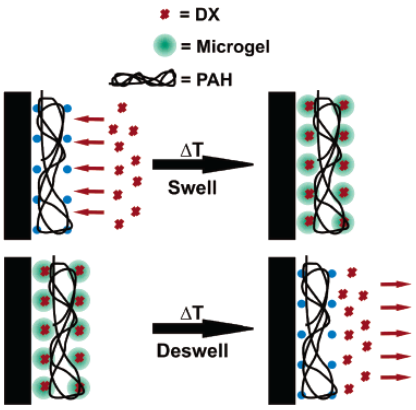

Figure 2.2:(upper) Schematic of loading of drug molecules using temperature controlled microgel. (lower) Schematic of drug release using temperature controlled microgel.[39-40]

As stated in Chapter 1, external stimuli responsive materials are utilized in a wide array of fields. The other portion of this work is concerned with thin films and hydrogels that were engineered to control temperature,[6, 72] pH,[6, 73] and hydrophilicity.[18] The Lyon group uses reversible temperature responsive microgels to control release of insulin and doxorubicin.[39-40] With a decrease in temperature below the lower critical solution temperature (LCST), the microgels swell and the small molecules are loaded into the gel network. With an increase above the LCST, the pharmeceuticals are released from the microgel as it shrinks. This is depicted in Figure 2.2.

This example illustrates the sophistication of the robust, switchable materials available for study. This thesis will contribute understanding of transport in similar crowded environments.

2.3 Single Molecule Regime

2.3.1 Advantages of the Single Molecule Regime

The observations and results of this thesis are based on single molecule regime

observations. We used these methods to discuss and comment on transport in heterogeneous environments at the nanoscale.

Contrary to the single molecule regime, ensemble measurements include and report an average behavior of the molecules within the system. While the average behavior of a system gives information on a system, focusing only on the global description neglects the potential for realizing the presence of less common, yet equally or more important events. The single molecule regime has the sensitivity to realize the full spectrum of behavior, since information about the system is garnered from each molecule. This type of sensitivity is required when measuring heterogeneous analytes or environments.

Single molecule investigations have grown to include a wide array of systems and applications. Some of these techniques are in extensive use in the present research group. Single molecule fluorescent resonant energy transfer (smFRET) is used to measure conformational changes of proteins, RNA and small DNA molecules[74-77], and reaction kinetics.[78] Force microscopies like AFM[49-50, 79-82] and optical tweezers[83-84] are used to determine physical properties of biological molecules and assess surface interaction. Single particle tracking (SPT) has allowed the prospect of guiding nanoparticles and monitoring local heating effects within biological membranes. [59]

The sensitivity of the single molecule regime lends itself well to fundamental studies of functionalized surfaces. The advantage of realizing all of the types of interactions present within the nanostructures will aid in the design and usage of specialized materials.

2.3.2 History of FCS

Chapter 3 offers experimental details of FCS, as it is the featured technique of this work. Here, I propose to outline the timeline of the technique and highlight its present day usage. Although FCS is an ensemble technique, we have used parameters and treatments that give us information about the behavior of single molecules.

Invention and implementation of FCS was approached for different reasons: to explore reaction kinetics,[85-87] molecular transport[85] and rotational diffusion.[88-89] In this way, it was meant to combine the efficacy of temperature or pressure jumps and Dynamic Light Scattering for biophysical queries.[90] Initially, the technique was performed in a setup similar to UV/Vis spectroscopy[91]; transfer of the technique to confocal microscopy soon followed.[92] Staying close to the field it was invented to improve, FCS began to be used as a technique used for biophysical problems such as DNA binding reaction kinetics,[93] measuring the dynamics of lipid bilayers, [94-95] and the dynamics and structures of biopolymers.[96-99]

FCS was not regarded as accessible until decades later, when Eigen, Rigler and coworkers improved the technique to include advances such as the usage of avalanche photon detectors (as opposed to photomultiplier tubes), incorporating optics to realize a small detection volume, and inclusion of a pinhole in the image plane to improve signal-to-noise.[100-102] These technological advances elevated the technique to the single molecule regime.[103-106]

Since then, FCS has been used to measure protein-dye and quantum dot photophysics,[107-110] monitoring triplet state dynamics[111] and photon antibunching.[112-113]

Many bio-related sciences use FCS to decipher the inner workings of living cells.[114-120] Recent findings are pushing frontiers in investigating rotational dynamics. [121-122]

FCS has also spurred proverbial cousins. Two photon FCS achieves higher optical resolution. [123] FRET-FCS measures both conformational dynamics as well as transport.[124-127] Scanning FCS, which will be discussed more in later chapters, is more sensitive to slower dynamics.[128-132] Image Correlation Spectroscopy is a manifestation that correlates images rather than a raw signal.[133-135]

2.3.3 Advantages of FCS

FCS can be contrasted with other techniques that seek to offer similar information. Fluorescence recovery after photobleaching (FRAP) can also give diffusion characteristics. This technique requires a higher concentration of particles, since its premise is to photobleach a spot and record the time needed for viable fluorophores to re-enter the bleached spot. Also the bleaching of the spot can damage the sample and definitely damages the probes. FCS is non-invasive and non-destructive.[136] Dynamic light scattering (DLS) is the scattering counterpart to FCS. Yet, the fact that FCS is selective for fluorescence abolishes the increased background signal present in DLS and offers a sensitivity that DLS cannot.[90] FCS can also measure chemical kinetics,[91, 93, 137-138] rotational diffusion,[88] adsorption,[136] anomalous diffusion[117, 139-140] and multiple transport processes.[141-142]

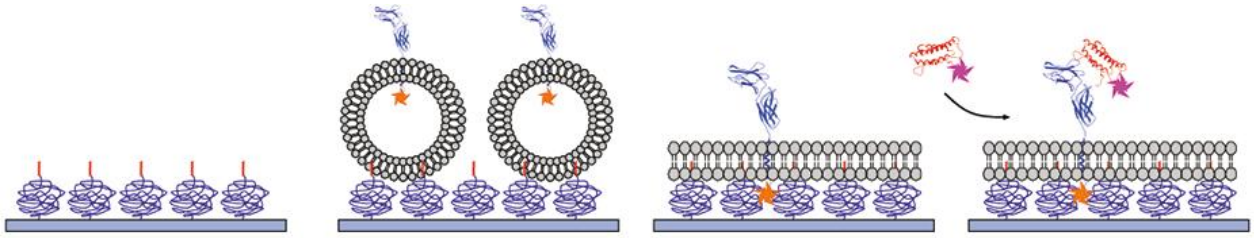

Figure 2.3: Schematic of the membrane assembling on the polymer brush, with the membrane receptor intact. The binding of the ligand to the receptor was also measured.[143]

A good example of the incorporation of FCS and other techniques that operate in the single molecule regime to measure the dynamics of a biologically relevant system is that of Roder, et. al.[143] The authors used FCS, SPT, and other single molecule methods to monitor the creation of polymer supported membranes and the mobility of the embedded membrane proteins.[143] A schematic is shown in Figure 2.3. FCS is used to monitor the free diffusion of the protein ligand in solution. To further benefit from the FCS technique, the authors monitored binding to the membrane protein, which was nearly immobilized in the polymer-supported lipid membrane. This study was complemented by analysis of SPT trajectories, which confirmed both the free diffusion and the adsorption events.

This thesis will utilize FCS and single molecule analysis methods to garner information about events within and at the interface of soft surfaces. This information will contribute to the fundamental knowledge of functionalized and responsive surfaces and the way small molecules and proteins interact with the aforementioned surfaces.

Chapter 3

Fluorescence Correlation Spectroscopy

3.1 FCS Theory

The utility of FCS methods arises from the Stokes-Einstein relation, which describes the rate of diffusion of particles as a function of particle characteristics:

$$D = \frac{k_B \cdot T}{6\pi \cdot \eta \cdot R_h} \qquad \text{Equation 3.1}$$

Here, the diffusion coefficient, D, is proportional to the temperature of the solvent, T, and inversely proportional to the viscosity of the medium and the hydrodynamic radius of the particle, η and R_h, respectively.

The diffusion coefficient in Equation 3.1, is related to the characteristic diffusion time, τ_D, through a laser beam focal area by:

$$\tau_D = \frac{r_0^2}{4D} \qquad \text{Equation 3.2}$$

where r_0 is the beam waist radius, which can be determined through measurements of diffusion times through the volume for particles of known size.[101] It is important to note that these calibration criteria were employed to ensure that the confocal conditions were internally consistent throughout the experiment.

Through Equations 3.1 and 3.2, knowledge of characteristic diffusion times for a particle interacting in some system enables the extraction of specific information on

environment and/or particle parameters. The diffusion times can be determined by FCS analysis. As measurements are taken, fluorescence signal fluctuates in accordance with the movement of a diffusing fluorescent molecule within the excitation focal volume. A simple autocorrelation of the fluorescence intensity signal can draw out the necessary information for the characterization of the molecule or environment. Elson and Madge, starting from a normalized autocorrelation function, G(τ):

$$G(\tau) = \frac{\langle \delta F(t) \cdot \delta F(t+\tau) \rangle}{\langle F(t) \rangle^2} \qquad \text{Equation 3.3}$$

derived an analytical expression relating the correlation function to the characteristic diffusion time.[85] In Equation 3.3, $\langle F(t) \rangle$ is the average of the fluorescence signal over time, *t*, and $\delta F(t) = F(t) - \langle F(t) \rangle$ is the expression that describes the fluctuation of the signal around the mean value. The autocorrelation is a measure of self-similarity of the signal over a set of lag times, ranging from τ_0 to τ_{max}. (For representative autocorrelation curves for the samples measured for this study, see Appendix A.)

The initial findings of Elson and Madge derived the autocorrelation function for 2D diffusion within a detection volume with a Gaussian intensity profile for x and y. Aragon and Pecora expanded the expression to describe a detection volume with a Gaussian intensity profile for x, y, and z:[89]

$$G(\tau) = \frac{1}{V_{eff} \langle C \rangle} \cdot \frac{1}{\left(1 + \frac{\tau}{\tau_d}\right)} \cdot \frac{1}{\left(1 + \left(\frac{r_0}{z_0}\right)^2 \left(\frac{\tau}{\tau_d}\right)\right)^{1/2}} \qquad \text{Equation 3.4}$$

where V_{eff} is the effective volume, ‹C› is the concentration of the dye, τ is the lag time, τ_d is the characteristic diffusion time, and z_0 is the beam height.

For systems where multiple species are present, a multiple-component expression is used, where n_i is the brightness and C_i is the concentration of the species i.[141-142] :

$$G(\tau) = \frac{\Sigma n_i^2 \langle C_i \rangle^2 G_i(\tau)}{(\Sigma n_i \langle C_i \rangle)^2} \qquad \text{Equation 3.5}$$

Autocorrelation data show the distribution of particle size and diffusion speeds within the solution, which makes it possible to distinguish between free diffusion, hindered diffusion, and anomalous adsorption behavior.

3.2 FCS Setup

A solid state laser was the excitation source (VERDI, Coherent). The 532 nm light was circularly polarized, filtered, and expanded to overfill the back aperture of an oil immersion microscope objective (FLUAR 100x, 1.3 NA, Carl Zeiss, GmBH). After excitation, the fluorescence was captured by the same objective[144] and isolated by a dichroic mirror (z532rdc, Chroma Technology) and a notch filter (NHPF-532.0, Kaiser). Fluorescence was then guided through a 50 μm pinhole to block out-of-focus light, increasing spatial resolution.[145] The resulting focal volume had a $1/e^2$ beam radius of ~230 nm and height of ~1 μm.[145] Photons were detected by avalanche photodiodes (APD; SPCM-AQR-15, Perkin-

Elmer). A piezo stage (P-517.3CL Physik Instrumente) and controller (SPM 100, RHK Technology) allowed the user to maneuver the sample in 3 dimensions. The output from the APDs was split to a photon counting board (PMS-400-A, Boston Electronics Corporation) and a 2D imaging system (RHK Technology). This setup is pictured in Figure 3.1. For each condition, the focal volume was calibrated in order to ensure that no experimental condition altered the confocal beam geometry. It was found that the beam geometry was consistent throughout the experiments.

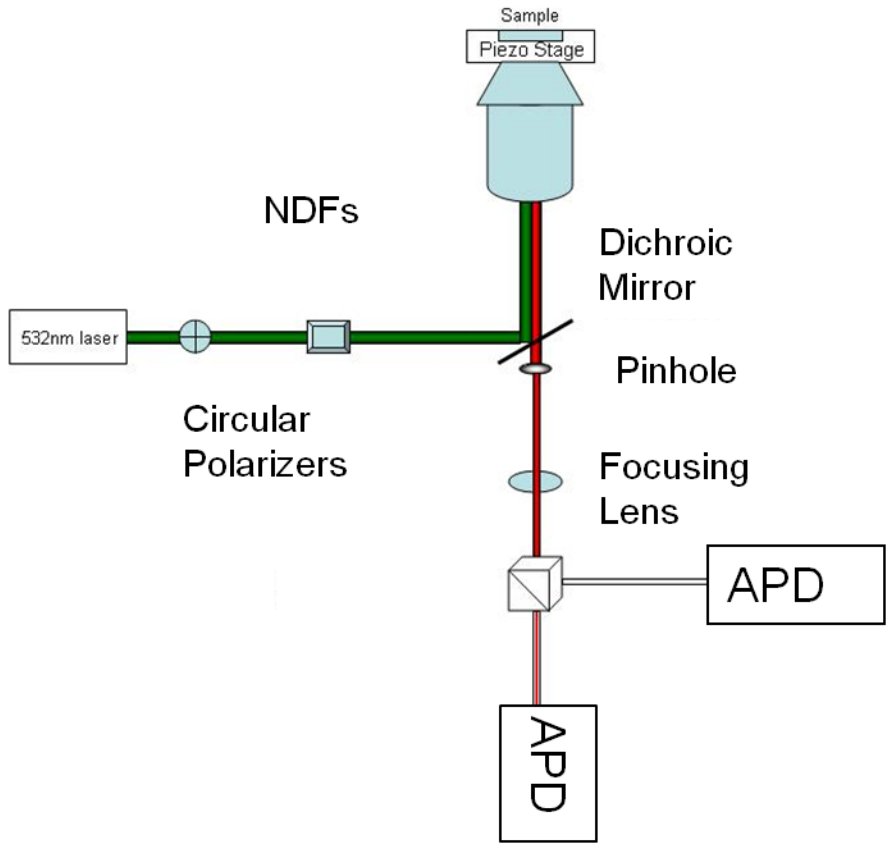

Figure 3.1: Homebuilt microscope used for the experiments.

3.3 Line Scan FCS

For line scan FCS, the focal volume is scanned along a predetermined length continuously (Figure 3.2a). This is in opposition to the stationary focal volume of traditional FCS. This scanning is performed with a user-defined velocity (υ).

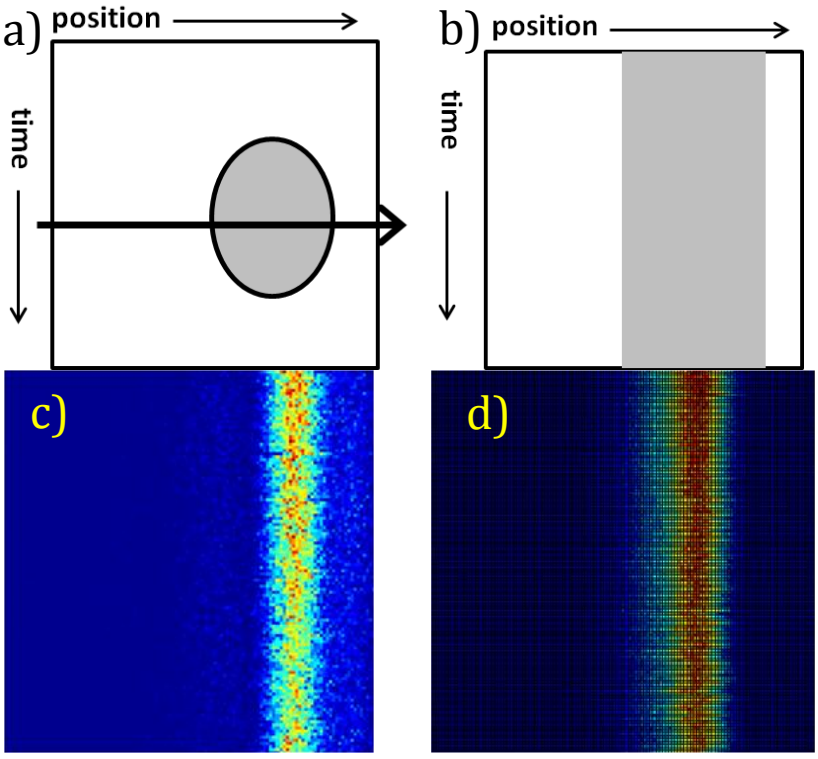

Figure 3.2: a) a schematic of a line scan trajectory across a bead, b) a schematic of the resultant trace, c) an image from the slow raster scan program, in which an image is created directly from collected photons, d) an image from fast line scan time trajectories, in which counts vs. time are collected and later assembled into an image.

In order to calibrate the line-scan method, a stationary bead was scanned. For these measurements, a 2μm line was scanned, with the bead within the area of interest. Figure 3.2 depicts the schematics and actual images. Figure 3.2a is a schematic of what the program has been designed to perform. The focal volume traces a line across the bead, which was given a user specified length and a user specified amount of time. The result of this scan should look like that in Figure 3.2b where the x-axis is position and the y-axis is time t_i, where t_i is an integer multiple (i) of the scanning period (T_p). Figure 3.2c is an actual scan from raster program that is slower than our line scan

program. The raster scan program is designed to automatically plot intensities as a function of position, writing out the image, with a user-defined time bin. Alternately, the line scan program only collects trajectories of intensity. Therefore, an additional program was written to align the time traces and produce an image, as seen in Figure 3.2d. The program also corrects for the speed up/slow down velocities that occur at the beginning and end of the line scan as well as the time needed to return the piezo stage to the starting point. We used this image to compare to the trajectory we obtained in the line scan program, Figure 3.2d. For both Figure 3.2c and d, the length of the line, i.e. the length of the x-axis, was 2 μm. Figure 3.2c was taken at 128ms/line; the image is approximately 16s of data. Figure 3.2d was obtained at 26ms/line; the image is approximately 3s of data. Although the line scan program is an order of magnitude quicker than the raster scanning program, T_p defines the minimum diffusion time. In this way, line scan FCS is adequate for measuring slow diffusion, as the minimum diffusion time that it can measure is the amount of time it takes to complete a linear scan, and is limited by the scanning setup and T_p.

For each sample, 10^4 line scans were acquired. We found that at large t_i, or lag times, the correlation curves $G(0, t_i)$ have little information about the diffusion coefficient. Therefore we calculated the autocorrelation with slightly fewer lag times. The autocorrelation curve is calculated on a logarithmic scale. The choice of a pixel size (s) ≈ r_0 leads to a correlation curve which exhibits much less statistical noise than for $s << r_0$.[132] The more accurate model takes into account the finite size of the pixel:[130-131]

$$G(0,\tau_i) = \frac{1}{C\pi s^2}\left(\sqrt{\pi}\mu_i erf(\mu_i) + e^{-\mu_i^2} - 1\right)$$

$$\mu_i = \frac{s}{\sqrt{r_0^2 + 4D\tau_i}} \qquad \text{Equation 3.6}$$

Equation 3.6 could be valid for any diffusion coefficient, but diffusion that is on the order of the scanning time changes the shape, and therefore accuracy, of the autocorrelation curve.[132] Therefore, line scan FCS is adequate for measuring slow diffusion, like we find in these soft surface systems.

3.4 FCS to Measure Surface Interactions

The fluctuating intensity characterized by FCS arises from the motion of fluorescent molecules as they pass through a tightly focused focal volume[146] as shown in Figure 3.3, which depicts our sample/observation volume geometry. For this study, measurements were acquired with the focal volume placed first at the surface of the coverslip (Figure 3.3a), corresponding to an offset of 0.5 μm of the beam waist from the surface), and at successively deeper positions within the bulk sample (Figure 3.3b and c). Therefore, the findings represent diffusion characteristics of the dyes in question as a function of distance from the coverslip surface.

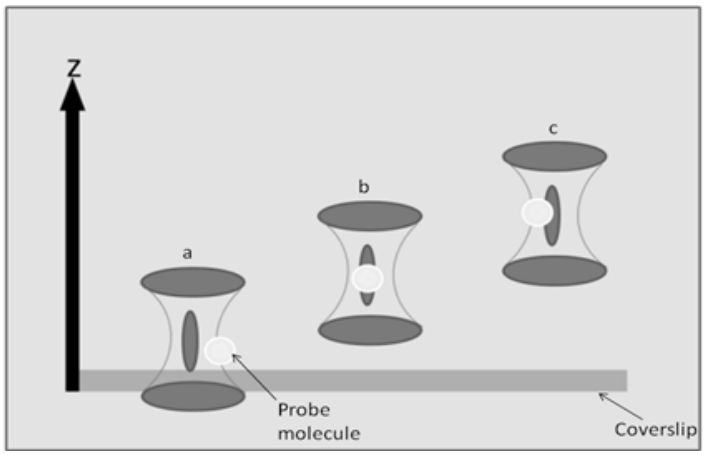

Figure 3.3: Placement of the bottom coverslip surface with respect to the focal volume.

There is some degree of uncertainty in the position of the focal volume with respect to the surface that can be quantified. Contributors to the uncertainty in position are the focus set point and focus drift. The focus set point was established prior to acquiring each sample by focusing the laser beam at the surface of the coverslip (i.e., at a depth of zero microns into the sample). This focus set point was selected by adjusting the sample position along the z axis until the light scattered from the surface of the coverslip, as viewed on a CCD camera, was at its minimum area/maximum intensity. The uncertainty in setting the focus visually was determined to be ± 75 nm. This uncertainty arises from the limitation of visual discrimination of changes in the focusing spot within this 150 nm range. The second contributor to uncertainty is focus drift during the 5 minute sample acquisition period. To minimize the effect of this source of error, the visual focus was checked at the conclusion of every measurement and its z axis location compared to the location recorded at the beginning of the measurement. The uncertainty associated with focus drift was ± 0.17 μm; acquisition periods for which the drift was greater than this were re-sampled.

In considering the position of the focal volume with respect to the surface, and the resulting intersection of the focal volume with the surface/bulk portions of the sample, a discussion of the focal volume profile in z is also merited. Based on the work of Hess and

Webb,[123] the focal volume profile for a high NA, overfilled ($\beta < 1$, $\beta = r_{microscope\ aperture}/r_{pin\text{-}hole}$), optical system with an aperture size of 7.68 o.u. ($r_{ou} = r_{pin\text{-}hole} * 2\pi NA/\lambda M$; M = magnification of the objective) is nearly Guassian in z over the $1/e^2$ intensity range, and has half length dimensions of ~0.5 μm which agrees with our estimated focal volume $1/e^2$ dimensions. At these conditions, ~94% of signal is measured from the $1/e^2$ -focal volume and the remaining 6% occur outside of these bounds. With these considerations, when setting the focus position (center of the focal volume along the z axis) to 0.5 μm above the surface of the coverslip, we are able to position the entire focal volume in the sample, while intersecting the surface region of interest. It is important to note that there is continuity to the measurements: since the focal volume is ~2 μm in the z dimension, taking measurements in 0.5 μm steps ensures that an overlap of data acquisition is present.

Chapter 4

Dye Diffusion at Surfaces

4.1 Abstract

Fluorescence correlation spectroscopy and single molecule burst analysis were used to measure the effects of glass surface interactions on the diffusion of two common fluorescent dyes, one cationic and one anionic. The presence of dye-surface interactions as a function of distance from the surface was investigated. Use of a three-axis piezo stage, combined with reference calibration measurements, enabled the accurate acquisition of surface-distance dependent transport data. This analysis reveals attractive interactions between the cationic dye and the surface, which significantly alter the extracted diffusion values and persist in the measurements up to 1.0 μm from the surface. The Coulomb attraction between the cationic dye and the surface also results in rare, long-lived association events that lead to irreproducibility in extracted diffusion values. In addition to an assignment of the association lifetime for these events, this paper demonstrates that, if experiments must be performed with cationic probes near a glass surface, the use of solution electrolytes can eliminate deleterious dye-surface interactions, as the dyes were tested in a variety of environments. Finally, our data demonstrate that a better dye choice is an anionic probe, which exhibits no depth-dependence of diffusion characteristics above a glass surface.

4.2 Introduction

In the present work, we report on the presence and extent of interactions between

glass support substrates and two commonly used fluorescent probes of opposite charge, as a function of distance from the support surface. The data presented are important because many photophysical experiments using a variety of molecular fluorescent dyes are performed on glass substrates. Although the objective of the aforementioned experiments may not involve the glass-solvent interface, the presence of interfacial interactions can persist up to distances of 1 μm from the surfaces which significantly impact extracted parameters, and thus affect interpretation of data. There are several phenomena that might influence data interpretation.

One property that can be affected significantly by surface interactions is dye photophysics. Both free and bound configurations of dyes have been used to probe kinetics, conformational dynamics, and the influence of surfaces on molecular photophysics.[147-151] When experimental spectral or time windows overlap with surface-induced changes to photophysical lifetimes and spectral characteristics, data interpretation becomes complicated.

Another concern is surface chemical interactions that occur at an interface. In the case of the glass/water interface, it is well known that a charged double layer forms that can be nanometers thick depending on the ionic strength of the solute.[152-153] The electrical double layer can shield the dye from the surface resulting in differences of behavior as a function of environment. Dynamic behavior of molecules at the surface can also exhibit dependence on the silica termination/silanol chemistry.[154] This chemistry can be modified through oxygen plasma cleaning, which produces densely populated hydroxyl-terminated silica surfaces,[155] as shown in Figure 4.1. The water solvent organization at the interfaces

is significantly altered from that of bulk water.[156-157] Additionally, studies have shown that the translational diffusion of water is markedly different within confined regions, such as micelles and nanopores.[158-159] Furthermore, each of the previous factors can be drastically altered as a function of solution ionic strength.

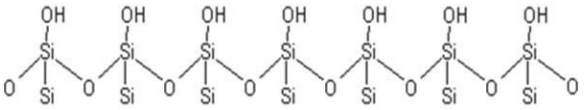

Figure 4.1: Illustration of plasma cleaned silica (glass) surface.

As stated, identifying and understanding these interactions is important because of their ability to alter the integrity of data analysis in the many experimental systems that are conducted close to surfaces.[160-163] Specifically, fluorescence correlation spectroscopy (FCS), although not designed to probe surface interactions, is frequently performed near a glass surface and thus the surface interactions and their impact on the data must be understood. FCS and its more advanced cousins such as dual-focus FCS, scanning FCS, and two-photon FCS have recently developed in order to overcome some of the intrinsic limitations of conventional FCS.[164-170] These advances have allowed us to probe transport at and near membrane interfaces. Attempts to measure transport in such heterogeneous, crowded, or charged environments present their own innate challenges to data collection and analysis.[142, 171-177] Since such environments also present an interfacial measurement to some degree, it becomes important to quantify the interaction of probes with the interfaces as a separate issue. Calibrating the focal volume for the objective, laser wavelength, the chemical makeup and thickness of the coverslip, and the medium are critical to acquiring accurate, reproducible diffusion data.[178-179] As we will demonstrate, choice of measurement distance from the support interface, dye charge, and solution electrolytic properties are other

crucial factors.

Rhodamine 6G (R6G), a cationic dye, is common in fluorescence experiments[180-186] and there have been several reports of its interfacial properties. For example, the probe has been shown to aggregate at the air/water interface using confocal fluorescence microscopy.[185-186] Further evidence has been reported that R6G is not only attracted to silica, but it also orders itself with respect to silanol groups.[180] In contrast, Boutin and coworkers did not observe attractive interactions in their study of hydrophilic surfaces.[181] Instead, those studies reported the largest attraction of R6G to hydrophobic surfaces. One purpose of the current work is to determine which of these earlier observations is correct, namely whether attractive interactions are observed between R6G and a hydrophilic glass surface when performing FCS, and the extent of any interactions.

Other common dyes lack the extensive information on surface interactions that is present for R6G, and of particular interest are dyes with different charge value and distribution. The current work delves deeper into the effects of surface interactions by characterizing, as a function of distance from a hydrophilic glass interface, the mobility and local concentration of both cationic and anionic dyes using FCS and single molecule burst analysis. In order to extend previous studies, and to provide a quantitative analysis of the depth-dependence of measurements, the current work utilizes a three-axis piezo stage controller, which provides nanometer accuracy of the sample positioning.

In this study, we use confocal FCS to quantify the presence of dye-surface interactions between a glass surface and the cationic and anionic dyes R6G and AlexaFluor 555® (Alexa), respectively, as a function of distance from the surface. These studies are

performed in aqueous media under a variety of electrolytic conditions. By comparing diffusion times for the two dyes under the various conditions, it was found that surface interactions with the cationic R6G contribute significantly to measured diffusion rates out to a focus position depth of 1.0 μm from the glass surface. Additionally, the surface interactions led to rare, but long-lived association events that introduce irreproducibility in extracted diffusion constants. In contrast, the anionic dye did not exhibit surface interactions, and thus its measured diffusion rate was constant and reproducible at all distances measured. Single molecule burst analyses of single fluorescent events confirm that R6G is more concentrated near the surface and spends more time in the laser focal volume. The data acquired at various pH and electrolyte conditions support the hypothesis that the primary interactions between R6G and the glass surface are Coulombic. The authors would offer the practical advice that if R6G is used in water, an electrolyte solution should be employed to eliminate surface interactions. Blip dwell-time analyses yield a characteristic association time for R6G at the surface of 0.71 ms.

4.3 Methods and Materials

4.3.1 Materials and Sample Preparation

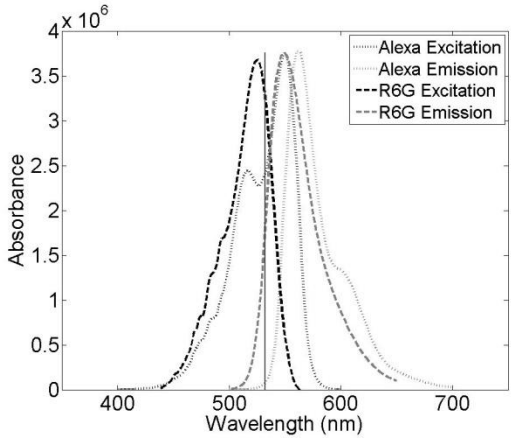

Figure 4.2: Absorption and emission spectra of

Rhodamine 6G (solid) and Alexa Fluor® 555 (dotted). The excitation source is also illustrated (vertical line).

Many of the details of the sample preparation, setup, theory, data analysis and acquisition have been previously reported.[142, 170] Orange fluorescent carboxylate-modified FluoSphere beads (max abs/em: 540/560 nm) were used to calibrate the focal volume for the current FCS measurements at all depths measured. Both 40 and 100 nm beads were used; the 40 nm beads were prepared at 1:10000 dilution and the 100 nm beads were at 1:1000 dilution, in water. Both R6G (max abs/em: 530/566 nm) and Alexa (max abs/em: 555/565 nm) were diluted to approximately 100 pM for signal versus concentration optimization.[187] Figure 4.2 depicts the excitation and emission spectra of the two dyes, with the laser excitation line indicated. Due to differences in extinction and quantum yield at the excitation wavelength, the Alexa solutions were measured with a power density of ~2100 W/cm^2 and the R6G solutions were measured with a power density of ~800 W/cm^2.

NaCl (5M, Sigma-Aldrich), KOH (85+%, Sigma-Aldrich) and spectroscopic grade H_2SO_4 (J. T. Baker) were diluted to 0.001N solutions serving as differing environments for the fluorescent dyes. The basic solution used was pH 11.0; the acidic solutions were pH 1.0 & 3.0. Measurements were taken in each of the four solutions (aqueous, acidic, basic, and electrolytic) and at four depths (0.5, 1.0, 1.5, and 2.0 μm). No. 1 coverslips were rinsed in Hyclone Molecular Biology (MB) grade water (VWR) before undergoing oxygen plasma cleaning for 2 minutes. The coverslips were stored in a dessicator until use.

4.4 Results & Discussion

4.4.1 Depth Analysis

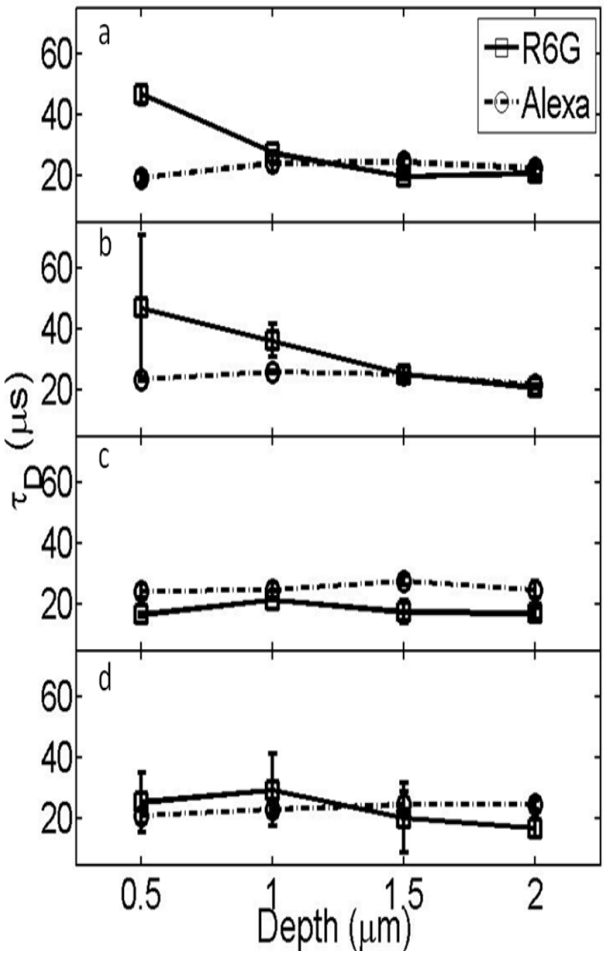

Figure 4.3: Plots of the average τ_D vs. depth of R6G and Alexa in aqueous (a), acidic (b), basic (c), and electrolytic (d) solutions. The spread in τ_D values at each depth reflects the reproducibility from multiple measurements. Lines between points are included only as a guide for the eye.

The depth dependence of the extracted diffusion time, τ_d, for the cationic R6G in water is shown in Figure 4.3a. The diffusion time for R6G is more than twice as long when measured close to the glass surface. For measurements taken further than 1 μm from the glass surface, the diffusion values converge to a diffusion time of 22 μs.[188] In contrast, diffusion times for the anionic Alexa dye in water are not depth dependent, as is shown in Figure 4.3a. It should be noted that the self-consistent data obtained for Alexa diffusion at all depths establishes that the slowed diffusion measured for R6G when close to the surface does not arise as an artifact of focal volume perturbation by the surface or from changes in the refractive index, but from real perturbation of R6G diffusion. Thus, the longer R6G diffusion times close to the glass surface are clear evidence of attractive interactions between the cationic dye and the hydrophilic hydroxyl-terminated silica surface. They also provide at least partial insight

into the wide range of reported values for the diffusion time of R6G.[148, 187-188] Among the many possible explanations for these discrepancies are surface effects, as our results clearly demonstrate.

Because the focal volume encompasses the region close to the surface where attractive interactions may occur, and also extends into the bulk solution, fluctuations measured within this extended focal volume are expected to reflect both surface-hindered diffusion and bulk diffusion of the dyes. FCS analysis conducted with a two-component fit[141, 189] was unable to reliably extract the two expected components, however, due to limitations in resolving diffusion for two components when diffusion times are similar.[189] Instead, other techniques both chemical and analytical are necessary to further test the hypothesis that our measurements are sensitive to attractive interactions, and to quantify these interactions, between the dye and surface.

4.4.2 Ionic Condition Analysis

The slow diffusion times measured for R6G close to the glass surface exhibited a strong dependence on the ionic conditions, as shown in Figure 4.3b-d. The depth dependence was observed in acidic conditions (pH 1.0 and 3.0) but not basic (pH 11.0) or electrolytic (0.001N NaCl) conditions. The pH 3.0 data are of particular significance. As shown in Figure 4.3b, there is a large standard deviation of extracted diffusion values closest to the glass surface under these conditions. Large standard deviations in FCS data suggest the presence of anomalous events such as aggregation or adsorption.[183] We would expect chemisorption events in the case of a Coulombic attraction between the cationic R6G and an anionic surface. The isolectric point (IEP) of silica is reported to be at pH 2.0,

and can be dependent on the hydration of the surface.[190] Other studies have confirmed that below pH 2, glass coverslips are positively charged and from pH 2-5, the surface is negatively charged.[182] Thus, even under our acidic experimental conditions at pH 3, the negatively charged surface can be expected to attract the cationic R6G, leading to both to a slow diffusion time and a large spread in the error due to anomalous adsorption events. We performed additional depth dependent experiments at pH 1.0, below the reported isoelectric point[190] (data not shown), and our results differ from the findings of Chen and coworkers in that surface interactions are not eliminated even at this pH. This can be explained by differences in the experimental conditions. The coverslips in our study were plasma cleaned, which increases surface hydration levels, and thus alters the surface IEP. There is experimental evidence that the IEP of a solid oxide/hydroxide is decreased when the level of surface hydration is increased.[190] According to this information, along with the data presented in Figure 4.3b and our findings during attempts to further acidify the surface (to pH 1.0), it is not practical to use acid to switch the surface charge when using plasma-treated glass coverslips.

Whereas measurements in aqueous and acidic solvent reveal a dependence of diffusion times on distance from the interface, neither the electrolytic nor basic conditions exhibit a comparable dependence. This reflects a lack of strong interfacial interactions between the dye and the surface in these conditions. Aligning the Gouy-Chapman and Stern models for the composition of ion concentration near a charged surface, the differential behavior of R6G mobility measured near the interface in aqueous and acidic conditions as compared to basic and ionic solutions may be related to the identity of the counter ions

available to form the adsorbed and diffusive layers.[191] The use of MB water in all of the dye solutions ensures that the only ions present are those that have been purposefully introduced, and the inherent hydronium/hydroxide pairs. In the case of the aqueous and acidic measurements, our data shows that the cationic dye participates at the surface along with the expected hydronium ions in neutralization of the negative surface charges. However, in the case of the basic and ionic environments, the respective cations (Na^+ and K^+) are available to compose the Stern layer, and our data indicates that there is significant inhibition of surface interactions for the cationic dye.[192]

These data are supported by other studies that report attractive interactions between R6G and silica surfaces.[183-184] Of additional importance is a study in which attractions were observed in the case of hydrophobic surfaces, but not hydrophilic surfaces.[181] Our work demonstrates that attractive conditions are present in the case of the hydrophilic, polar SiOH surface.

It is important to note the lack of surface interactions under any conditions for the anionic Alexa dye. The lack of measureable effects on the behavior of anionic Alexa dye molecules can be attributed to charge exclusion from the negatively charged surface. This insensitivity to the glass surface makes Alexa a reasonable substitute for R6G in studies that require measurement close to this interface.

4.4.3 Frequency Analysis

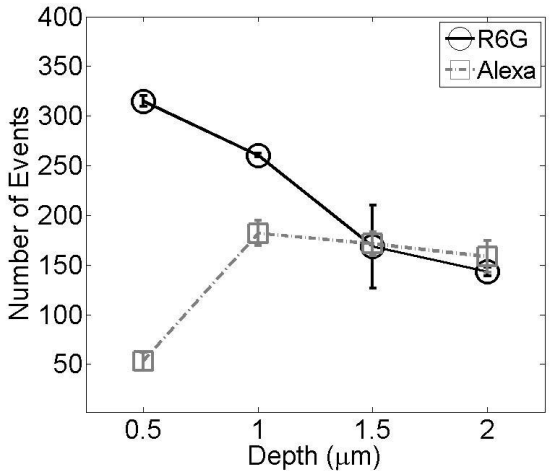

Figure 4.4: Mean events for R6G and Alexa in aqueous conditions. The spread in intensity values at each depth reflect reproducibility from multiple experiments. Lines are drawn as a guide for the eye.

A single molecule blip frequency analysis was performed to test the hypothesis that attractive forces are responsible for the slower R6G diffusion near the surface. If this hypothesis is correct, then we would expect to find a higher local concentration of R6G dye near the surface. Since our data is collected in the time domain rather than from an autocorrelator acquisition board, it is possible to obtain data such as single event frequency, intensity, and duration values. Figure 4.4 displays the average number of events (with standard deviations over multiple samples) obtained from data in 100 μs time bins versus the distance from the coverslip for the two dyes in aqueous solution. The increase in events observed near the surface arises from an increase in the average number of molecules in the focal volume per 100 μs bin time. The frequency trends shown here confirm that the local concentration of R6G is higher at the surface, as would be expected if there are significant attractive forces between the cationic dye and the coverslip surface. Additionally, the single blip analysis also demonstrates a repulsive decrease in local concentration of the anionic Alexa dye near the surface, an expected result, but one that is averaged out by the simpler ensemble FCS analysis performed above. Similar trends are found in the case of the acidic condition and are reported in Appendix A.

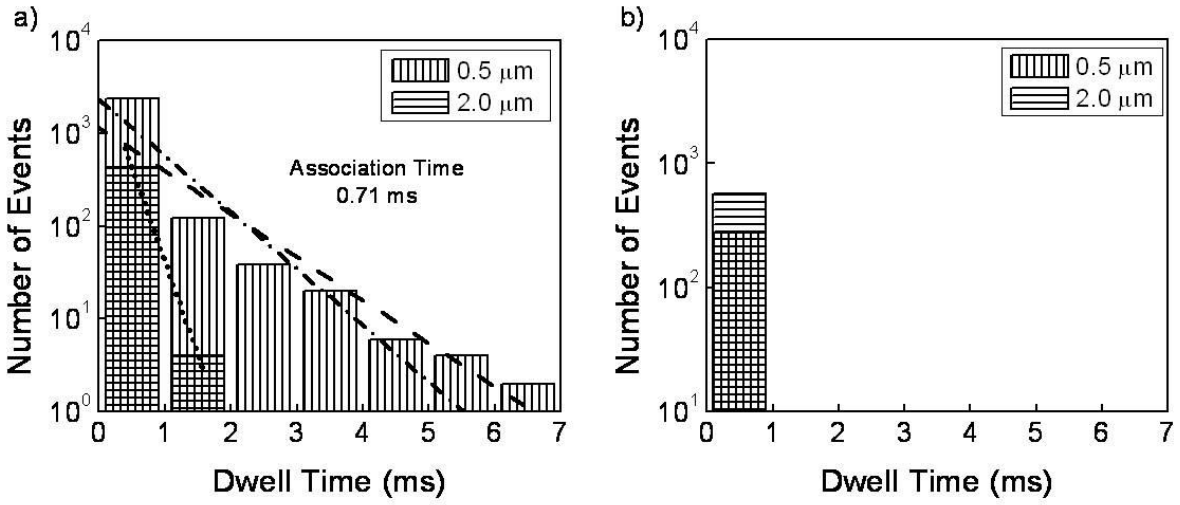

Figure 4.5: Dwell time histograms for R6G (a) and Alexa (b) in water. In (a) the 0.5μm data was fitted to an exponential (dashed line) and decomposed into the IRF (dotted line) and the pure data (dot-dashed line).

4.4.4 Blip Dwell Time Analysis

The blip frequency and FCS data both demonstrate attractive forces between the R6G dye and the surface that result in an overall measured slower diffusion time. An additional question about the extent of the attractive forces can be asked. Others have studied the orientational effects of silica on R6G and have found that the dye trapped in a silica cage rigidly orients itself with respect to the walls of the cage which are comprised of Si-OH bonds,[180] suggesting chemical coordination between the dye and the silica. In order to test for the presence of long-lived association events, we performed a blip dwell-analysis. As shown in Figure 4.5, a fluorescence blip dwell-time analysis was performed for each dye in water at 100 μs time bins (note that these bins are an order of magnitude larger than the 10 μs bins used for diffusion measurements) at 0.5 μm and 2.0 μm from the surface. In Figure 4.5a, at 0.5 μm, there are a large number of fluorescent events that are several milliseconds long for R6G. These dwell times are much longer than the diffusion

time measured for R6G near the surface (~40 μs). It is also important to note that the measured number of events for these dwells represent minimum values because, despite the low excitation fluence in our FCS measurements, photobleaching limits detection of dwell times longer than several milliseconds. These observed long focal volume dwell times deviate considerably from those expected from a typical distribution, as evidenced by the bulk data displayed in Figure 4.5a. The dwell time distribution is significantly broadened near the surface when compared with diffusion in the bulk. These long dwell times are consistent with adsorption events. The present analysis reveals that there is a prolonged interaction of the R6G with the surface, consistent with chemisorption events described earlier.[180] In conjunction with the frequency analysis data presented in Figure 4.4, and the large standard deviations shown in Figure 4.3, the dwell-time data support the presence of rare, long-lived association events that are consistent with adsorption/desorption processes.[193] As shown in Figure 4.5b, and consistent with the FCS data, the Alexa dye conforms to a model of simple diffusion, even close to the coverslip.

One of the concerns in the study conducted by Schuster and coworkers[183] was their inability to determine the attachment times for R6G to the surface. Using the dwell time analysis shown in Figure 4.5a, we were able to fit the bulk and close-to-surface data to exponential decay functions. The data measured close to the surface represents a convolution of long surface association events, bulk diffusion characteristics, and our instrument response function (IRF). To extract the characteristic association time for molecules at the interface from this data, the convoluted data (dashed line in Figure 4.5) was decomposed into two exponential functions (dotted and dot-dashed lines in Figure 4.5,

respectively), representing the association-data function, and the combined bulk diffusion and IRF functions as obtained experimentally from measurements at 2.0 um away from the surface. The association-data function was extracted through Fourier deconvolutions of the two fitted exponentials. Fitting the resulting pure data function yields an association time. In this manner we establish that, in aqueous conditions, R6G shows a characteristic association time of 0.71 ms. Again, this is a low estimate of actual association lifetimes because detection of longer-lived events is reduced by photobleaching.

4.5 Conclusions

The current studies offer evidence that R6G is attracted to a hydrophilic hydroxyl-terminated silica surface under aqueous and acidic conditions above the protonation point of the hydroxyl surface group. These studies suggest that, in order to avoid conditions in which surface interactions affect acquired data, diffusion studies using R6G should be performed at least 1 μm from the surface for confocal conditions, or salt should be added to shield the surface attraction when using the cationic R6G. Blip dwell-time analyses yield an R6G surface association time of 0.71 ms. The anionic Alexa dye is not attracted to hydroxyl-terminated silica, and thus presents itself as a good alternative to R6G as a diffusion probe when studies are to be performed near glass or hydrophilic substrates in aqueous conditions.

4.6 Acknowledgements

The authors would like to thank Alexei Tcherniak and David Solis of the Link Group at Rice University, along with Prof. Link, for their helpful discussions.

Chapter 5

Permeability of Anti-Fouling PEGylated Surfaces

5.1 Abstract

The present work reports on *in situ* observations of the interaction of organic dye probe molecules and dye-labeled protein with different poly(ethylene glycol) (PEG) architectures (linear, dendron, and bottle brush). Fluorescence correlation spectroscopy (FCS) and single molecule event analysis were used to examine the nature and extent of probe-PEG interactions. The data support a sieve-like model in which size-exclusion principles determine the extent of probe-PEG interactions. Small probes are trapped by more dense PEG architectures and large probes interact more with less dense PEG surfaces. These results, and the tunable pore structure of the PEG dendrons employed in this work, suggest the viability of electropolymerizable materials for tunable surfaces.

5.2 Introduction

The present work reports on *in situ* observations of the interaction of various probe molecules with PEGylated surfaces. Poly(ethylene glycol) (PEG) is used in a variety of surface preparations because of its hydrophilicity, low toxicity, and its suppression of nonspecific protein adsorption [70, 194-199]. Despite the wide use of PEGs in dental, ophthalmological, and surgical applications for anti-fouling purposes, a greater molecular-scale understanding of its mechanism of activity is still desirable. Given the structural and applications evidence for the relationship between structure and function in PEGylated

surfaces [46, 68-70], it is important to pursue an understanding of how various PEGylated surfaces resist nonspecific protein adsorption [200]. More broadly, a better molecular-scale description of transport at soft interfaces would benefit both ion-exchange and size exclusion chromatographic separations sciences [201-202], and the scientific understanding of chromatography, therapeutic separations, biosensors, and immunoassay.

X-ray photoelectron spectroscopy, ellipsometry, fluorescence spectroscopy, theoretical modeling and other techniques extensively support the anti-fouling properties of PEGylated surfaces [28, 46, 67-68, 198-200, 203-210]. However, questions remain about the dynamics and mechanisms that direct how these surfaces serve as a physical barrier, decrease adsorption events, and/or repel proteins. It is likely that the mechanism underlying function of soft PEG interfaces is more complicated than a simple physical barrier. The mechanism may depend on the polymer chemistry involved in the fabrication of the surface, including methods involving end-grafting to a surface, radical-initiated polymerization, cross-linking and co-block polymerization [24, 33, 211]. These methods of chemical synthesis can produce products that vary in length, density, and architecture.

Both polymer length and shape appear to be important parameters for controlling surface properties. All chain lengths show some resistance to nonspecific protein adsorption [69-70, 200, 212-216]. Short oligo(ethylene glycols) (OEGs), of fewer than 11 monomers [217], decrease the van der Waals interactions between the surface and protein [215] and offer a layer of water protection [218]. Longer PEGs have been reported to operate based on steric repulsion, chain flexibility, hydrophobic forces, and entropic costs [67, 198-199, 219]. Polymer shape also contributes to functionality, as cross-linked star-shaped polymers have been

observed to be superior in the reduction of nonspecific protein adsorption due to the dense matrix of chains on the surface [31, 220]. Bottle-brush polymers have an intricate layering of "bristles" that presents a thicket of PEG chains [27-28]. Apart from the chemical and steric repulsive forces listed above, sieve-like behaviors have been observed in cyclic voltammetry studies [69], in which molecules have been observed to permeate both low and high molecular weight (MW) polymers.

In the present work, a variety of PEG brushes are studied, including linear, dendron, and bottle brush PEGs. For simplicity, the term PEG will be used for both higher MW PEGs and lower MW OEGs, and length differences will be explained in the text. We used confocal FCS and single event analysis to quantify the presence and extent of interactions between PEG and the cationic Rhodamine 6G (R6G) and anionic AlexaFluor 555® (Alexa) dyes as a function of distance from the surface. We have successfully used these techniques to study transport at charged and crowded interfaces and with heterogeneous mixtures [122, 142, 170, 221]. Others have recently reported the successful use of FCS to understand probe-polymer brush interactions [222]. When measuring close to the substrate interface, it is important to consider dye-surface interactions [221]. In order to offer insight into these questions we report evidence of the interaction of small molecules and proteins with linear and other forms of PEG brushes (Figure 5.1).

We have also used novel electropolymerized PEG dendrons [223] to modify the pore size (distance between PEG chains) near the surface in efforts to study the tuning of the molecular sieve. FCS analysis of translational diffusion of the dyes in the presence of the polymer revealed two distinct components: a fast, bulk-like component and a slow,

hindered component. By comparing diffusion times for the R6G and Alexa dyes under the various conditions, it was found that interactions with the polymer contribute significantly to diffusion rates measured by FCS out to a focal position of at least 1.0 μm from the glass surface. Similar studies on PEG dendrons support a physical sieve-like model for molecular diffusion near PEGylated interfaces. Lastly, we explored biocompatibility with the protein α-lactalbumin.

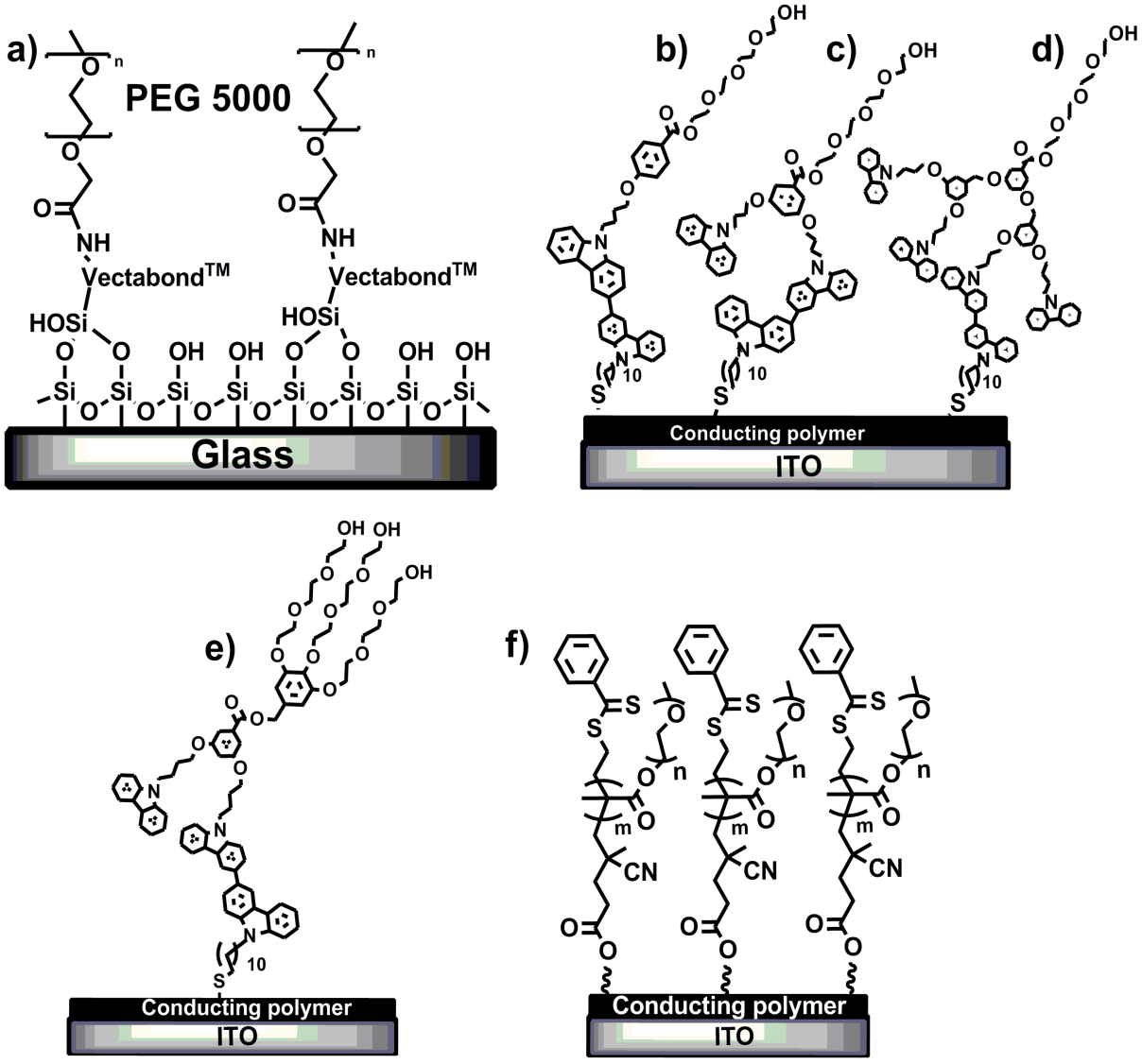

Figure 5.1: Depiction of the surfaces used in this study. All details of surface modification are described in the text. (a) Structure of linear PEG brushes grafted to a glass surface. Additional PEG brushes were prepared with G_nCbztEG Janus-type dendrons on ITO surfaces. Janus-type dendrons are "double-faced" molecules. In

this case, one face is the carbozole end, which is grafted onto the ITO surface, and the other face is the PEG chain extended in solution. Dendron generations used in this study include: (b) G_0CbztEG (c), G_1CbztEG (d), G_2CbztEG and (e) branched G_1CbztEG. The dendrons are abbreviated as Gn in the text, with the branched dendron as GnB, (f) Structure of bottle brush polymers, with a PMMA backbone and PEG 'bristles'.

5.3 Methods and Materials

5.3.1 Materials and Linear PEG Preparation

Many of the details of the sample preparation, setup, and theory have been previously reported [122, 142, 170, 221]. 100 nm orange fluorescent carboxylate-modified FluoSphere beads (max abs/em: 540/560 nm) beads (1:1000 dilution) were used to determine the focal volume for the FCS measurements. Rhodamine 6G (max abs/em: 530/566nm) and AlexaFluor® 555 (max abs/em: 555/565 nm) were diluted to approximately 100 pM for signal versus concentration optimization. NaCl (5M, Sigma-Aldrich), KOH (85+%, Sigma-Aldrich), RbOH (Sigma Aldrich) and spectroscopic grade H_2SO_4 (J. T. Baker) were diluted to a 0.001N solutions supplying the differing environments for the fluorescent dyes. The basic solutions were pH 11.0 and 8.0; the acidic solution was pH 3.0. Hyclone Molecular Biology grade (MB) water (VWR) was used for all dilutions. No. 1 coverslips were rinsed in the MB-grade water and plasma cleaned in oxygen for 2 minutes. For PEGylation, the coverslips were pre-treated with an amino-silane linker, Vectabond™ (Vector Laboratories). The reagent was dissolved in acetone and the plasma cleaned slides were submerged followed by a MB water rinse and drying with N_2. An aqueous mixture containing 25% PEG 5000 (Fluka) and 11% $NaHCO_3$ (7.5%, Sigma-Aldrich) was then applied to the cavity of a custom silicon chamber. The mixture was allowed to dry for 4 hours, followed by a MB water rinse and drying with N_2. Figure 5.1a depicts the resulting PEGylated slide. Measurements were taken in each of the four solutions (aqueous, acidic, basic, and electrolytic) and at four depths (0.5, 1.0, 1.5, and 2.0

μm).

5.3.2 PEG Dendron Synthesis[223]

The three different generations of PEGylated carbazole linear dendrons, G_0CbztEG, G_1CbztEG and G_2CbztEG, were synthesized (Scheme S1-2) by first preparing the three different generations of carbazole-terminated dendrons made through a sonochemical Mitsonobu type etherification method [224-225]. The carbazole carboxylic acid dendrons were then functionalized with tetraethylene glycol units via dicyclohexylcarbodiimide coupling. ^{1}H NMR and MALDI-TOF spectrometry confirmed the structures of the desired G_nCbztEG molecules. (The dendrons are abbreviated as Gn in the remainder of the discussion, with the branched dendron as GnB). Details of the linear-dendron synthesis can be found elsewhere [223, 226]. Figure 5.1b-d depicts the the dendrons, from n = 0, 1, and 2. Figure 5.1e depicts the branched version of n = 1.

Thin films were fabricated onto indium tin oxide (ITO) coated cover slips employing an ex-situ electrochemical polymerization technique, preventing the use of glass coverslips. All electropolymerizations were performed using an Autolab PGSTAT 12 potentiostat (Metrohm) coupled with an SPR instrument (Autolab ESPRIT from Eco Chemie) which was controlled by GPES version 4.9 software provided by MetrOhm and Eco Chemie. The electropolymerization was performed using cyclic voltammetry (CV) in a three-electrode cell containing 20 μM PEGylated carbazole dendron monomers and 0.1 M tetrabutylammonium hexafluorophosphate (TBAP) as supporting electrolyte in chromatographic grade acetonitrile by sweeping the voltage from 0 V to 1.3 V for 20 cycles at a scan rate of 50 mV/s against a Ag/AgCl non-aqueous reference electrode and Pt

counter-electrode.

5.3.3 PEG Bottle Brush Synthesis[22]

Reagent chemicals were purchased from Aldrich and were used without further purification unless otherwise indicated. Tetrahydrofuran (THF) used in the synthesis and polymerization reactions was distilled from sodium/benzophenone ketyl. Methyl methacrylate (MMA, 99+%) and poly(ethylene glycol) methyl ether methacrylate (PEGMEMA) (MW 300) monomers, were passed through a column with alternating layers of activated basic alumina and inhibitor remover replacement packing to remove the inhibitor and were stored at -20 °C. The chain transfer agent (CTA), 3,5-bis(4-(9*H*-carbazol-9-yl)butoxy)benzyl 4-cyano-4-(phenylcarbonothioylthio)pentanoate (Cbz-CTA) was synthesized according to the method reported by Patton *et al* [25].

Electrochemical deposition was performed with a Parstat 2263 (Princeton Applied Research) instrument using PowerSuite software. All experiments were carried out using a three-electrode set-up where the ITO cover slip was used as the working electrode, Pt wire as the counter electrode and Ag/AgCl as the reference electrode. The use of electropolymerization techniques prevented the use of glass coverslips. A solution of the CTA (0.5 mM) and the supporting electrolyte, tetrabutylammonium hexafluorophosphate (TBAH) (0.1 M) in THF was used for preparing the electro-generated CTA film. Potentiostatic experiment was employed to deposit the CTA using a constant potential of 1.4 V for 240 seconds.

In a typical run, a solution of PEGMEMA (4945 mg, 16.48 mmol), AIBN (0.9 mg, 0.0055 mmol) and 25 mL of dry THF (for PEGMEMA polymerization) were degassed in a

Schlenck tube by bubbling with N_2 gas for 30-45 minutes. The degassed solutions were transferred to another Schlenck tube backfilled with N_2 gas containing the CTA-modified ITO cover slips through a cannula. The flask was placed in a preheated oil bath at 60 °C for 3 hours. The slides were then subjected to Soxhlet extraction overnight using THF as solvent to remove any unbound polymers.

5.3.4 Characterization of the Surface

The surfaces were analyzed by means of AFM, XPS, CV, and ellipsometry. The analyses of the surfaces are described in Appendix B.

5.3.5 Protein Labeling and Purification

Alexa Fluor® 555 succinimidyl ester (1 mg in dimethylformamide; Invitrogen Corp) was used to label a-lactalbumin (10 mg; Sigma-Aldrich) in 1 mL of 0.1 M sodium bicarbonate buffer, pH 7.4 to preferentially label the protein amine terminus rather than the ϵ-amino groups of the lysines, according to the manufacturer's protocol.

The reaction was incubated at room temperature for 1 hour under constant mixing, and stopped with 0.1 mL of freshly-prepared 1.5 M hydroxylamine, pH 8.5. The labeled protein was dialyzed against water for 24 hours and then against 10 mM Tris, 100 mM NaCl at pH 8 for 24 hours.

To ensure complete removal of the unincorporated fluorophore, PD-10 desalting columns and/or gel filtration chromatography was used. Gel filtration was carried out on a Pharmacia FPLC system using Sephadex 10/300 GL (GE Healthcare) with 10 mM Tris and 100 mM NaCl at pH8 as running buffer. The fractions with an estimated fluorophore-to-protein ratio of 1± 0.2 were used for the studies.

5.4 Results & Discussion

5.4.1 Single versus Multiple Species Analysis

Single-component diffusion algorithms are sufficient for describing dye diffusion near a glass interface. This is illustrated in Figures 5.2a and b for R6G and Alexa, respectively. As has been described previously [221], the cationic R6G dye exhibited Coulombic interactions with the glass while the anionic Alexa dye did not measurably interact with the surface. This can be seen in comparisons of the measurement close to and including the surface (0.5 μm, see section in Experimental describing geometry of focal volume) versus within the bulk solution (2.0 μm). However, analysis of experiments for the present interfacial measurements required a more sophisticated fitting algorithm, as discussed below.

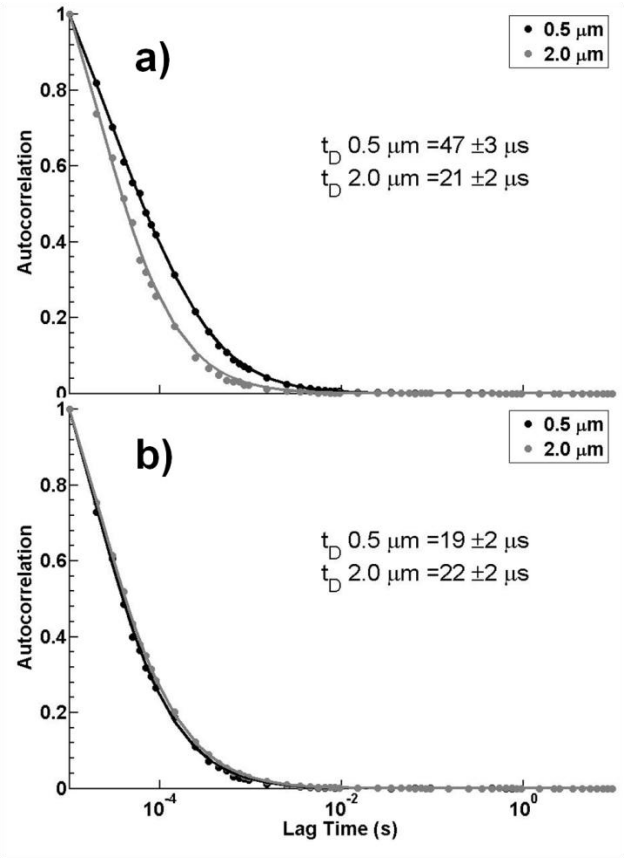

Figure 5.2: Single species averaged autocorrelation curves for R6G (a) and Alexa (b). Data sets from very close to the coverslip (0.5 μm, black) and far from the coverslip (2.0 μm, gray) are shown. The average diffusion times, with error, are also displayed. R6G displays an interaction with the surface; Alexa does not show any change in diffusion behavior near the surface.

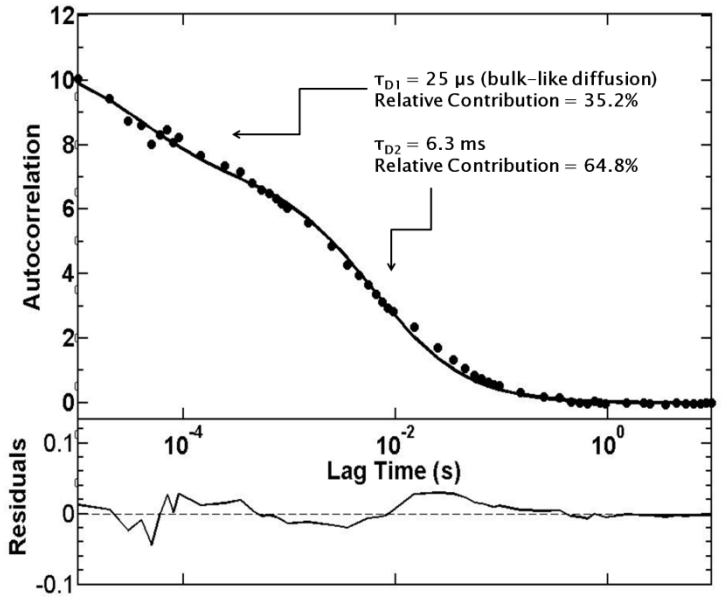

Figure 5.3: Example of an autocorrelation curve of R6G within linear PEG brush at depth of 1.0 µm fit with the two species equation. The filled circles represent the autocorrelation data and the line is the fit to the data, with residuals plotted below. The diffusion parameters show evidence of surface interaction in the significant contribution of the slow component, as compared to the bulk-like fast component (which was fit to the observed parameter of an aqueous solution).

5.4.2 Diffusion in the Presence of PEG

FCS was used to examine translational diffusion of free dyes in the presence of the linear PEG-functionalized surface depicted in Figure 5.1a. In these studies, the observed autocorrelation curves clearly indicate the presence of both free diffusion and a slower diffusion component. The two distinct diffusion regimes are obvious in the data analysis, as shown in Figure 5.3. Two-component analysis [136, 141] quantifies the fast component, which indicates free diffusion in bulk solution, and a slower component that indicates interaction between the dye and the PEG surface. The fast component was comparable to the measured diffusion constant for R6G in water. The characteristic bulk diffusion times were 21 ± 2 µs and 21 ± 3 µs for the hard (glass) and soft(PEGylated) surface measurements, respectively.

Hindered diffusion due to interaction with polymer brush-solvent interfaces has recently been attributed to coupling to surface polymer modes [222]. Other possible explanations include Coulombic forces between the dye and the PEG, and chemical

interactions such as hydrogen bonding or hydronium/hydroxide ion adsorption.[227] Distinguishing between each of these interactions was tested by following the relative contribution of surface diffusion in the confocal observation volume as a function of depth and altered solution chemistry. Thus, additional analyses were performed at various distances from the cover slip surface, as well as in different solution conditions, as discussed below.

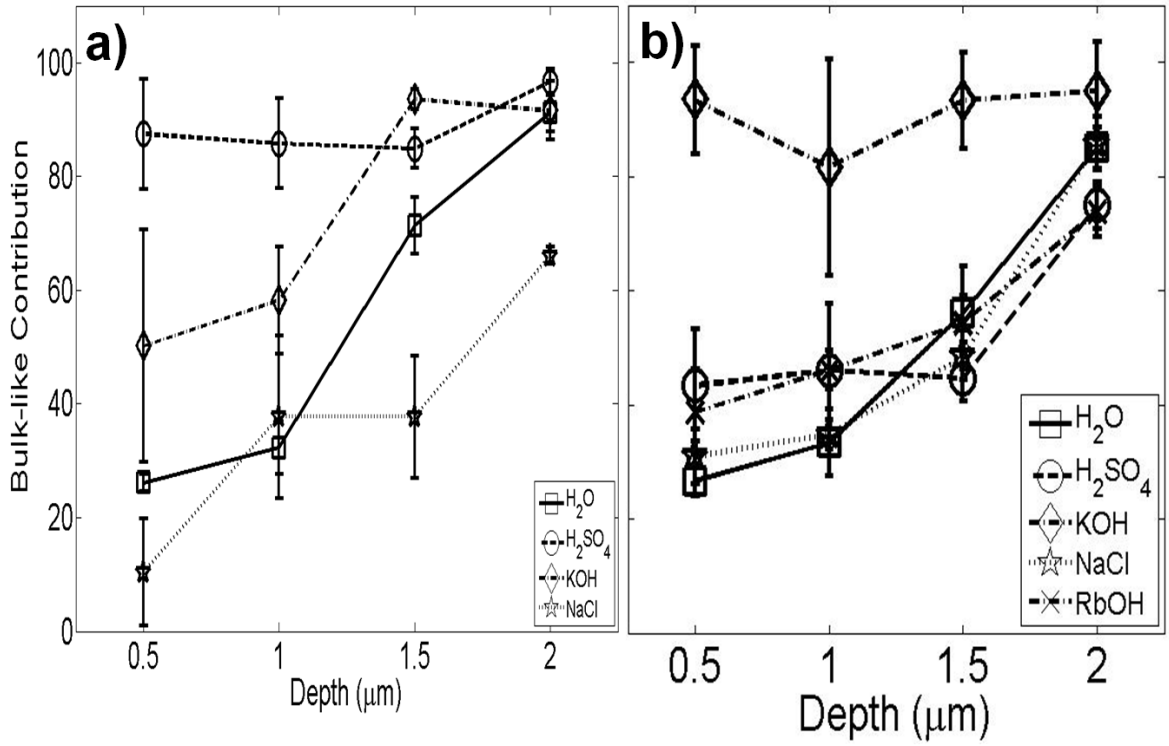

Figure 5.4: From the amplitudes of the autocorrelation curves of the data, the percent contribution of the fast, bulk-like component was determined. Here, we compare all values for all depths for R6G (a) and Alexa (b). It can be seen that an increase in the percentage of the bulk-like diffusion occurs as the focal volume shifts from the surface in nearly all cases. The lack of interaction in the acidic environment (pH 3, H_2SO_4) for cationic R6G and in the basic environment (pH 11, KOH) for anionic Alexa is shown by the high percentage of bulk-like diffusion at all depths. The aqueous (pH 6 MB water) and electrolytic (0.001N, NaCl) environments are unaffected. The same experiment was done for Alexa in an alternate base (pH 8, RbOH).The lines are included as a guide for the eye.

Depth-dependent measurements were performed using both cationic R6G and anionic Alexa dyes in neutral, aqueous solvent. As expected, the bulk-like contributions increased as the center of the focal volume was moved further from the surface (Figure 5.4). When

the observation volume includes the surface (0.5 and 1.0 μm), there is a large contribution of slow diffusion, whereas, further from the surface (1.5 and 2.0 μm), the interaction with the polymer is no longer apparent, as evidenced by the higher contribution of the bulk-like diffusion component. The changes are observed at distances further than the PEG brush thickness of 40 nm because of the geometry of the focal volume extends to include the polymer layer even when the center of the focus is above the thin-layer (focal height is ~1 μm; see Experimental Section). The long component is attributed to hindered diffusion. The presence of hindered and bulk diffusion is suggestive of sieve-like behavior of the linear PEG brush. Further experiments were performed to elucidate the nature of this sieve-like behavior.

The diffusion was studied in aqueous (pH 6.0, MB water), electrolytic (0.001N NaCl), basic (pH 11.0, 0.001N KOH; pH 8.0, 0.001N RbOH for Alexa), and acidic (pH 3.0, 0.001N H_2SO_4) conditions (Figure 5.4). The most striking observation is that acidic conditions most strongly decrease hindered diffusion of the cationic dye, (Figure 5.4a) whereas basic conditions most strongly decrease hindered diffusion of the anionic dye (Figure 5.4b). There are several possible explanations for the observed changes in diffusion characteristics. First, it is possible that changes to the PEG structure or chemistry are the primary force driving the observed surface interactions. Next, it is possible that changes to the dye structure or effective dye size are primarily responsible. Finally, Coloumb interactions could play a role. The elimination of surface interactions in acidic solution for R6G and basic solution for Alexa is strong evidence that the primary driving force is not changes in PEG structure, as any ionic effects on the neutral PEG brush would be the

reflected in similar fashion regardless of the identity of the dye probe at the concentration of the measurements [228-230]. However, the intermediate effects of KOH on the cationic dye diffusion (Figure 5.4a) suggest that PEG chemistry/structure does play some role. Another potential factor, the alternation of the dye chemistry due to photochemistry or diffusion behavior, can be ruled out because the dye absorption/emission spectra remain independent of pH over a large range [231-232]. An additional possible mechanism is the displacement of the native counterion of the dye. A larger counterion could explain the change in occurrence of hindered diffusion and is consistent with a sieve-like model for the PEG brush structure-function relationship.

The dyes, in the solution conditions that reduce PEG interactions, are solvated by different ions than in their native salt form. R6G is received as a chloride salt. The hydration shell of chloride is reported to be smaller than that of sulfate, with the radii reported as 5.79 and 5.76 Å, respectively [233]. However, since sulfate is a divalent ion, it will coordinate with two dye molecules, resulting in a hydrodynamic radius that is more than twice the size of the original salt. Thus, a larger coordination shell and resulting size exclusion are a likely explanation for the elimination of hindered diffusion in R6G under acidic conditions.

Alexa is received as a sodium salt; the potassium cation of the hydroxide is larger, as well. Computational studies have reported that the hydrated shell radii of sodium and potassium are 2.37 and 2.80 Å, respectively [234]. However, the relative size change of the newly complexed dyes cannot explain the observed results for Alexa because the use of the Rubidium hydroxide, with an even larger counterion, does not eliminate hindered diffusion

(Figure 5.4b). The strong size exclusion is limited to the KOH conditions. Additionally, some decrease in hindered diffusion in KOH conditions is observed with the cationic R6G dye (Figure 5.4a).

A more likely explanation for the slower diffusion rates in the presence of potassium ion is its complexation by PEG chains, which can act as pseudo-crown ethers, with an especially-tuned affinity for potassium ions [235-236]. This complexation can cause the PEG chains to shrink, thus excluding the dye from the PEG brush, and can be observed in the hydroxide measurements of both the dyes (Figure 5.4), but more dramatically with the Alexa dye. As mentioned above, experiments with another alkaline hydroxide, RbOH, confirm that the potassium hydroxide data are anomalous. Thus, the results on linear PEG brushes, in addition to earlier studies[69, 237-238], confirm that PEG brushes are not physical barriers. Instead, the results support a model wherein linear PEG brushes are permeable, comprise sieve-like structures with which solutes can interact, and that the extent of interaction can be controlled by either changing the solute size or changing the sieve size. The size exclusion hypothesis can be further tested using PEG dendrons, which allow controllable cavity spacing by the degree of branching of the polymer. An explanation of these findings follows.

5.4.3 Diffusion in the Presence of Varying Pore Sizes

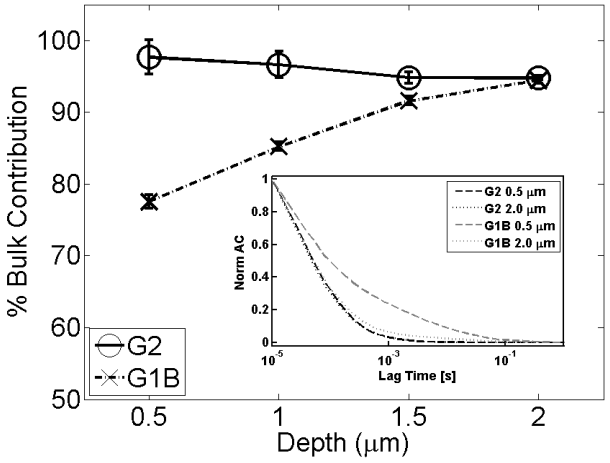

Figure 5.5: Comparison of the interaction of Alexa probe on G2 and G1B dendronized surfaces. The rising contribution of the fast, bulk-like species over the G1B dendron is indicative of the interaction of the probe with the surface. The lines are included as a guide for the eye. Inset features a comparison of the normalized autocorrelation curves for G2 and G1B dendrons at 0.5 and 2.0 um from the surface.

In these experiments, the PEGylated dendrons depicted in Figures 5.1b-e were used to test the hypothesis of size-dependent, sieve-like behavior for PEG brushes. Because R6G exhibits surface dependent diffusion and photophysics [221, 239-240], Alexa was chosen as the primary probe for these studies. Four generations of Janus-type linear-dendrons were analyzed. The ellipsometric thicknesses of each brush were 0.9, 1.4, 2.8, and 1.8 ± 0.1 nm for G0, G1, G2, and G1B, respectively. As the dendron generation proceeds from G0 to G2, the density of PEG on the surface decreases due to the spatial requirements of the carbazole on the surface; subsequently, the pore size increases. Theoretical calculations of the pore sizes of the dendritic PEGs have been calculated based on ellipsometric thickness and the MW of the molecules[21]. The grafting densities were 3.4, 2.4, and 1.3 molecules/nm^2 for the G0, G1, and G2 surfaces, respectively.

The amount of interaction of the probe with the PEG brush depends strongly on the relative packing densities of the PEG dendrons. The autocorrelation curves for all dendron systems are included in *the Supplemental Material (Figure S11).* It was found that as the dendron dimension increased from G0 to G2, and the brush density decreased, the probe dye exhibited correspondingly less interaction with the brush surface. This can be seen

from the amount of surface diffusion in the autocorrelation curves. The two extreme cases are compared in Figure 5.5, wherein the relative amounts of bulk-like diffusion of the G2 and G1B dendrons are shown. The Alexa dye showed no interaction with the G2 dendron, and considerable interactions with the G1B dendron. At all depths, diffusion over the G2 surface matches that of the probe in solution. This observation demonstrates that the least dense G2 dendron brush minimizes probe interactions with the surface. In contrast, the more dense G1B dendron brush exhibited strong probe interactions.

These results demonstrate clearly that, although the PEG chain structure might be preferred for biological applications because of its permeability to water and oxygen, its presence forms sieve-like pores, which can act as traps for diffusing molecules. This property might or might not influence anti-fouling efficacy, as in recent studies, the G2 dendron brush was found to exhibit anti-fouling behavior [223].

5.4.4 Permeability of Bottle Brush Polymer Surfaces

This notion of a sieve-like PEG structure was explored in a more extreme case, in which the bottle-brush PEG, illustrated in Figure 5.1f, was used as the substrate. The bottle brush polymer used in this study has recently been found to display antifouling properties[22]. However, this was measured after incubation, rinsing, and drying of the sample. In our case, we monitored the probe, Alexa, over a surface that had been freshly prepared ('untreated') with the dye solution versus a surface that had been allowed to incubate for 2 hours in water ('incubated'). The results can be seen in Table 1. The diffusion time of the 'incubated' sample is slower than that of the 'untreated' sample. This effect illustrates the strong interactions of the Alexa probe with the bottle-brush.

The extreme hydrophilicity of this system was apparent as the diffusion time of the Alexa probe was found to depend greatly on the exposure time of the sample to water. Our diffusion analyses, the results of which are summarized in Table 1, demonstrate an increase in permeability with exposure time. An increase in permeability as a result of incubation seems to be in contrast with a recent study in which a decrease in protein adsorption was observed for brushes of similar architecture after incubation of the sample [241]. There are two possibilities for the decrease in protein adsorption with surface treatment. One is the possibility that the decrease in adsorption occurred because of the vacuum treatment of the surface in these experiments. Under vacuum conditions, the forced collapse of the polymer may interfere with its preferred architecture. Incubation then allows the polymer to return to its native configuration. In our case, allowing the surface to remain in solution results in added hydration of the brush and possible reorientation of the PEG sidechains. This more flexible, hydrated structure provides more opportunity for the molecules to diffuse through the polymer and interact with the surface. These results show that the methods of measuring protein adsorption do not give a complete picture of the interaction of molecules with a surface. The second possibility is size-exclusion of the proteins from the dense surface, which is discussed below.

Condition of Sample	Slow Component Diffusion Time
Untreated	46 ± 4 μs
Incubated	1.2 ± 0.8 ms

Table 5.1: The diffusion times of the Alexa probe in the untreated and incubated samples. The marked slowing of the probe in the incubated environment illustrates the permeability of the bottle brush polymerized surface.

5.4.5 Protein-PEG Interactions

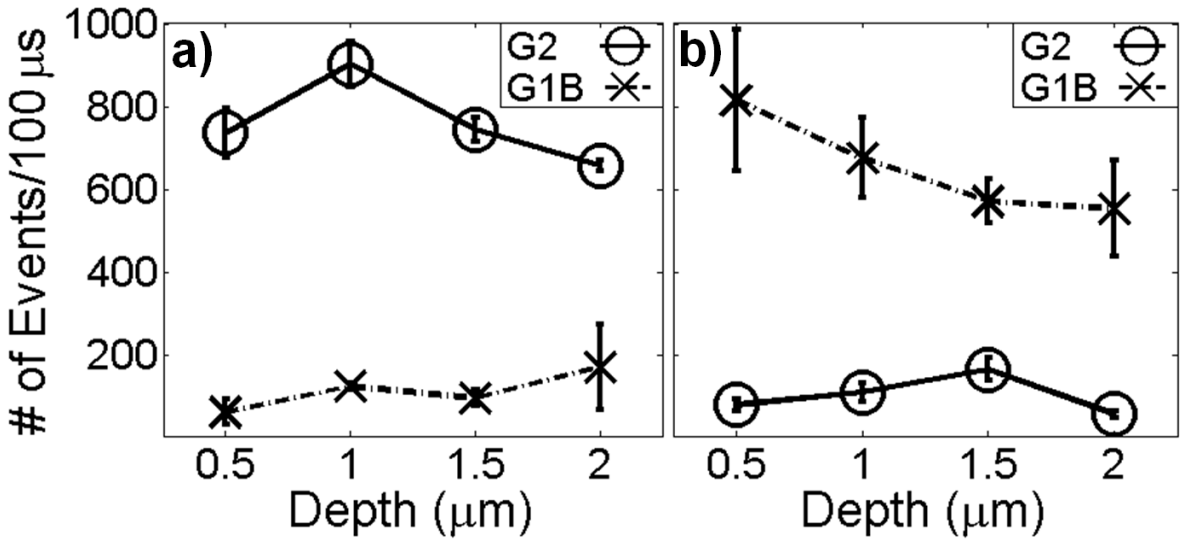

Figure 5.6: Single molecule blip frequency analysis of the Alexa-labeled α-lactalbumin (a) and free Alexa dye (b) diffusing over the G2 and G1B dendronized surfaces. The error bars for each point reflect reproducibility from multiple experiments. For the protein sample, a nearly ten-fold increase in the number of events was observed near the less-dense G2 surface as compared to the more-dense G1B surface. For the free dye sample, the opposite trend was observed. The lines are included as a guide for the eye.

The dendrons that resulted in interaction (G2, Figure 5.1d) and exclusion (G1B, Figure 5.1e) of the organic dye probe (Figure 5.5) were tested with Alexa-labeled α-lactalbumin. The recovered characteristic diffusion times were 636 ± 90 µs and 161 ± 64 µs over the G1B and G2 surfaces, respectively (data not shown). The protein diffuses more slowly than the organic dye, as expected because of its larger size. However, the diffusion times obtained by FCS suggest that the protein exhibits the opposite trend in surface interactions with the two dendron brushes than that observed with the smaller dye probe.

To further assess the permeability of the surfaces, a single molecule blip frequency analysis was performed. Our diffusion data are collected in the time domain, which allows multiple analyses of the trajectories, such as single event (blip) frequency, intensity, and

duration values. Figure 5.6 displays the average number of events (with standard deviations over three samples) obtained for each acquisition period (trajectories binned up from 10 μs to 100 μs) as a function of distance from the dendronized coverslip surface for the dye-labeled protein (Figure 5.6a) and the free dye (Figure 5.6b). In the absence of any interactions between the dendron-treated surfaces and the probes, the frequency of observed events should be constant regardless of the measurement position, because it reflects the probe concentration, which was constant for the two samples. Blip frequency analysis of the Alexa-labeled α-lactalbumin (Figure 5.6a) reveals an order of magnitude higher event frequency near the linear G2 brush surface as compared to near the branched G1B brush surface. This indicates that the concentration of protein is higher near the less-dense G2 surface than near the more-dense G1B surface. In direct contrast, similar analysis of the free Alexa dye (Figure 5.6b) reveals the opposite trend, and thus indicates a higher dye concentration near the G1B surface than near the G2 surface.

Further experiments are underway to assess possible ionic, hydrophobic, and any additional interactions modulating the protein-brush system. In the interim, however, it is possible to make some preliminary assessment of the driving-forces. Because both the Alexa-dye and the Alexa-labeled α-lactalbumin are negatively charged under the measurement conditions, it is unlikely that charge-charge interactions are responsible for the opposite trend in interaction with the dendronized surfaces. It seems likely that the difference lies in size-exclusion effects. The G2 dendronized surface offers larger pores with space between the PEG chains, thus allowing the protein to penetrate into and interact with the brush. The smaller free Alexa dye can freely diffuse into and out of the brush. The

G1B dendronized surface presents smaller pores, thus excluding the larger protein but trapping the smaller dye. The strong protein-G2 interaction, combined with recent results that demonstrate the increased protein anti-fouling properties of the G2 brush [223], together highlight that anti-fouling properties do not necessarily correlate with exclusion. These experiments further support the sieve-like properties of PEG and illustrate how the degree of permeability is dependent upon both the density of the chains on the surface and the size of the diffusion species. These experiments also illustrate that surface engineering can combine the attributes of these properties to produce an optimum surface for advanced functional surface applications.

5.5 Conclusions

We have measured the diffusion of cationic and anionic dyes in a variety of PEG structures. Both the cationic and the anionic dyes show a fast and slow component in the autocorrelation analysis. The slow component is evidence of the dye interacting with the polymer. These experiments reveal evidence of PEG pseudo-crown ether behavior in the presence of K, which can be seen in reduced interaction of the dyes with the PEG brush. Additionally, these experiments performed in multiple conditions prove that the PEG brush is permeable. We have also observed what we hypothesize to be size exclusion effects when allowing the dyes to exchange their native counterion for a larger one. In these instances, the dyes with larger hydrodynamic radii are excluded from interaction with the linear PEG. We have varied the pore size of the polymer at the surface with PEG dendrons and observed that density of PEG is also an important parameter. Overall, we found that there is a strong relationship between the probe size, mobility, and density of PEG on the

surface. Small probes get trapped by highly dense PEG architectures and exhibit interactions with moderately dense architectures. Large probes readily interact with sparsely populated PEG surfaces and are excluded from dense PEG architectures. The dendrons measured in this work offer the ability to vary both pore size and PEG density which allows fabrication of tunable surfaces.

5.6 Acknowledgements

The authors would like to thank Roderick Pernites of the Advicula group at University of Houston for his initial characterization work. The Welch Grant E-1264, as awarded to Richard Willson, supported the protein work. C. Landes thanks the Norman Hackerman Welch Young Investigator Program at Rice University. The NSF CBET-0854979 as awarded to Rigoberto C. Advincula, supported the PEG linear-dendron synthesis and studies. Acknowledgment is also made to the Donors of the American Chemical Society Petroleum Research Fund for partial support of this research.

Chapter 6

Fluorescence Correlation Spectroscopy Study of Protein Transport and Dynamic Interactions with Clustered-Charge Peptide Adsorbents

6.1 Abstract

Ion-exchange chromatography (IEX) relies on electrostatic interactions between the adsorbent and the adsorbate, and is used extensively in protein purification. Conventional IEX utilizes ligands that are singly charged and randomly dispersed over the adsorbent, creating a heterogeneous distribution of potential adsorption sites. Clustered-charge ion exchangers exhibit higher affinity, capacity, and selectivity than their dispersed-charge counterparts of the same total charge density. In the present work, we monitored the transport behavior of an anionic protein near clustered-charge adsorbent surfaces using Fluorescence Correlation Spectroscopy. We can resolve protein free diffusion, hindered diffusion and association with bare glass, agarose-coated, and agarose-clustered peptide surfaces, demonstrating that this method can be used to understand and ultimately optimize clustered charge adsorbent and other surface interactions at the molecular scale.

6.2 Introduction

Chromatographic separation of proteins is a ubiquitous processing step in both

pharmaceutical manufacturing and basic research applications. Ion-exchange chromatography (IEX), which relies on electrostatic interactions between charged adsorbents and protein molecules, is the most widely used chromatographic protein purification process [242] IEX can separate mixtures of biomolecules with high selectivity, including molecules with small differences in charge [64, 243-245]. Conventional IEX utilizes ligands that are singly charged and randomly dispersed over the adsorbent [243] creating a landscape of widely varying charge density, including isolated charges not expected to contribute to adsorption, and randomly-created patches of high local charge expected to dominate adsorption [246]

We previously showed that immobilizing charges in uniform groups creates "clustered-charge ion exchangers" which are more effective than their dispersed adsorbent counterparts with the same total charge density [64, 244] Specifically, clustered-charge adsorbents exhibit enhanced affinity and capacity of protein adsorption and greater selectivity in favor of proteins with patches of high local surface charge density. In related work, it was also demonstrated that a polymer brush with embedded cationic patches can sharply separate proteins with similar numbers of charges [247] Thus, clustered-charge adsorbents show promise for improving the purification of charged biomolecules.

IEX has been combined with confocal microscopy to characterize adsorption behavior on the macroscopic level [248-251] and the adsorption of dye molecules on silica chromatographic substrates on the single molecule level [252] Theoretical modeling has also been applied to the study of these systems [253] The investigation of IEX with realistic protein adsorbates at microscopic levels, however, has yet to be performed. Monitoring ion-

exchange adsorption at the single-molecule level includes interactions and dynamics of the probe molecule with the functionalized surfaces and in bulk solution [66, 254-258]

In order to understand and optimize IEX at the single molecule level, several experimental hurdles must be overcome. First, it must be possible to prepare, label, and isolate adsorbates for analysis at a purity that is appropriate for single-molecule scale experiments. Next, it is necessary to monitor and tune transport of the analyte to the IEX matrix. Finally, it is necessary to minimize or eliminate unwanted nonspecific interactions and to differentiate between them and the desired specific interactions. The first component, the preparation and characterization of single-molecule quality agarose and peptide-functionalized agarose substrates, is detailed in the Experimental section. The remainder of the current work as described below demonstrates the achievement of the latter two of these pre-requisite steps on the path towards the single-molecule study of protein chromatographic separation.

We have used fluorescence correlation spectroscopy (FCS) to probe the dynamics and interactions of various probe molecules with hard and soft surfaces [122, 170, 221, 259] In particular, we have shown that it is possible to position the ~2 μm high confocal Gaussian beam to span the solid-liquid interface using a piezo-electric positioning stage, such that hindered diffusion due to interfacial effects can be distinguished from free diffusion. Using this technique, in combination with single-molecule imaging and analysis algorithms, we can resolve and differentiate between nonspecific and specific interactions of the protein with the functionalized surface. These dynamics are important in understanding and optimizing the microscopic processes underlying chromatographic performance.

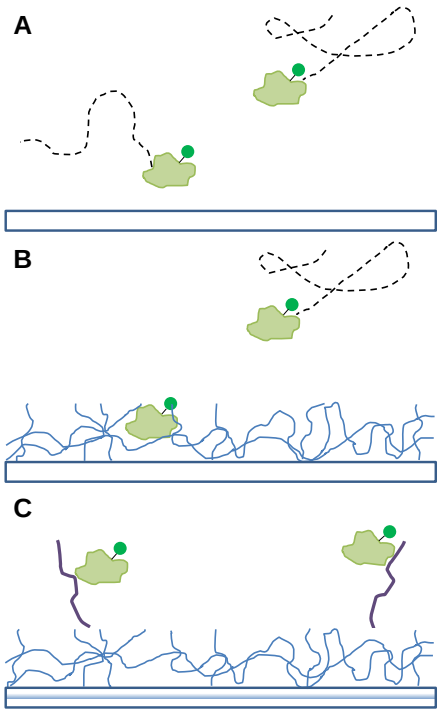

Figure 6.1: Cartoon depiction of the dye-labeled protein diffusing over the three surfaces used in this work. Bare glass surface (A), agarose-coated surface (B), peptide- functionalized surface (C).

The dynamics of single molecules of Alexa Fluor 555 ® (Alexa 555) dye and Alexa 555-labeled α-lactalbumin protein were studied above glass (Figure 6.1A), spin-coated agarose thin films (Figure 6.1B), and cluster-charged peptide (penta-argininamide)-functionalized agarose surfaces (Figure 6.1C). We monitored the interactions of the anionic protein with the anionic glass support, the agarose support matrix and the cationic anion-exchange ligands. Using free Alexa 555 dye as a reference, the hindered diffusion of single molecules of the Alexa 555-labeled protein in the presence of the clustered-charge ligands was quantified. Our ability to resolve protein free diffusion, hindered diffusion and association with the surface demonstrates that this method can be effectively used to characterize clustered-charge IEX at the single-molecule scale.

6.3 Materials and Methods

All chemicals were obtained from Sigma-Aldrich unless otherwise noted. Much of the experimental methodology has previously been reported [64, 122, 170, 221, 244, 259]

6.3.1 Agarose Surface Preparation

All solutions were prepared with DI water unless otherwise noted. No. 1 glass slides (VWR, 22 x 22 mm) were cleaned in a TL1 solution (4% (v/v) H_2O_2 (Fisher Scientific) and 13% (v/v) NH_4OH) at 80 °C for 90 seconds and then plasma cleaned in O_2, on medium

power, for 2 min (Harrick Plasma, PDC-32G). Silicon templates (Grace Biolabs) were placed on the slides and 1 mL of hot 1% (w/w) agarose solution (US Biological) was spun onto the slides at 2000-3000 rpm (Model WS 400A 8NPP/Lite spin coater, Laurell Technologies Corp.). To immobilize the peptide, agarose surfaces were activated with aldehyde groups by treating the surfaces with 20 mM $NaIO_4$ for 30 min as described in Afanassiev et al. [260] After washing with DI water and drying with He gas, the activated surfaces were treated with a 5 nM solution of the penta-argininamide peptide (Biomatik, NH_2-GGRRRRRamide; the amide form of the peptide was used to eliminate the negative charge on the C- terminus as previously described [261-262]) in coupling buffer (100 mM Na_3PO_4 (EM Science), 150 mM NaCl (Mallinckrodt Chemical), pH 7.2). The peptides were immobilized on the surface with several drops of 20 mM $CNBH_4$ (Pierce, diluted in 25% EtOH / 75% PBS) at 4 °C for 30 min. Excess uncoupled peptide was removed by rinsing with coupling buffer, and unreacted aldehyde sites were reduced with 66 mM $NaBH_4$ (in 25% EtOH / 75% PBS) at 4 °C for 5 min. The surfaces were finally rinsed gently with DI water and stored at 4˚C, if not used immediately.

6.3.2 Fluorescence Labeling of α-Lactalbumin

Labeling was done according to the manufacturer's protocol. Alexa 555 (max abs/em 555/565 nm) succinimidyl ester was dissolved in dimethylformamide at a concentration of 10mg/ml and 0.1ml of dye solution was slowly added to 1ml of 10 mg/ml Ca^{2+} depleted α-lactalbumin (Figure 6.2) dissolved in 0.1 M $NaHCO_3$ buffer, pH 7.4 , to preferentially label the protein amine terminus rather than lysine ϵ-amino groups [263] Initially, the protein was labeled with Tetramethylrhodamine isothiocyanate (TRITC) dye (max abs/em: 540/580nm, as shown in Fig 5). However, Alexa replaced TRITC due to higher photostability and brightness of the Alexa Fluor® dyes [232] The reaction was incubated at room temperature for 1 hour under constant mixing, and stopped with 0.1 mL of freshly-prepared 1.5 M hydroxylamine, pH 8.5. The labeled protein was dialyzed against water for 24 hours and then against 10 mM Tris and 100 mM NaCl at pH 8.0 for 24 hours. To ensure complete removal of the unincorporated fluorophore, PD-10 desalting columns and/or gel filtration chromatography was used. Gel filtration was carried out on a Pharmacia FPLC system using Sephadex 10/300 GL (GE Healthcare) with 10 mM Tris and 100 mM NaCl at pH 8.0 as running buffer. The fractions with an estimated fluorophore-to-protein ratio of 1 ± 0.2 were used for the studies.

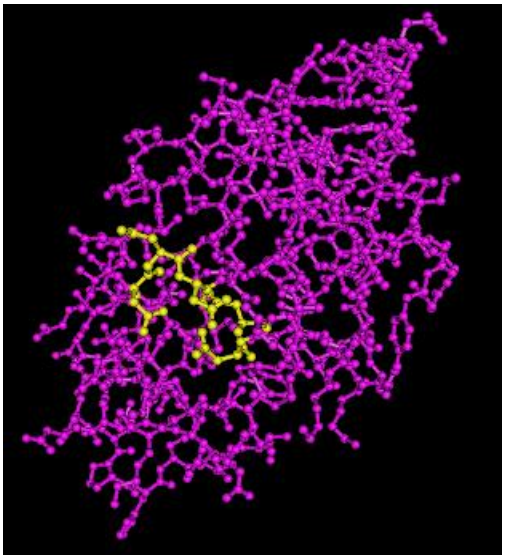

Figure 6.2: Structure of $Ca2^{+}$ depleted -lactalbumin with five aspartate residues highlighted in yellow shown using Cn3D 4.1 viewer. This region of -lactalbumin with a large number of aspartate residues, which forms a cluster of negative charge, has been shown to be the binding site of the calcium ion.

6.4 Results and Discussion

6.4.1 Agarose Surface Characterization

Ellipsometry (M-2000 ellipsometer, J.A. Woollam) was used to determine that the agarose and peptide-functionalized agarose surfaces were 88.6 ± 1.9 nm thick using the Cauchy dispersion model for transparent media. This makes the thin film 5% of the FCS beam height. To confirm the successful immobilization of the peptide and to check the heterogeneity of the substrate, we used a BODIPY 650-labeled peptide (K(BODIPY650)GGRRRRR-amide) immobilized on the agarose matrix as described above.

Figure 6.3 shows a scanning confocal image of the dye-labeled peptide-functionalized agarose surface. The image confirms the successful immobilization of the clustered peptides, the efficiency of washing of the agarose surface post immobilization, and control of cluster density for single-adsorbate analysis. The characteristic inter-peptide spacing was calculated to be approximately 1 µm.

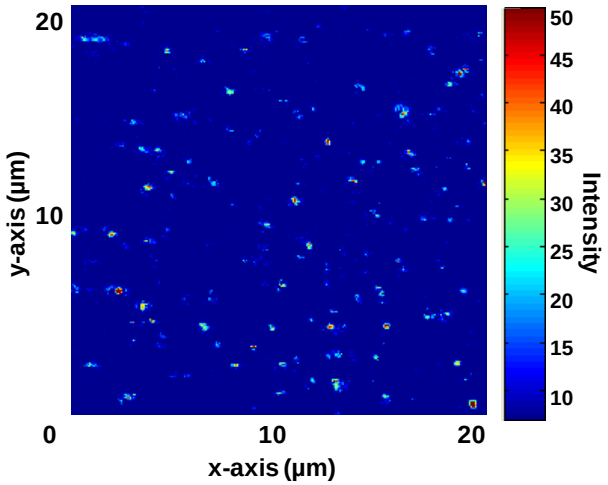

Figure 6.3: 20x20 µm image of BODIPY650-labeled peptide-agarose slide. Continuous scanning confirmed single-state photobleaching, implying that the bright features arise from single-dye labeled peptide molecules. The average inter-peptide spacing is 1 µm,

It was also necessary to characterize the presence of any detectable background fluorescence from the agarose film or peptide adsorbents, and to determine if there was significant nonspecific protein adsorption to the agarose support. This was achieved by scanning confocal imaging of the agarose support, with and without peptide

functionalization, in the presence and absence of TRITC-labeled α-lactalbumin. The results are shown in Figure 6.4A-D, in which it is demonstrated that there was negligible fluorescence background from the agarose support and that there was negligible nonspecific protein adsorption. In particular, protein adsorption was only observed to occur when the agarose support was functionalized with peptides.

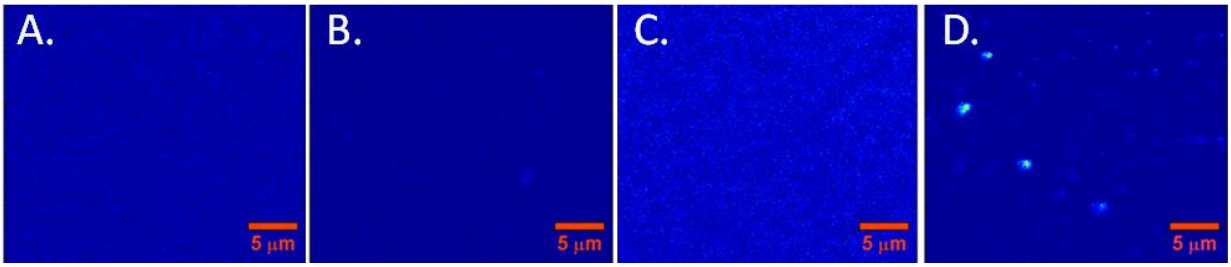

Figure 6.4: Scanning confocal images of: A) agarose film on glass, showing that agarose itself is not fluorescent at our excitation/emission conditions (532 nm/633 nm); B) agarose functionalized with penta-argininamide peptide charge clusters, showing that peptide immobilization does not introduce fluorescence; C) agarose with flowing TRITC-labeled α-lactalbumin in solution, showing distributed background fluorescence of flowing protein, but no localized adsorption events; D) agarose with peptide clusters after flowing TRITC-labeled α-lactalbumin in solution, showing discrete protein adsorption events.

6.4.2 Diffusion of protein and free dye over treated surfaces

In Figure 6.5, diffusion coefficients extracted from autocorrelation analysis are compared for free Alexa 555 dye (top panel) and Alexa 555-labeled α-lactalbumin (bottom panel) over glass, agarose, and penta-argininamide-functionalized agarose surfaces both in the bulk solution and near the surface. We observed that the anionic Alexa 555 dye exhibits no interaction with the anionic glass surface (Figure 6.5A), since the measured diffusion coefficients are identical whether the confocal observation volume included the surface or was centered in the bulk solvent. This is expected, as we have previously reported that the anionic Alexa 555 shows negligible nonspecific interactions with anionic glass surfaces, in contrast to the commonly used cationic probe Rhodamine 6G [221, 239-240] As

expected, the mobility of the dye is greatly reduced upon conjugation to α-lactalbumin (Figure 6.5D), which has a much larger hydrodynamic radius [264] However, that comparable bulk and interfacial diffusion coefficients for the Alexa 555-labeled α-lactalbumin indicates that there are negligible weak non-specific interactions between the protein and the glass surface, as was observed for the Alexa 555 alone.

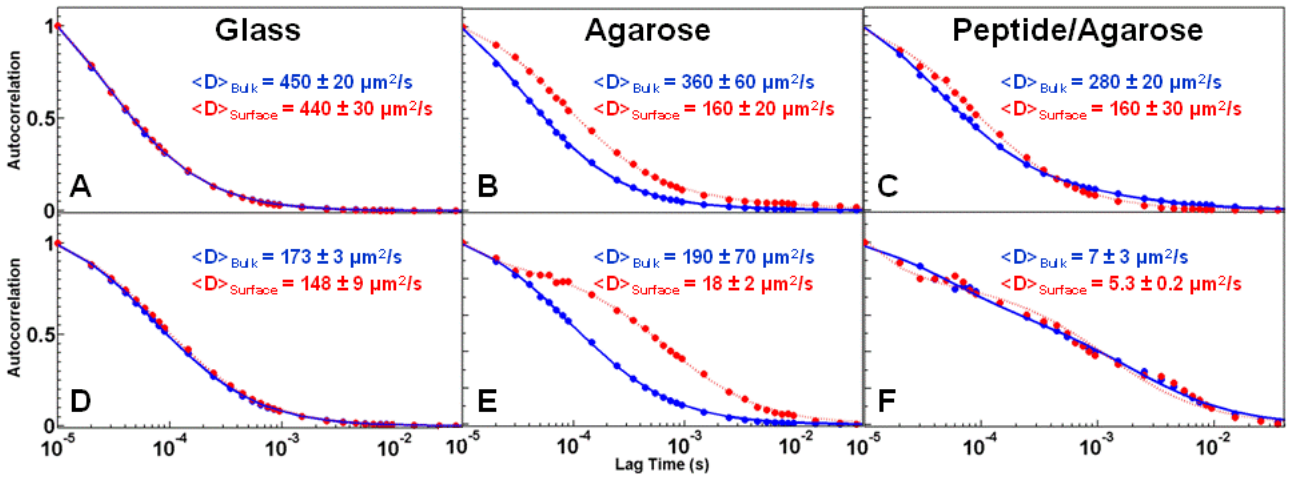

Figure 6.5: Autocorrelation curves for Alexa 555 (top; A-C) and Alexa 555- labeled α-lactalbumin (bottom; D-F). The measurements were taken over glass (A, D), agarose (B, E), and penta-argininamide aldehyde agarose (C, F) surfaces. The measurements were taken with the confocal observation volume focused either in the bulk solution (blue) or including the surface (red) in 10 mM Tris-HCl, 10 mM NaCl, pH 8.0 at 22.1°C.

As expected, both Alexa 555 and Alexa 555-labeled α-lactalbumin exhibit free diffusion when the confocal observation volume is focused in the bulk solution, far from the agarose-functionalized surface (Figures 6.5B and E, respectively; blue). When the observation volume includes the agarose-functionalized surface, however, both Alexa 555 and Alexa 555- labeled α-lactalbumin exhibit marked decreases in measured diffusion coefficients (Figures 6.5B and E, respectively; red). This indicates that the diffusion of both analytes is hindered by the agarose support; the protein was hindered more strongly, likely because of its larger size.

The observed hindered diffusion could be caused by steric, electrostatic, and

chemical contributions. First, agarose is known to form relatively large pores that can range from 9 to 90 nm in size [265-266] As we have recently shown, soft porous substrates can form sieve-like structures that sterically hinder the diffusion of probes such as dyes and proteins via hydrostatic effects [259] Other proposed steric interactions that have been identified by FCS include coupling to higher-order polymer vibrational modes [222] Thus, the overall effect of steric interactions would be to decrease solute mobility near, on and inside the porous substrate, which is consistent with the observed effects. Electrostatic interactions would be expected to yield repulsive forces between the anionic probes and slightly negatively charged agarose substrates. Repulsive forces (in contrast to attractive electrostatic interactions) would not cause a decrease in mobility, as observed here. Instead , repulsive forces would cause a decrease in surface concentration, as we have demonstrated via single event analysis and will discuss later in the manuscript [221] Finally, it is possible that the protein's hindered diffusion could result from hydrogen bonding between the protein and the support matrix [267-268] This type of behavior has been observed with lysozyme, which is structurally similar to α-lactalbumin [269-270] Single molecule imaging, and the extensive successful practical use of agarose-based adsorbents, offer strong evidence that there are only negligible nonspecific chemical interactions between the protein and agarose. Thus, based both on our experimental analysis and on our more detailed recent study of sieve-like behavior of porous soft interfaces [259] we believe that the primary contributor to the modification of protein mobility in agarose is steric interactions.

That we observe steric interactions between the agarose surface and both Alexa 555 and Alexa 555- labeled α-lactalbumin protein analytes contradicts an earlier study in which

minimal steric surface interactions were observed when Fluorescence Recovery After Photobleaching (FRAP) was used to measure diffusion coefficients for α-lactalbumin interacting with 2% agarose [271] There are several possible explanations. First, uncertainties in laser beam dimensions in FRAP experiments could lead to misrepresentation of diffusion coefficients and hydrodynamic radii. In contrast, the current work employs a characterization of the confocal beam dimensions as part of every measurement to ensure that accurate confocal beam dimensions are used in calculating diffusion coefficients [122, 142, 170, 221, 259] Next, the present measurements employ a piezoelectric sample stage with nanometer stability precision for accurately (and reproducibly) positioning the confocal observation volume with respect to the thin supported film. As these and other depth-dependent measurements clearly demonstrate [221] only by accurately overlapping the center of the Gaussian focal volume with the thin supported film is it possible to quantify the small contributions from surface interactions (see Methods section for discussion on focal volume). As demonstrated in Figure 6.5, if the measurement is performed in the bulk of the solution (and away from the surface), bulk diffusion dominates the signal, and surface interactions are negligible. Finally, because the FRAP study employed 2% agarose, the smaller pore size, relative to that in the 1% agarose use in the present work, would further exclude the dye and protein analytes and perhaps minimize the observable effects of surface interactions.

Anomalously slow diffusion, which is evidence of long-lived association interactions between the α-lactalbumin and the surface, is observed with the penta-argininamide - functionalized agarose surfaces (Figure 6.5F). The corresponding dye control, in which

only hindered diffusion is observed with the Alexa 555 probe, is shown in Figure 6.5C. A further control, in which association-induced anomalous diffusion is demonstrated to occur only at discrete positions on the sparsely peptide-functionalized agarose surface, is discussed below. The slow fitted diffusion coefficients, and the dominance of these events in the detected signal, even when the beam has been moved into the solvent, are indicative of association events [221] When long-lived interactions are the predominant phenomenon, these events dominate the autocorrelation decay curves, even when measuring further away from the surface. This results from the nature of FCS phenomenology, and is discussed in previous work [142]. The anomalously long extracted diffusion coefficient indicates long-range Coulombic interactions between the cationic charge-clustered penta-argininamide and the anionic probe molecules, and is consistent with previous work on the adsorption of proteins on penta-argininamide clustered-charge adsorbents [64] Future efforts will employ single event analysis to extract association/dissociation constants under conditions relevant to practical separations, as demonstrated previously [221]

6.4.3 Heterogeneity of the Agarose Surface

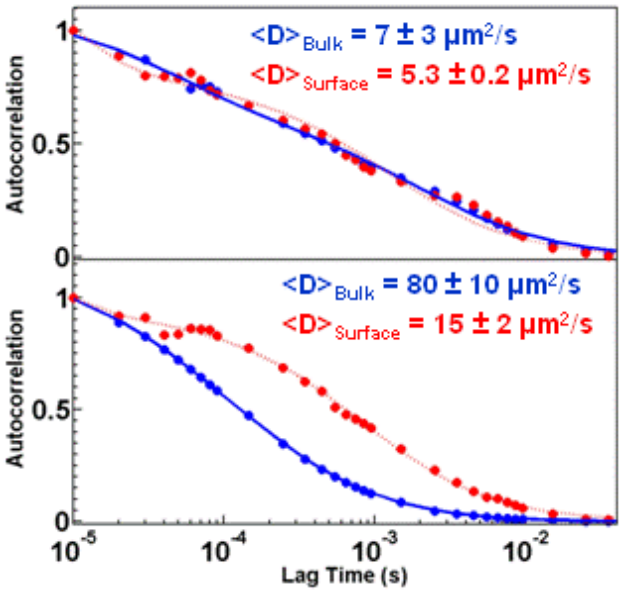

Figure 6.6: Autocorrelation curves for α-lactalbumin at different locations on a peptide functionalized agarose surface measured in the bulk (blue) and at 0.5 μm from the surface (red). Measurements at certain locations on the same sample indicate only nonspecific interactions dominate transport phenomena (top panel). Measurements at other locations indicate strong interactions between the protein and the peptide-functionalized agarose surface (bottom panel).

We would expect the slowest diffusion component, which we assign to protein-peptide associations, to be a localized observation. This is because the inter-peptide spacing is approximately 1 μm, and because the confocal beam radius is approximately 215 nm, and therefore the peptide spacing is sparse enough to differentiate between agarose-hindered diffusion and peptide association-induced anomalous diffusion on the same sample. This is demonstrated in Figure 6.6, in which anomalous diffusion, indicating association events, is only observed at certain positions on the sample, as would occur when the observation volume overlaps a penta-argininamide-functionalized region. By moving to other portions of the same sample, it is possible to extract the same hindered diffusion data as would be expected if the protein were only above the bare agarose surface.

6.4.4 Protein-Peptide Interactions

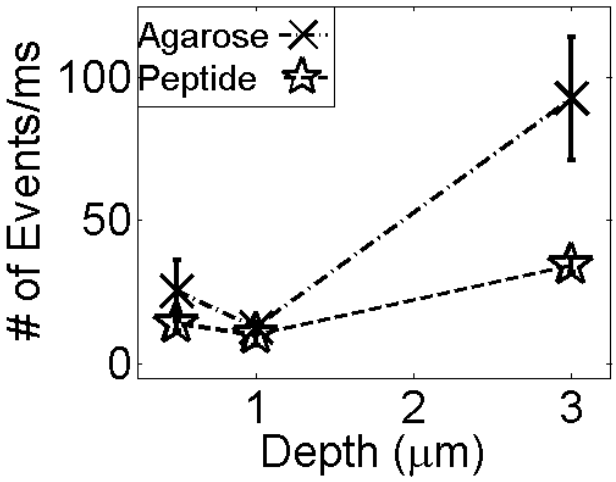

Figure 6.7: Single molecule blip frequency analysis of the Alexa 555-labeled α-lactalbumin diffusing over the agarose and peptide-functionalized agarose surfaces. The spread in intensity values for each point reflects reproducibility from multiple experiments. The negatively charged agarose repels the protein as shown by a smaller number of events near the surface as compared to the measurements in the bulk. The lines are included as a guide for the eye.

We also used single-event frequency analysis to characterize repulsive interactions between probes and surfaces, which are more difficult than attractive interactions to assess with traditional FCS analysis. Repulsion is important, however, because it is the competition between specific adsorptive attractions and non-specific desorptive repulsive interactions, tuned with various elution buffers, that controls separation efficiency and resolution. We successfully demonstrated that it is possible to study repulsive interactions using single event (blip) frequency analysis of single events in which a dye-labeled analyte diffuses into the observation volume, is detected, and diffuses out again. Figure 6.7 displays the average number of events (with standard deviations over three samples) obtained for each acquisition period (trajectories binned up from 10 μs to 1 ms) as a function of distance from the surface for the dye-labeled protein over both agarose and penta-argininamide functionalized agarose surfaces. Whereas the relative number of observed fluorescence events is constant (within the measurement error) at all distances from the peptide-functionalized surfaces, there were fewer detected fluorescence events near the pure agarose surface than in the bulk solvent. As discussed above, it is important

to note that any detection of surface interactions far from the surface results from the nature of the confocal excitation volume (as discussed above), rather than from long-distance persistence of surface interactions.

The blip frequency analysis in Figure 6.7 clearly demonstrates a decrease in the number of diffusion events close to the surface for the protein-agarose system. This would be expected in a system in which electrostatic repulsion, in the absence of specific binding, causes a decrease in concentration near the support. The Coulombic repulsion between the like-charged protein and agarose resulted in a decreased number of events (and thus adsorbate concentration), closer to the surface.

With the peptide functionalized surface, the effects are less dramatic, as there are also attractive forces between the penta-argininamide and the protein, in addition to nonspecific repulsive forces. In the presence of the ligands, the protein has a higher probability of staying close to the surface. This is not seen in an overall increase in the number of events close to the surface, however, because the proteins are inclined to stick to the ligands, which restricts the diffusion and lowers the number of pure diffusion events observed. Even so, due to the heterogeneity of the surface (Figure 6.6), there is still a probability that the proteins will be repelled from the surface into the bulk. This probably accounts for the slight increase in the number of events of the peptide-agarose surface moving from near the surface to the bulk solution, and also for the greater variability in the number of detected events close to the peptide-functionalized surface.

6.5 Conclusions

We have demonstrated the feasibility of each of the separate steps required for

characterizing protein ion-exchange separations on a single molecule scale. We have prepared clustered-charge functionalized surfaces that show definite electrostatic interaction versus bulk diffusion. We have shown that it is possible to distinguish between free diffusion, hindered diffusion resulting from steric interactions with the interface, and electrostatic association. The benchmarks presented here for sample preparation and analysis will allow us to understand and optimize the clustered-charge ion exchange parameters at the molecular scale in future experiments.

6.6 Acknowledgements

Support for this work was provided by the National Science Foundation and the National Institutes of Health.

Chapter 7

Strong Affinity of Anionic Dye to pH Responsive Material Probed by Traditional and Scanning FCS

7.1 Abstract

The present work reports on observations of the interaction of cationic and anionic organic dye probe molecules with a poly(2-(dimethylamino) ethyl-methacrylate) (PDMAEMA) brush architecture at basic and acidic pHs. Traditional and scanning Fluorescence correlation spectroscopy (FCS) were used to examine the nature and extent of probe-polymer interactions. The data support observations of strong Coulombic interactions between the anionic probe and the brush in an acidic environment. The probes are also found to have a preferential affinity for the brush. These results, and the responsive properties of the PDMAEMA brush employed in this work, contribute to the basic understanding of transport in external stimuli responsive materials for tunable surfaces.

7.2 Introduction

The present work reports on observations of the interaction of various probe molecules with surfaces polymerized with stimuli responsive polymers, namely poly(2-(dimethylamino) ethyl-methacrylate) (PDMAEMA). Recently, interest in and usage of switchable polymers has risen. Materials that have the ability to sense changes in properties such as temperature, pH, and/or ionic concentration are especially desirable for

varied applications.[5, 7-13] The weak polyelectrolyte PDMAEMA has potential to be used in a variety of surface preparations due to its response to pH and temperature[6, 13, 16]. Other applications include diagnostics and controlled drug delivery.[272-274]

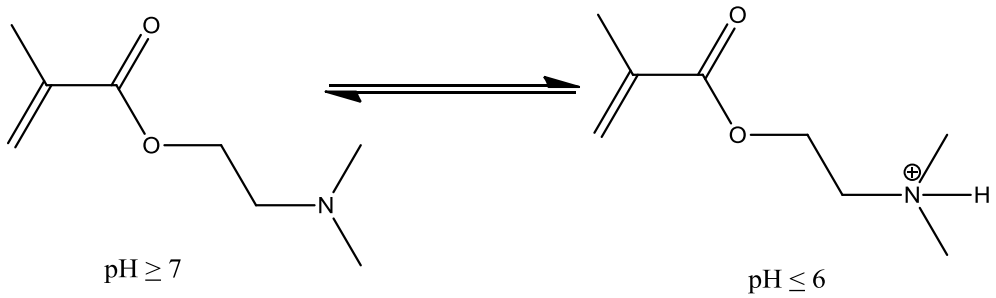

Figure 7.1: Schematic of the unprotenated (l) and protenated (r) DMAEMA monomer with corresponding pH conditions.

Due to the potential for use in switchable applications, and because of the relationship between structure and function in stimuli responsive thin film surfaces, it is important to pursue an understanding of how PDMAEMA brush-modified surfaces affect transport of molecular ions as a function of pH. These analyses are important because environmental pH is used to control thickness, composition, and ionization in the building phases of these polymers.[275-276] More broadly, a better molecular-scale description of transport at soft interfaces would benefit both biomedical and pharmaceutical applications, and the basic understanding of the discrete switchability of these smart surfaces.

Weak polyelectrolytes have been reported to have more complicated folding and unfolding transitions than the coil-to-globule model previously embraced.[277] Due to the mobility of the charges along the weak polyelectrolyte backbone, in contrast to the static charges of strong polyelectrolytes, the transition from coil to globule is not a straightforward one. Many intermediate states may be sampled as the charges move along the backbone, and those states are heavily dependent on pH. Wang and coworkers assessed

the local pH around polymer strands in comparison to the bulk pH in polymer-free solutions of FITC.[277] The difference between the local and bulk pH enlarged with increasing MW, due to the larger number of mobile charges.

FCS has been used to explore the importance fine evaluation and characterization of polyelectrolyte surfaces.[121-122, 170, 259] In the present work, we used traditional FCS, and line scan FCS to quantify the presence and extent of interactions between PDMAEMA, the cationic Rhodamine 6G (R6G), and anionic AlexaFluor 555® (Alexa) dyes as a function of distance from the surface. Recently, we have successfully used these techniques to study transport at charged and crowded interfaces and with heterogeneous mixtures.[121-122, 170, 221, 259] When measuring close to the substrate interface, it is important to consider dye-surface interactions. In order to offer insight into these questions we report evidence of the interaction of small molecules with different thicknesses/lengths of PDMAEMA brushes. FCS analysis of translational diffusion of the anionic dye in the presence of the polymer revealed strong interaction in acidic environment. Scanning FCS was used to confirm the interaction, since it is more sensitive to slower diffusion. To our knowledge, this is the first application of line scan FCS to a materials, rather than a biological, system.

7.3 Materials and Methods

Many of the details of the sample preparation, setup, and theory have been previously reported[121-122, 142, 170, 221, 259]. 100 nm orange fluorescent carboxylate-modified FluoSphere beads (max abs/em: 540/560 nm) beads (1:1000 dilution) were used to determine the focal volume for the FCS measurements. Rhodamine 6G (max abs/em: 530/566nm) and AlexaFluor® 555 (max abs/em: 555/565 nm) were diluted to

approximately 100 pM for signal versus concentration optimization. KOH (85+%, Sigma-Aldrich) and spectroscopic grade H_2SO_4 (J. T. Baker) were diluted to a 0.001N solutions supplying the basic and acidic environments for the fluorescent dyes, respectively. The basic solution was pH 11.7; the acidic solution was pH 3.5. Hyclone Molecular Biology grade (MB) water (VWR) was used for all dilutions. No. 1 borosilicate coverslips were cleaned using a TL1 wash (80º C 1:1:6 mixture of NH_3OH:30% H_20_2:H_2O), followed by oxygen plasma cleaning for 2 minutes. Measurements were taken in each of the three solutions (aqueous, basic, and acidic) and at four depths (0.5, 1.0, 1.5, and 2.0 μm)/ two depths (0.5 and 2.0 μm).

2-(Dimethylamino)ethylmethacrylate (DMAEMA, 99%) was purchased from Acros Organics. Before polymerization inhibitor was removed by passing the compound through a tube containg alternating layers of inhibitor remover and alumina. 1,1,4,7,10,10-hexamethyl triethylenetetramin (HMTETA, 97%) and copper(I)bromide (CuBr) were purchased from Aldrich and Alfa Aesar respectively, and used without any modification.

7.3.1 Preparation and Characterization of the PDMAEMA Surface

Self assembled monolayers of ATRP-silane were prepared according to literature, and depicted in Figure 7.2.[26] The surface initiated atom transfer radical polymerization ATRP (SI-ATRP) of PDMAEMA was performed using a typical 3 schlenk tube system. The first schlenk tube contained 5.04 ml of DMAEMA and 40.8 mL of HMTETA dissolved in 30 ml of acetone and degassed

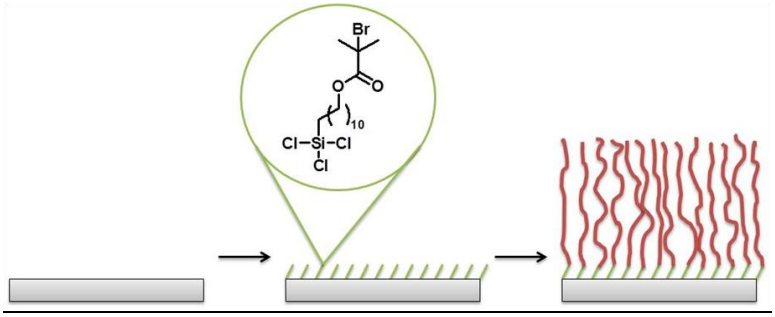

Figure 7.2: Depiction of the polymerization process.

with N_2 for 30 min. The second and third schlenk tubes contained 21.6 mg of CuBr and the ATRP-silane monolayer coated slide respectively. Upon degassing, the contents of the tube 1 and 2 were combined and allowed to stir for 10 min. Then the solution was transferred to the modified film substrate and allowed to polymerize for the desired time.

Null ellipsometry was used to determine the thickness of the brush films. All measurements were conducted using a null-ellipsometer operating in polarizer-compensator-sample-analyzer (Multiskop, Optrel Berlin) mode. As a light source, a He–Ne laser (632.8 nm) was applied, and the angle of incidence was set to 608˚.

Table 7.1: Ellipsometry Data

Dry thickness	
Thin brush: (6 hr)	12 ± 2 nm
Middle brush: (12 hr)	38 ± 3 nm
Thick brush: (24 hr)	82 ± 4 nm
Thickness at pH 3	
Thin brush: (12.4 ± 1.2 nm)	15 ± 1 nm
Middle brush: (38.4 ± 3.1 nm)	50 ± 2 nm
Thick brush: (82.2 ± 4.5 nm)	108 ± 4 nm
Thickness at pH 11	
Thin brush: (12.4 ± 1.2 nm)	10.2 ± 0.3 nm
Middle brush: (38.4 ± 3.1 nm)	26 ± 3 nm
Thick brush: (82.2 ± 4.5 nm)	62 ± 2 nm

7.4 Results & Discussion

7.4.1 Cationic vs. Anionic Probe

PDMAEMA is a weak polybase. In acidic pHs, the amine group of the DMAEMA becomes protenated. The Coulombic repulsion that occurs as the protenated groups remain in close proximity on the polymer chain results in an elongation of the chain.[6, 13] Therefore, the brush swells to relieve the Coulombic strain. This can be seen in Table 7.1. The thickness of the brushes at acidic pHs is greater than that of the dry thickness. This change is clear for the Middle and Thick brushes. This provides evidence that the brush is affected by the surplus of hydronium ions.

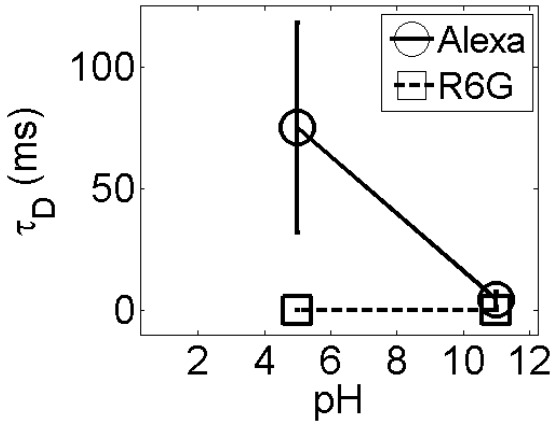

Figure 7.3: Plot of diffusion times as a function of pH near the surface of the Middle brush. These were acquired with traditional FCS. Both the cationic (square marker) and the anionic (circle marker) probes are featured. The cationic probe shows no evidence of interaction at either pH. The anionic probe heavily interacts at pH 5. The anionic probe shows no evidence interaction at pH 11.

Conversely, in basic pHs the amine group of the DMAEMA does not have a charge, and therefore shrinks.[6, 13] This can also be seen in Table 7.1. The thickness of the brushes at basic pHs is less than that of the dry thickness. This change is clear for the Middle and Thick brushes. This provides evidence that the brush has a response to basic environments as well. In low pHs, the brush swells, as the hydronium ions are attracted to the anionic backbone and repel from each other. In high pHs, without this Columbic interaction, the

brush collapses on itself.[6, 13] The switching of the brush affects the probes, as can be seen in Figure 7.3.

Figure 7.3 describes the trend of diffusion times as a function of pH for both the cationic and anionic probe as measured using traditional FCS measured near the surface (0.5 μm from the surface). The three environmental pHs used in this study were pH 5 and 11.

These environmental effects are also evident in Figure 7.3. At high pH (pH = 11), neither probe exhibited interaction with the brush. The diffusion times were comparable to those of the probes in bulk solution;[221] the diffusion times for the cationic and anionic probes were 38 ± 5 μs and 45 ± 3 μs, respectively. It is evident that in its collapsed state, the brush did not garner interaction of the probes. At low pH, the cationic probe did not exhibit interaction with the brush. The diffusion time at this condition remained comparable to that of the probe in bulk solution;[221] the diffusion time of the cationic probe was 43 ± 3 μs. At low pH (pH = 5), the cationic probe appeared excluded from the brush in favor of the hydronium ions present in the solution. However, at low pH, the anionic probe exhibited interaction with the brush. The diffusion times were much longer than those of the probes in bulk solution, at 76 ± 45 ms. The diffusion of the anionic probe in the acidic environment is three orders of magnitude longer than the anionic probe in the basic environment and the cationic probe in both environments. The Coloumbic interaction between the anionic probe and the protonated brush is evident in this analysis. There is a large spread in the data for the anionic probe at the low pH. Large standard deviations in FCS data suggest the presence of anomalous events such as aggregation or adsorption.[183] Adsorption events

would be expected with a strong Coulombic attraction between the probe and brush.

7.4.2 Complete Solvation of Probe by Brush

Additionally, a near complete solvation of the anionic probe in the weak polyelectrolyte was observed at low pH (data not shown). From the intensity trajectories, events are distinguishable from noise due to the larger fluctuations in signal. Since we can control the piezo stage with nanometer precision, we took data at a focal depth of 0.5 μm from the surface, as well as 1.5 μm from the surface. These depths shall be termed 'near the surface' and 'in the bulk', respectively. It was observed that intensity trajectories for the cationic probe exhibited fluctuations in signal consistent with those expected for diffusion events. This means that there were probes diffusing through the focal volume at both depths. However, for the anionic probes, fluctuations consistent with diffusion events were only observed near the surface. In the bulk solution, the signal collected proved to be mostly noise. This indicates that the anionic probe has a strong affinity for the protonated brush.

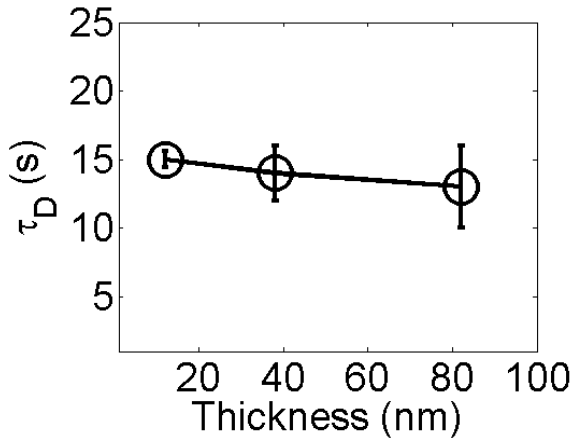

Figure 7.4: Plot of diffusion times as a function of brush thickness (all three brushes are represented) in environment of pH 5. These were acquired with line-scan FCS. Only the anionic probe is featured; the diffusion time remains constant even as the density of the brush changes.

7.4.3 Scanning FCS Analysis

Line scan FCS was used to further probe the interaction of the anionic probe near the surface in the pH 5 environment. Traditional FCS can be insensitive to longer

lived events since, even though the excitation fluence of our experiments is low, probability of photobleaching heightens for slower diffusing probes.[129] Figure 7.4 displays the characteristic diffusion times as a function of ellipsometric thickness. The Thin (12 nm), Middle (38 nm), and Thick (82 nm) brushes are all represented on this plot.

As previously stated, traditional FCS resulted in a characteristic diffusion time of 76 ± 45 ms of the anionic probe in the Middle PDMAEMA brush at a pH of 5. In contrast, line scan FCS resulted in a much longer diffusion time of 14 ± 2 s in the same conditions. There were 2 orders of magnitude in difference between the two types of measurements. This revealed an extremely strong interaction of the anionic probe to the protonated state of the PDMAEMA brush that was not measureable in traditional FCS. Yet, what was not distinguishable was whether the interaction was absolutely hindered diffusion or if it was an average between adsorption events, hindered diffusion, and free diffusion. We plan to use wide field imaging techniques to further probe those details.

Additionally shown in Figure 7.4 was the observation that the diffusion time did not change as a function of brush thickness. We have recently observed that brush thickness can affect the transport through neutral polymer brush architectures.[259] However, that was not the result observed in this system. The presence of mobile cations along the polymer backbone and the strong Coulombic interactions between the probe and the protonated PDMAEMA structure may negate the effects of density previously found.[277]

7.5 Conclusions

In the present work, we sought to investigate transport with PDMAEMA, a pH-

responsive polymer brush that shrinks in basic pHs and swells in acidic pHs. Traditional and line scan FCS techniques were used to probe this interaction near the surface with cationic and anionic dyes in an acidic and basic environment. Traditional FCS reveals no interaction of the cationic probe with the brush, as the diffusion constants are comparable to those of free diffusion. Traditional FCS does show an interaction between the anionic probe and the brush in the acidic environment. Scanning FCS has been proven the more sensitive technique for slow diffusion. Studies done with line scan FCS revealed a very strong interaction of the anionic probe with the brush, which was hinted at by the results from traditional FCS. In addition to the results founded by the FCS techniques, we observed an extreme affinity for the anionic probe to the polymer in low pHs, as there are a negligible number of events in bulk solution compared to those near the surface.

Chapter 8

Conclusions & Future Directions

8.1 Conclusions

The push for technological advances in the biomedical industry calls for new materials that will specifically interact with intended species and respond as the environment changes. Engineered nanostructured materials offer the benefit of tunability; these tunable properties present opportunities to develop highly efficient substrates and devices. It is therefore necessary to establish a fundamental and comprehensive understanding of the heterogeneous processes involved in transport within these nanostructured materials. I have focused on the transport in both functionalized and stimuli-responsive surfaces using FCS to determine the extent of interaction of relevant probes.

Chapter 4 investigates the presence of an interaction between two oppositely charged and well-known probes and hydrophilic hydroxyl-terminated silica surfaces. The cationic probe (R6G) displays a Coulombic interaction with the silica surface for conditions in which the surface hydroxyls are protonated. This study offers a mechanistic response to the wide range of characteristic diffusion times that have been reported for R6G over glass surfaces. It also suggests that for accurate analysis the cationic probe should be measured at least 1 μm from the surface for confocal conditions, or salt should be added to shield the surface attraction. It also resolves Alexa to be a more robust probe than R6G since it did not exhibit surface interactions that strongly affected the transport dynamics.

Chapters 5 and 6 investigate the interaction of free dye and dye-labeled proteins over functionalized surfaces. Chapter 5 presents a PEGylated surface that has been modified with a series of dendrons that offer increasing ligand space as well as a bottle brush polymer that represents an extremely crowded surface. In the case of the free dye, two components were extracted from the FCS analysis. The slow component is evidence of the free dye interacting with the polymer whereas the fast component is consistent with free diffusion. As a function of ligand density and probe size, this proved the PEGylated surface was permeable and showed effects of size exclusion.

Chapter 6 presents a agarose matrix functionalized with clustered-charge peptides; this surface is offered as an alternative to the current singly-charged peptide stationary phases in use for separations. The study shows evidence of free diffusion, hindered diffusion as a result of steric interactions with the agarose support, and electrostatic association with the peptides.

Chapter 7 investigates transport within a polymer brush that responds to pH, also introducing the technique of scanning FCS to the investigations. The interactions of cationic and anionic probes are assessed in a pH-responsive polymer brush. This brush is a weak polybase; it shrinks in high pH and swells in low pH environments. An interaction of the anionic probe with the brush in low pH solutions is evident. Traditional FCS reveals a characteristic diffusion time for the anionic probe that is orders of magnitude larger than

the characteristic diffusion time of a free probe. Scanning FCS is more apt to measure diffusion times on this timescale. In addition to the strong interaction between the probe and polymer brush we observe an extreme affinity for the anionic probe to the polymer in low pHs, as there are a negligible number of events in bulk solution.

8.2 Future Directions

Current literature shows that transport within nanostructured materials are of importance. The work of this thesis presents potential for additional work with these surfaces, some currently underway in the Landes Research Group.

8.2.1 Temperature Control

With the invention and implementation of equipment that finely controls a temperature gradient across a sample, there is the potential to exploit and examine the effects of pH and temperature on the PDMAEMA brush simultaneously. Earlier preliminary results within the research group indicate the applicability of using FCS to identify molecular transport mechanisms for the probes in the brush.

8.2.2 Diffusion Along the Axis of the Polymer

With the implementation of scanning FCS, exerted through nanometer-precision control of piezo stages, the next step is to examine behavior away from the surface. There has been reported evidence of charge hopping in layers of polymeric materials. Scanning along the axis of the polymer will give information on transport mechanisms in **z**.

8.2.3 Wide Field Microscopy

With the realization of slow dynamics as a result of interactions with the surfaces

and techniques used in this work, a real-time picture of such binding events would garner more information about the dynamics of the species of interest. Preliminary results show that data collection and analysis is feasible.

References

1. Li, C.; Mishchenko, A.; Wandlowski, T., Charge transport in single molecular junctions at the solid/liquid interface. *Top Curr Chem* **2012,** *313* (Copyright (C) 2012 U.S. National Library of Medicine.), 121-88.
2. Fan, F.-R. F.; Yang, J.; Cai, L.; Price, D. W., Jr.; Dirk, S. M.; Kosynkin, D. V.; Yao, Y.; Rawlett, A. M.; Tour, J. M.; Bard, A. J., Charge Transport through Self-Assembled Monolayers of Compounds of Interest in Molecular Electronics. *Journal of the American Chemical Society* **2002,** *124* (Copyright (C) 2012 American Chemical Society (ACS). All Rights Reserved.), 5550-5560.
3. Haiss, W.; Van, Z. H.; Higgins, S. J.; Bethell, D.; Hoebenreich, H.; Schiffrin, D. J.; Nichols, R. J., Redox State Dependence of Single Molecule Conductivity. *Journal of the American Chemical Society* **2003,** *125* (Copyright (C) 2012 American Chemical Society (ACS). All Rights Reserved.), 15294-15295.
4. Donhauser, Z. J.; Mantooth, B. A.; Kelly, K. F.; Bumm, L. A.; Monnell, J. D.; Stapleton, J. J.; Price, D. W., Jr.; Rawlett, A. M.; Allara, D. L.; Tour, J. M.; Weiss, P. S., Conductance switching in single molecules through conformational changes. *Science (Washington, DC, U. S.)* **2001,** *292* (Copyright (C) 2012 American Chemical Society (ACS). All Rights Reserved.), 2303-2307.
5. Bashir, R.; Hilt, J. Z.; Elibol, O.; Gupta, A.; Peppas, N. A., Micromechanical cantilever as an ultrasensitive pH microsensor. *Applied Physics Letters* **2002,** *81* (Copyright (C) 2012 American Chemical Society (ACS). All Rights Reserved.), 3091-3093.
6. Jia, H.; Wildes, A.; Titmuss, S., Structure of pH-Responsive Polymer Brushes Grown at the Gold-Water Interface: Dependence on Grafting Density and Temperature. *Macromolecules (Washington, DC, U. S.)* (Copyright (C) 2011 American Chemical Society (ACS). All Rights Reserved.), Ahead of Print.
7. Kanekiyo, Y.; Ono, Y.; Inoue, K.; Sano, M.; Shinkai, S., 'Molecular-imprinting' in polyion complexes which creates the 'memory' for the AMP template. *J. Chem. Soc., Perkin Trans. 2* **1999,** (Copyright (C) 2012 American Chemical Society (ACS). All Rights Reserved.), 557-562.
8. Lochhead, R.; Padman, V.; Anderson, L.; Wilgus, L. A.; McDaniel, P.; LaBeaud, L.; Davis, K.; Hoff, E.; Epler, J., Skin care polymer IP trends. *Household Pers. Prod. Ind.* **2010,** *47* (Copyright (C) 2012 American Chemical Society (ACS). All Rights Reserved.), 71-76.
9. Lochhead, R. Y., A review of recent advances in the polymeric delivery of attributes in cosmetics and personal care products. *ACS Symp. Ser.* **2010,** *1053* (Copyright (C) 2012 American Chemical Society (ACS). All Rights Reserved.), 3-22.
10. Peteu, S. F.; Oancea, F.; Sicuia, O. A.; Constantinescu, F.; Diinu, S., Responsive Polymers for Crop Protection. *Polymers (Basel, Switz.)* **2010,** *2* (Copyright (C) 2012 American Chemical Society (ACS). All Rights Reserved.), 229-251.
11. Tokarev, I.; Minko, S., Stimuli-responsive hydrogel thin films. *Soft Matter* **2009,** *5* (Copyright (C) 2011 American Chemical Society (ACS). All Rights Reserved.), 511-524.
12. Tokarev, I.; Motornov, M.; Minko, S., Molecular-engineered stimuli-responsive thin polymer film: a platform for the development of integrated multifunctional intelligent

materials. *J. Mater. Chem.* **2009,** *19* (Copyright (C) 2011 American Chemical Society (ACS). All Rights Reserved.), 6932-6948.
13. Tokarev, I.; Tokareva, I.; Minko, S., Optical Nanosensor Platform Operating in Near-Physiological pH Range via Polymer-Brush-Mediated Plasmon Coupling. *ACS Appl. Mater. Interfaces* **2011,** *3* (Copyright (C) 2011 American Chemical Society (ACS). All Rights Reserved.), 143-146.
14. Analysis, B. R. M. Global Medical Markets for Nanoscale Materials and Devices 2008.
15. Sun, T.-L.; Qing, G.-Y., Biomimetic Smart Interface Materials for Biological Applications. *Adv. Mater. (Weinheim, Ger.)* **2011,** *23* (Copyright (C) 2012 American Chemical Society (ACS). All Rights Reserved.), H57-H77.
16. Butun, V.; Armes, S. P.; Billingham, N. C., Synthesis and aqueous solution properties of near-monodisperse tertiary amine methacrylate homopolymers and diblock copolymers. *Polymer* **2001,** *42* (Copyright (C) 2012 American Chemical Society (ACS). All Rights Reserved.), 5993-6008.
17. de Vos, W. M.; Meijer, G.; de Keizer, A.; Cohen Stuart, M. A.; Kleijn, J. M., Charge-driven and reversible assembly of ultra-dense polymer brushes: formation and antifouling properties of a zipper brush. *Soft Matter* **2010,** *6* (11), 2499-2507.
18. He, X.; Yang, W.; Pei, X., Preparation, Characterization, and Tunable Wettability of Poly(ionic liquid) Brushes via Surface-Initiated Atom Transfer Radical Polymerization. *Macromolecules (Washington, DC, U. S.)* **2008,** *41* (Copyright (C) 2012 American Chemical Society (ACS). All Rights Reserved.), 4615-4621.
19. Wu, T.; Efimenko, K.; Genzer, J., Preparing High-Density Polymer Brushes by Mechanically Assisted Polymer Assembly. *Macromolecules* **2001,** *34* (4), 684-686.
20. Li, D.; Sheng, X.; Zhao, B., Environmentally Responsive "Hairy" Nanoparticles: Mixed Homopolymer Brushes on Silica Nanoparticles Synthesized by Living Radical Polymerization Techniques. *J. Am. Chem. Soc.* **2005,** *127* (17), 6248-6256.
21. Ma, H.; Wells, M.; Beebe, T. P., Jr.; Chilkoti, A., Surface-initiated atom transfer radical polymerization of oligo(ethylene glycol) methyl methacrylate from a mixed self-assembled monolayer on gold. *Adv. Funct. Mater.* **2006,** *16* (Copyright (C) 2011 American Chemical Society (ACS). All Rights Reserved.), 640-648.
22. Tria, M. C. R.; Grande, C. D. T.; Ponnapati, R. R.; Advincula, R. C., Electrochemical Deposition and Surface-Initiated RAFT Polymerization: Protein and Cell-Resistant PPEGMEMA Polymer Brushes. *Biomacromolecules* **2010,** *11* (12), 3422-3431.
23. An, S. W.; Thirtle, P. N.; Thomas, R. K.; Baines, F. L.; Billingham, N. C.; Armes, S. P.; Penfold, J., Structure of a Diblock Copolymer Adsorbed at the Hydrophobic Solid/Aqueous Interface: Effects of Charge Density on a Weak Polyelectrolyte Brush. *Macromolecules* **1999,** *32* (Copyright (C) 2011 American Chemical Society (ACS). All Rights Reserved.), 2731-2738.
24. Mert, O.; Doganci, E.; Erbil, H. Y.; Demir, A. S., Surface Characterization of Poly(L-lactic) Acid-Methoxy Polyethylene Glycol Diblock Copolymers by Static and Dynamic Contact Angle Measurements, FTIR and ATR-FTIR. *Langmuir* **2008,** *24* (3), 749-757.
25. Patton, D. L.; Taranekar, P.; Fulghum, T.; Advincula, R., Electrochemically Active Dendritic−Linear Block Copolymers via RAFT Polymerization: Synthesis, Characterization, and Electrodeposition Properties. *Macromolecules* **2008,** *41* (18), 6703-6713.
26. Yu, K.; Wang, H.; Xue, L.; Han, Y., Stimuli-Responsive Polyelectrolyte Block

Copolymer Brushes Synthesized from the Si Wafer via Atom-Transfer Radical Polymerization. *Langmuir* **2007,** *23* (Copyright (C) 2012 American Chemical Society (ACS). All Rights Reserved.), 1443-1452.
27. Zhou, Y.; Liedberg, B.; Gorochovceva, N.; Makuska, R.; Dedinaite, A.; Claesson, P. M., Chitosan-N-poly(ethylene oxide) brush polymers for reduced nonspecific protein adsorption. *J. Colloid Interface Sci.* **2006,** *305* (1), 62-71.
28. Olanya, G.; Thormann, E.; Varga, I.; Makuska, R.; Claesson, P. M., Protein interactions with bottle-brush polymer layers: Effect of side chain and charge density ratio probed by QCM-D and AFM. *J. Colloid Interface Sci.* **2010,** *349* (1), 265-274.
29. Groll, J.; Amirgoulova Elza, V.; Ameringer, T.; Heyes Colin, D.; Rocker, C.; Nienhaus, G. U.; Moller, M., Biofunctionalized, ultrathin coatings of cross-linked star-shaped poly(ethylene oxide) allow reversible folding of immobilized proteins. *J Am Chem Soc* **2004,** *126* (13), 4234-9.
30. Heyes, C. D.; Groll, J.; Moeller, M.; Nienhaus, G. U., Synthesis, patterning and applications of star-shaped poly(ethylene glycol) biofunctionalized surfaces. *Molecular BioSystems* **2007,** *3* (6), 419-430.
31. Heyes, C. D.; Kobitski, A. Y.; Amirgoulova, E. V.; Nienhaus, G. U., Biocompatible surfaces for specific tethering of individual protein molecules. *J. Phys. Chem. B* **2004,** *108* (35), 13387-13394.
32. Wu, C.; Wang, X., Globule-to-Coil Transition of a Single Homopolymer Chain in Solution. *Phys. Rev. Lett.* **1998,** *80* (Copyright (C) 2011 American Chemical Society (ACS). All Rights Reserved.), 4092-4094.
33. Bhat, R. R.; Tomlinson, M. R.; Genzer, J., Orthogonal surface-grafted polymer gradients: A versatile combinatorial platform. *Journal of Polymer Science, Part B: Polymer Physics* **2005,** *43* (23), 3384-3394.
34. Semler, J. J.; Genzer, J., Design of random copolymers with statistically controlled monomer sequence distributions via Monte Carlo simulations. *J Chem Phys FIELD Full Journal Title:The Journal of chemical physics* **2006,** *125* (1), 014902.
35. Amirgoulova, E. V.; Groll, J.; Heyes, C. D.; Ameringer, T.; Roecker, C.; Moeller, M.; Nienhaus, G. U., Biofunctionalized polymer surfaces exhibiting minimal interaction towards immobilized proteins. *ChemPhysChem* **2004,** *5* (4), 552-555.
36. Gasteier, P.; Reska, A.; Schulte, P.; Salber, J.; Offenhaeusser, A.; Moeller, M.; Groll, J., Surface grafting of PEO-based star-shaped molecules for bioanalytical and biomedical applications. *Macromolecular Bioscience* **2007,** *7* (8), 1010-1023.
37. Groll, J.; Amirgoulova, E. V.; Ameringer, T.; Heyes, C. D.; Roecker, C.; Nienhaus, G. U.; Moeller, M., Biofunctionalized, ultrathin coatings of crosslinked star-shaped poly(ethylene oxide) allow reversible folding of immobilized proteins. *J. Am. Chem. Soc.* **2004,** *126* (13), 4234-4239.
38. Nel, A. E.; Madler, L.; Velegol, D.; Xia, T.; Hoek, E. M. V.; Somasundaran, P.; Klaessig, F.; Castranova, V.; Thompson, M., Understanding biophysicochemical interactions at the nano-bio interface. *Nat. Mater.* **2009,** *8* (Copyright (C) 2012 American Chemical Society (ACS). All Rights Reserved.), 543-557.
39. Nolan, C. M.; Serpe, M. J.; Lyon, L. A., Thermally modulated insulin release from microgel thin films. *Biomacromolecules* **2004,** *5* (Copyright (C) 2012 American Chemical Society (ACS). All Rights Reserved.), 1940-1946.

40. Serpe, M. J.; Yarmey, K. A.; Nolan, C. M.; Lyon, L. A., Doxorubicin Uptake and Release from Microgel Thin Films. *Biomacromolecules* **2005,** *6* (Copyright (C) 2012 American Chemical Society (ACS). All Rights Reserved.), 408-413.
41. Cheng, X.; Canavan, H. E.; Graham, D. J.; Castner, D. G.; Ratner, B. D., Temperature-dependent activity and structure of adsorbed proteins on plasma polymerized N-isopropyl acrylamide. *Biointerphases* **2006,** *1* (Copyright (C) 2012 American Chemical Society (ACS). All Rights Reserved.), 61-72.
42. Garty, S.; Kimelman-Bleich, N.; Hayouka, Z.; Cohn, D.; Friedler, A.; Pelled, G.; Gazit, D., Peptide-Modified "Smart" Hydrogels and Genetically Engineered Stem Cells for Skeletal Tissue Engineering. *Biomacromolecules* **2010,** *11* (Copyright (C) 2012 American Chemical Society (ACS). All Rights Reserved.), 1516-1526.
43. Maynard, H. D.; Heredia, K. L.; Li, R. C.; Parra, D. P.; Vazquez-Dorbatt, V., Thermoresponsive biohybrid materials synthesized by ATRP. *J. Mater. Chem.* **2007,** *17* (Copyright (C) 2012 American Chemical Society (ACS). All Rights Reserved.), 4015-4017.
44. Tan, H.; Ramirez, C. M.; Miljkovic, N.; Li, H.; Rubin, J. P.; Marra, K. G., Thermosensitive injectable hyaluronic acid hydrogel for adipose tissue engineering. *Biomaterials* **2009,** *30* (Copyright (C) 2012 American Chemical Society (ACS). All Rights Reserved.), 6844-6853.
45. Nozaki, D.; Pastawski, H. M.; Cuniberti, G., Controlling the conductance of molecular wires by defect engineering. *New J. Phys.* **2010,** *12* (Copyright (C) 2012 American Chemical Society (ACS). All Rights Reserved.), No pp. given.
46. Schlapak, R.; Armitage, D.; Saucedo-Zeni, N.; Chrzanowski, W.; Hohage, M.; Caruana, D.; Howorka, S., Selective protein and DNA adsorption on PLL-PEG films modulated by ionic strength. *Soft Matter* **2009,** *5* (3), 613-621.
47. Gong, P.; Genzer, J.; Szleifer, I., Phase behavior and charge regulation of weak polyelectrolyte grafted layers. *Phys Rev Lett FIELD Full Journal Title:Physical review letters* **2007,** *98* (1), 018302.
48. Zustiak, S. P.; Boukari, H.; Leach, J. B., Solute diffusion and interactions in cross-linked poly(ethylene glycol) hydrogels studied by Fluorescence Correlation Spectroscopy. *Soft Matter* **2010,** *6* (15), 3609-3618.
49. Preiner, J.; Ebner, A.; Chtcheglova, L.; Zhu, R.; Hinterdorfer, P., Simultaneous topography and recognition imaging: physical aspects and optimal imaging conditions. *Nanotechnology* **2009,** *20* (Copyright (C) 2012 American Chemical Society (ACS). All Rights Reserved.), 215103/1-215103/9.
50. Zhu, R.; Ebner, A.; Kastner, M.; Preiner, J.; Howorka, S.; Hinterdorfer, P., Topography and Recognition Imaging of Protein-Patterned Surfaces Generated by AFM Nanolithography. *ChemPhysChem* **2009,** *10* (Copyright (C) 2012 American Chemical Society (ACS). All Rights Reserved.), 1478-1481.
51. Chen, Y.-C.; Xie, R.; Yang, M.; Li, P.-F.; Zhu, X.-L.; Chu, L.-Y., Gating characteristics of thermo-responsive membranes with grafted linear and crosslinked poly(N-isopropylacrylamide) gates. *Chem. Eng. Technol.* **2009,** *32* (Copyright (C) 2012 American Chemical Society (ACS). All Rights Reserved.), 622-631.
52. Ito, T.; Sato, Y.; Yamaguchi, T.; Nakao, S.-I., Response Mechanism of a Molecular Recognition Ion Gating Membrane. *Macromolecules* **2004,** *37* (Copyright (C) 2012 American Chemical Society (ACS). All Rights Reserved.), 3407-3414.
53. Schepelina, O.; Zharov, I., PNIPAAM-Modified Nanoporous Colloidal Films with

Positive and Negative Temperature Gating. *Langmuir* **2007,** *23* (Copyright (C) 2012 American Chemical Society (ACS). All Rights Reserved.), 12704-12709.
54. Qing, G.; Wang, X.; Jiang, L.; Fuchs, H.; Sun, T., Saccharide-sensitive wettability switching on a smart polymer surface. *Soft Matter* **2009,** *5* (Copyright (C) 2012 American Chemical Society (ACS). All Rights Reserved.), 2759-2765.
55. Reddy, T. T.; Kano, A.; Maruyama, A.; Hadano, M.; Takahara, A., Thermosensitive Transparent Semi-Interpenetrating Polymer Networks for Wound Dressing and Cell Adhesion Control. *Biomacromolecules* **2008,** *9* (Copyright (C) 2012 American Chemical Society (ACS). All Rights Reserved.), 1313-1321.
56. Vinogradov, S. V., Colloidal microgels in drug delivery applications. *Curr. Pharm. Des.* **2006,** *12* (Copyright (C) 2012 American Chemical Society (ACS). All Rights Reserved.), 4703-4712.
57. Zhang, J.; Misra, R. D. K., Magnetic drug-targeting carrier encapsulated with thermosensitive smart polymer: core-shell nanoparticle carrier and drug release response. *Acta Biomater.* **2007,** *3* (Copyright (C) 2012 American Chemical Society (ACS). All Rights Reserved.), 838-850.
58. Budhlall, B. M.; Marquez, M.; Velev, O. D., Microwave, Photo- and Thermally Responsive PNIPAm-Gold Nanoparticle Microgels. *Langmuir* **2008,** *24* (Copyright (C) 2012 American Chemical Society (ACS). All Rights Reserved.), 11959-11966.
59. Urban, A. S.; Fedoruk, M.; Horton, M. R.; Radler, J. O.; Stefani, F. D.; Feldmann, J., Controlled Nanometric Phase Transitions of Phospholipid Membranes by Plasmonic Heating of Single Gold Nanoparticles. *Nano Lett.* **2009,** *9* (Copyright (C) 2012 American Chemical Society (ACS). All Rights Reserved.), 2903-2908.
60. Anikin, K.; Roecker, C.; Wittemann, A.; Wiedenmann, J.; Ballauff, M.; Nienhaus, G. U., Polyelectrolyte-mediated protein adsorption: fluorescent protein binding to individual polyelectrolyte nanospheres. *J. Phys. Chem. B* **2005,** *109* (12), 5418-5420.
61. Yonet-Tanyeri, N.; Evans, R. C.; Tu, H.-L.; Braun, P. V., Molecular Transport Directed via Patterned Functionalized Surfaces. *Adv. Mater. (Weinheim, Ger.)* **2011,** *23* (Copyright (C) 2011 American Chemical Society (ACS). All Rights Reserved.), 1739-1743.
62. Chunder, A.; Etcheverry, K.; Londe, G.; Cho, H. J.; Zhai, L., Conformal switchable superhydrophobic/hydrophilic surfaces for microscale flow control. *Colloids Surf., A* **2009,** *333* (Copyright (C) 2012 American Chemical Society (ACS). All Rights Reserved.), 187-193.
63. Yager, P.; Edwards, T.; Fu, E.; Helton, K.; Nelson, K.; Tam, M. R.; Weigl, B. H., Microfluidic diagnostic technologies for global public health. *Nature (London, U. K.)* **2006,** *442* (Copyright (C) 2012 American Chemical Society (ACS). All Rights Reserved.), 412-418.
64. Fu, J. Y.; Balan, S.; Potty, A.; Nguyen, V.; Willson, R. C., Enhanced Protein Affinity and Selectivity of Clustered-Charge Anion-Exchange Adsorbents. *Analytical Chemistry (Washington, DC, United States)* **2007,** *79* (Copyright (C) 2010 American Chemical Society (ACS). All Rights Reserved.), 9060-9065.
65. Etheve, J.; Dejardin, P.; Boissiere, M., Adsorption of lysozyme on a hemodialysis sulfonated polyacrylonitrile membrane, with and without preadsorbed poly(ethyleneimine) on the external faces. *Colloids and Surfaces, B: Biointerfaces* **2003,** *28* (Copyright (C) 2012 American Chemical Society (ACS). All Rights Reserved.), 285-293.
66. Yang, K.; Bai, S.; Sun, Y., Protein adsorption dynamics in cation-exchange chromatography quantitatively studied by confocal laser scanning microscopy. *Chem. Eng.*

Sci. **2008,** *63* (Copyright (C) 2011 American Chemical Society (ACS). All Rights Reserved.), 4045-4054.
67. Halperin, A., Polymer Brushes that Resist Adsorption of Model Proteins: Design Parameters. *Langmuir* **1999,** *15* (Copyright (C) 2010 American Chemical Society (ACS). All Rights Reserved.), 2525-2533.
68. Halperin, A.; Fragneto, G.; Schollier, A.; Sferrazza, M., Primary versus Ternary Adsorption of Proteins onto PEG Brushes. *Langmuir* **2007,** *23* (21), 10603-10617.
69. Schlapak, R.; Caruana, D.; Armitage, D.; Howorka, S., Semipermeable poly(ethylene glycol) films: The relationship between permeability and molecular structure of polymer chains. *Soft Matter* **2009,** *5* (21), 4104-4112.
70. Yang, Z.; Galloway, J. A.; Yu, H., Protein Interactions with Polyethylene Glycol Self-Assembled Monolayers on Glass Substrates: Diffusion and Adsorption. *Langmuir* **1999,** *15* (5), 8405-8411.
71. Altrock, E.; Muth, C. A.; Klein, G.; Spatz, J. P.; Lee-Thedieck, C., The significance of integrin ligand nanopatterning on lipid raft clustering in hematopoietic stem cells. *Biomaterials* **2012,** *33* (Copyright (C) 2012 American Chemical Society (ACS). All Rights Reserved.), 3107-3118.
72. Xue, C.; Yonet-Tanyeri, N.; Brouette, N.; Sferrazza, M.; Braun, P. V.; Leckband, D. E., Protein Adsorption on Poly(N-isopropylacrylamide) Brushes: Dependence on Grafting Density and Chain Collapse. *Langmuir* **2011,** *27* (14), 8810-8818.
73. Sanjuan, S.; Perrin, P.; Pantoustier, N.; Tran, Y., Synthesis and Swelling Behavior of pH-Responsive Polybase Brushes. *Langmuir* **2007,** *23* (Copyright (C) 2011 American Chemical Society (ACS). All Rights Reserved.), 5769-5778.
74. Darugar, Q.; Kim, H.; Gorelick, R. J.; Landes, C., Human T-cell lymphotropic virus type 1 nucleocapsid protein-induced structural changes in transactivation response DNA hairpin measured by single-molecule fluorescence resonance energy transfer. *J. Virol. FIELD Full Journal Title:Journal of Virology* **2008,** *82* (24), 12164-12171.
75. Taylor, J. N.; Darugar, Q.; Kourentzi, K.; Willson, R. C.; Landes, C. F., Dynamics of an anti-VEGF DNA aptamer: A single-molecule study. *Biochem. Biophys. Res. Commun. FIELD Full Journal Title:Biochemical and Biophysical Research Communications* **2008,** *373* (2), 213-218.
76. Taylor, J. N.; Makarov, D. E.; Landes, C. F., Denoising single-molecule FRET trajectories with wavelets and Bayesian inference. *Biophys. J.* **2010,** *98* (1), 164-173.
77. Ha, T.; Zhuang, X.; Kim, H. D.; Orr, J. W.; Williamson, J. R.; Chu, S., Ligand-induced conformational changes observed in single RNA molecules. *Proc. Natl. Acad. Sci. U. S. A. FIELD Full Journal Title:Proceedings of the National Academy of Sciences of the United States of America* **1999,** *96* (16), 9077-9082.
78. Collinson, M. M.; Wightman, R. M., Observation of Individual Chemical Reactions in Solution. *Science* **1995,** *268* (5219), 1883-1885.
79. Frisbie, C. D.; Rozsnyai, L. F.; Noy, A.; Wrighton, M. S.; Lieber, C. M., Functional group imaging by chemical force microscopy. *Science (Washington, D. C.)* **1994,** *265* (Copyright (C) 2012 American Chemical Society (ACS). All Rights Reserved.), 2071-4.
80. Noy, A.; Frisbie, C. D.; Rozsnyai, L. F.; Wrighton, M. S.; Lieber, C. M., Chemical Force Microscopy: Exploiting Chemically-Modified Tips To Quantify Adhesion, Friction, and Functional Group Distributions in Molecular Assemblies. *J. Am. Chem. Soc.* **1995,** *117*

(Copyright (C) 2012 American Chemical Society (ACS). All Rights Reserved.), 7943-51.
81. Preiner, J.; Losilla, N. S.; Ebner, A.; Annibale, P.; Biscarini, F.; Garcia, R.; Hinterdorfer, P., Imaging and Detection of Single Molecule Recognition Events on Organic Semiconductor Surfaces. *Nano Lett.* **2009,** *9* (Copyright (C) 2012 American Chemical Society (ACS). All Rights Reserved.), 571-575.
82. Stroh, C. M.; Ebner, A.; Geretschlaeger, M.; Freudenthaler, G.; Kienberger, F.; Kamruzzahan, A. S. M.; Smith-Gill, S. J.; Gruber, H. J.; Hinterdorfer, P., Simultaneous topography and recognition imaging using force microscopy. *Biophysical Journal* **2004,** *87* (Copyright (C) 2012 American Chemical Society (ACS). All Rights Reserved.), 1981-1990.
83. Jass, J.; Schedin, S.; Faellman, E.; Ohlsson, J.; Nilsson, U. J.; Uhlin, B. E.; Axner, O., Physical properties of Escherichia coli P pili measured by optical tweezers. *Biophysical Journal* **2004,** *87* (Copyright (C) 2012 American Chemical Society (ACS). All Rights Reserved.), 4271-4283.
84. Simpson, K. H.; Bowden, M. G.; Hook, M.; Anvari, B., Measurement of adhesive forces between S. epidermidis and fibronectin-coated surfaces using optical tweezers. *Lasers Surg Med* **2002,** *31* (Copyright (C) 2012 U.S. National Library of Medicine.), 45-52.
85. Elson, E. L.; Madge, D., Fluorescence Correlation Spectroscopy. I. Conceptual Basis and Theory. *Biopolymers* **1974,** *13* (1), 1.
86. Magde, D.; Elson, E.; Webb, W. W., Thermodynamic fluctations in a reacting system. Measurement by fluorescence correlation spectroscopy. *Phys. Rev. Lett.* **1972,** *29* (11), 705-8.
87. Magde, D.; Elson, E. L.; Webb, W. W., Fluorescence correlation spectroscopy. II. Experimental realization. *Biopolymers FIELD Full Journal Title:Biopolymers* **1974,** *13* (1), 29-61.
88. Ehrenberg, M.; Rigler, R., Fluorescence correlation spectroscopy applied to rotational diffusion of macromolecules. *Q Rev Biophys* **1976,** *9* (Copyright (C) 2012 U.S. National Library of Medicine.), 69-81.
89. Aragon, S. R.; Pecora, R., Fluorescence Correlation Spectroscopy as a Probe of Molecular Dynamics. *The Journal of Chemical Physics* **1976,** *64* (4), 1791-1803.
90. Elson, E. L., Quick tour of fluorescence correlation spectroscopy from its inception. *J. Biomed. Opt.* **2004,** *9* (Copyright (C) 2012 American Chemical Society (ACS). All Rights Reserved.), 857-864.
91. Magde, D.; Elson, E. L.; Webb, W. W., Fluorescence correlation spectroscopy. II. Experimental realization. *Biopolymers* **1974,** *13* (Copyright (C) 2012 American Chemical Society (ACS). All Rights Reserved.), 29-61.
92. Koppel, D. E.; Axelrod, D.; Schlessinger, J.; Elson, E. L.; Webb, W. W., Dynamics of fluorescence marker concentration as a probe of mobility. *Biophys. J.* **1976,** *16* (Copyright (C) 2012 American Chemical Society (ACS). All Rights Reserved.), 1315-29.
93. Magde, D.; Elson, E.; Webb, W. W., Thermodynamic fluctations in a reacting system. Measurement by fluorescence correlation spectroscopy. *Phys. Rev. Lett.* **1972,** *29* (Copyright (C) 2012 American Chemical Society (ACS). All Rights Reserved.), 705-8.
94. Fahey, P. F.; Koppel, D. E.; Barak, L. S.; Wolf, D. E.; Elson, E. L.; Webb, W. W., Lateral diffusion in planar lipid bilayers. *Science* **1977,** *195* (Copyright (C) 2012 American Chemical Society (ACS). All Rights Reserved.), 305-6.
95. Fahey, P. F.; Webb, W. W., Lateral diffusion in phospholipid bilayer membranes and

multilamellar liquid crystals. *Biochemistry* **1978,** *17* (Copyright (C) 2012 American Chemical Society (ACS). All Rights Reserved.), 3046-53.
96. Ehrenberg, M.; Rigler, R., Fluorescence spectroscopy applied to dynamics and structure of biopolymers. *Springer Ser. Opt. Sci.* **1976,** *3* (Copyright (C) 2012 American Chemical Society (ACS). All Rights Reserved.), 314-25.
97. Borejdo, J., Motion of myosin fragments during actin-activated ATPase: fluorescence correlation spectroscopy study. *Biopolymers* **1979,** *18* (Copyright (C) 2012 American Chemical Society (ACS). All Rights Reserved.), 2807-20.
98. Sorscher, S. M. *Studies of chromatin in situ by fluorescence correlation spectroscopy*; Univ. California: 1979; p 195 pp.
99. Sorscher, S. M.; Bartholomew, J. C.; Klein, M. P., The use of fluorescence correlation spectroscopy to probe chromatin in the cell nucleus. *Biochim. Biophys. Acta, Nucleic Acids Protein Synth.* **1980,** *610* (Copyright (C) 2012 American Chemical Society (ACS). All Rights Reserved.), 28-46.
100. Rigler, R.; Mets, U.; Widengren, J.; Kask, P., Fluorescence correlation spectroscopy with high count rate and low background: Analysis of translational diffusion. *Eur. Biophys. J. FIELD Full Journal Title:European Biophysics Journal* **1993,** *22* (3), 169-75.
101. Eigen, M.; Rigler, R., Sorting single molecules: application to diagnostics and evolutionary biotechnology. *Proceedings of the National Academy of Sciences of the United States of America* **1994,** *91* (13), 5740-7.
102. Hess, S. T.; Webb, W. W., Focal volume optics and experimental artifacts in confocal fluorescence correlation spectroscopy. *Biophys. J.* **2002,** *83* (Copyright (C) 2012 American Chemical Society (ACS). All Rights Reserved.), 2300-2317.
103. Maiti, S.; Haupts, U.; Webb, W. W., Fluorescence correlation spectroscopy: diagnostics for sparse molecules. *Proc. Natl. Acad. Sci. U. S. A.* **1997,** *94* (Copyright (C) 2012 American Chemical Society (ACS). All Rights Reserved.), 11753-11757.
104. Foldes-Papp, Z., Fluorescence fluctuation spectroscopic approaches to the study of a single molecule diffusing in solution and a live cell without systemic drift or convection: a theoretical study. *Current pharmaceutical biotechnology* **2007,** *8* (5), 261-73.
105. Foldes-Papp, Z., 'True' single-molecule molecule observations by fluorescence correlation spectroscopy and two-color fluorescence cross-correlation spectroscopy. *Experimental and molecular pathology* **2007,** *82* (2), 147-55.
106. Rigler, R., Fluorescence correlations, single molecule detection and large number screening. Applications in biotechnology. *J. Biotechnol.* **1995,** *41* (Copyright (C) 2012 American Chemical Society (ACS). All Rights Reserved.), 177-86.
107. Berland, K. M.; Shen, G., Investigating two-photon photophysics with fluorescence correlation spectroscopy. *Proc. SPIE-Int. Soc. Opt. Eng.* **2003,** *4963* (Copyright (C) 2012 American Chemical Society (ACS). All Rights Reserved.), 1-12.
108. Gaiotto, T.; Nguyen, H. B.; Jung, J.; Gnanakaran, G. S.; Schmidt, J. G.; Waldo, G. S.; Bradbury, A. M.; Goodwin, P. M., A photophysical study of two fluorogen-activating proteins bound to their cognate fluorogens. *Proc. SPIE* **2011,** *7905* (Copyright (C) 2012 American Chemical Society (ACS). All Rights Reserved.), 79050O/1-79050O/10.
109. Peters, R.; Goh, J. B.; Dinglasan, J.; Thakur, A.; Shehata, S.; Anderson, D. J.; Fradin, C., Investigation into the photophysics and diffusion properties of water soluble quantum dots using fluorescence correlation spectroscopy. *ECS Trans.* **2010,** *28* (Copyright (C) 2012

American Chemical Society (ACS). All Rights Reserved.), 243-255.
110. Muddana, H. S.; Morgan, T. T.; Adair, J. H.; Butler, P. J., Photophysics of Cy3-Encapsulated Calcium Phosphate Nanoparticles. *Nano Lett.* **2009,** *9* (Copyright (C) 2012 American Chemical Society (ACS). All Rights Reserved.), 1559-1566.
111. Martynski, M.; Zydlewicz, J.; Boens, N.; Molski, A., Determination of photophysical parameters from photon arrival time trajectories in single molecule fluorescence spectroscopy. *J. Chem. Phys.* **2005,** *122* (Copyright (C) 2012 American Chemical Society (ACS). All Rights Reserved.), 134507/1-134507/6.
112. Kask, P.; Piksarv, P.; Mets, U., Fluorescence correlation spectroscopy in the nanosecond time range: photon antibunching in dye fluorescence. *Eur. Biophys. J.* **1985,** *12* (Copyright (C) 2012 American Chemical Society (ACS). All Rights Reserved.), 163-6.
113. Sykora, J.; Kaiser, K.; Gregor, I.; Boenigk, W.; Schmalzing, G.; Enderlein, J., Exploring Fluorescence Antibunching in Solution To Determine the Stoichiometry of Molecular Complexes. *Anal. Chem. (Washington, DC, U. S.)* **2007,** *79* (Copyright (C) 2012 American Chemical Society (ACS). All Rights Reserved.), 4040-4049.
114. Allmeroth, M.; Moderegger, D.; Biesalski, B.; Koynov, K.; Roesch, F.; Thews, O.; Zentel, R., Modifying the Body Distribution of HPMA-Based Copolymers by Molecular Weight and Aggregate Formation. *Biomacromolecules* **2011,** *12* (Copyright (C) 2012 American Chemical Society (ACS). All Rights Reserved.), 2841-2849.
115. Chen, J.; Nag, S.; Vidi, P.-A.; Irudayaraj, J., Single molecule in vivo analysis of Toll-like receptor 9 and CpG DNA interaction. *PLoS One* **2011,** *6* (Copyright (C) 2012 American Chemical Society (ACS). All Rights Reserved.), e17991.
116. He, H.-T.; Marguet, D., Detecting nanodomains in living cell membrane by fluorescence correlation spectroscopy. *Annu. Rev. Phys. Chem.* **2011,** *62* (Copyright (C) 2012 American Chemical Society (ACS). All Rights Reserved.), 417-436.
117. Malchus, N.; Weiss, M., Anomalous Diffusion Reports on the Interaction of Misfolded Proteins with the Quality Control Machinery in the Endoplasmic Reticulum. *Biophys. J.* **2010,** *99* (Copyright (C) 2012 American Chemical Society (ACS). All Rights Reserved.), 1321-1328.
118. Michelman-Ribeiro, A.; Mazza, D.; Rosales, T.; Stasevich, T. J.; Boukari, H.; Rishi, V.; Vinson, C.; Knutson, J. R.; McNally, J. G., Direct measurement of association and dissociation rates of DNA binding in live cells by fluorescence correlation spectroscopy. *Biophys. J.* **2009,** *97* (Copyright (C) 2012 American Chemical Society (ACS). All Rights Reserved.), 337-346.
119. Muetze, J.; Ohrt, T.; Petrasek, Z.; Schwille, P., In vivo Fluorescence Correlation and Cross-Correlation Spectroscopy. *Springer Ser. Chem. Phys.* **2010,** *96* (Copyright (C) 2012 American Chemical Society (ACS). All Rights Reserved.), 139-154.
120. Vukojevic, V.; Papadopoulos, D. K.; Terenius, L.; Gehring, W. J.; Rigler, R., Quantitative study of synthetic Hox transcription factor-DNA interactions in live cells. *Proc. Natl. Acad. Sci. U. S. A., Early Ed.* **2010,** (Copyright (C) 2012 American Chemical Society (ACS). All Rights Reserved.), 1-6, 6 pp.
121. Reznik, C.; Berg, R.; Foster, E.; Advincula, R.; Landes, C. F., Transient Three-Dimensional Orientation of Molecular Ions in an Ordered Polyelectrolyte Membrane. *Journal of Physical Chemistry Letters* **2011,** *2* (6), 592-598.
122. Reznik, C.; Estillore, N.; Advincula, R. C.; Landes, C. F., Single Molecule Spectroscopy

Reveals Heterogeneous Transport Mechanisms for Molecular Ions in a Polyelectrolyte Polymer Brush. *J. Phys. Chem. B* **2009,** *113* (44), 14611-14618.
123. Hess, S. T.; Webb, W. W., Focal Volume Optics and Experimental Artifacts in Confocal Fluorescence Correlation Spectroscopy. *Biophys. J.* **2002,** *83* (4), 2300-2317.
124. Sahoo, H.; Schwille, P., FRET and FCS-Friends or Foes? *ChemPhysChem* **2011,** *12* (Copyright (C) 2011 American Chemical Society (ACS). All Rights Reserved.), 532-541.
125. Kim, H. D.; Nienhaus, G. U.; Ha, T.; Orr, J. W.; Williamson, J. R.; Chu, S., Mg2+-dependent conformational change of RNA studied by fluorescence correlation and FRET on immobilized single molecules. *Proc. Natl. Acad. Sci. U. S. A.* **2002,** *99* (Copyright (C) 2012 American Chemical Society (ACS). All Rights Reserved.), 4284-4289.
126. Larson, D. R.; Ma, Y. M.; Vogt, V. M.; Webb, W. W., Direct measurement of Gag-Gag interaction during retrovirus assembly with FRET and fluorescence correlation spectroscopy. *J. Cell Biol.* **2003,** *162* (Copyright (C) 2012 American Chemical Society (ACS). All Rights Reserved.), 1233-1244.
127. Torres, T.; Levitus, M., Measuring Conformational Dynamics: A New FCS-FRET Approach. *J. Phys. Chem. B* **2007,** *111* (Copyright (C) 2012 American Chemical Society (ACS). All Rights Reserved.), 7392-7400.
128. Petersen, N. O.; Johnson, D. C.; Schlesinger, M. J., Scanning fluorescence correlation spectroscopy. II. Application to virus glycoprotein aggregation. *Biophys. J.* **1986,** *49* (Copyright (C) 2011 American Chemical Society (ACS). All Rights Reserved.), 817-20.
129. Petrasek, Z.; Schwille, P., Precise measurement of diffusion coefficients using scanning fluorescence correlation spectroscopy. *Biophys. J.* **2008,** *94* (4), 1437-1448.
130. Ries, J.; Klose, C.; Walch-Solimena, C.; Schwille, P., How to measure slow diffusion in yeast cell membranes. *Proceedings of SPIE* **2008,** *6991* (Biophotonics: Photonic Solutions for Better Health Care), 69910W/1-69910W/8.
131. Ries, J.; Schwille, P., Studying slow membrane dynamics with continuous wave scanning fluorescence correlation spectroscopy. *Biophys. J.* **2006,** *91* (Copyright (C) 2011 American Chemical Society (ACS). All Rights Reserved.), 1915-1924.
132. Ries, J.; Chiantia, S.; Schwille, P., Accurate determination of membrane dynamics with line-scan FCS. *Biophys. J.* **2009,** *96* (Copyright (C) 2011 American Chemical Society (ACS). All Rights Reserved.), 1999-2008.
133. Petrov, E. P.; Schwille, P., State of the art and novel trends in fluorescence correlation spectroscopy. *Springer Series on Fluorescence* **2008,** *6* (Standardization and Quality Assurance in Fluorescence Measurements II), 145-197.
134. Thompson Nancy, L.; Lieto Alena, M.; Allen Noah, W., Recent advances in fluorescence correlation spectroscopy. *Curr Opin Struct Biol FIELD Full Journal Title:Current opinion in structural biology* **2002,** *12* (5), 634-41.
135. Wiseman, P. W.; Squier, J. A.; Ellisman, M. H.; Wilson, K. R., Two-photon image correlation spectroscopy and image cross-correlation spectroscopy. *J. Microsc. (Oxford)* **2000,** *200* (Copyright (C) 2012 American Chemical Society (ACS). All Rights Reserved.), 14-25.
136. Wirth, M. J.; Ludes, M. D.; Swinton, D. J., Analytic solution to the autocorrelation function for lateral diffusion and rare strong adsorption. *Applied Spectroscopy* **2001,** *55* (6), 663-669.
137. Elson, E. L.; Magde, D., Fluorescence correlation spectroscopy. I. Conceptual basis

and theory. *Biopolymers* **1974,** *13* (Copyright (C) 2012 American Chemical Society (ACS). All Rights Reserved.), 1-27.
138. Magde, D.; Webb, W. W.; Elson, E. L., Fluorescence correlation spectroscopy. III. Uniform translation and laminar flow. *Biopolymers* **1978,** *17* (Copyright (C) 2012 American Chemical Society (ACS). All Rights Reserved.), 361-76.
139. De Santo, I.; Causa, F.; Netti, P. A., Subdiffusive Molecular Motion in Nanochannels Observed by Fluorescence Correlation Spectroscopy. *Analytical Chemistry (Washington, DC, United States)* **2010,** *82* (3), 997-1005.
140. Hoefling, F.; Bamberg, K.-U.; Franosch, T., Anomalous transport resolved in space and time by fluorescence correlation spectroscopy. *Soft Matter* **2011,** *7* (Copyright (C) 2012 American Chemical Society (ACS). All Rights Reserved.), 1358-1363.
141. Haustein, E.; Schwille, P., Ultrasensitive Investigations of Biological Systems by Fluorescence Correlation Spectroscopy. *Methods* **2003,** *29* (2), 153-166.
142. Tcherniak, A.; Reznik, C.; Link, S.; Landes, C. F., Fluorescence Correlation Spectroscopy: Criteria for Analysis in Complex Systems. *Anal. Chem. (Washington, DC, U. S.) FIELD Full Journal Title:Analytical Chemistry (Washington, DC, United States)* **2009,** *81* (2), 746-754.
143. Roder, F.; Waichman, S.; Paterok, D.; Schubert, R.; Richter, C.; Liedberg, B.; Piehler, J., Reconstitution of Membrane Proteins into Polymer-Supported Membranes for Probing Diffusion and Interactions by Single Molecule Techniques. *Anal. Chem. (Washington, DC, U. S.)* **2011,** *83* (Copyright (C) 2012 American Chemical Society (ACS). All Rights Reserved.), 6792-6799.
144. Koppel, D. E.; Axelrod, D.; Schlessinger, J.; Elson, E. L.; Webb, W. W., Dynamics of fluorescence marker concentration as a probe of mobility. *Biophys. J. FIELD Full Journal Title:Biophysical Journal* **1976,** *16* (11), 1315-29.
145. Qian, H.; Elson, E. L., Analysis of confocal laser-microscope optics for 3-D fluorescence correlation spectroscopy. *Appl. Opt. FIELD Full Journal Title:Applied Optics* **1991,** *30* (10), 1185-95.
146. Haustein, E.; Schwille, P., Fluorescence Correlation Spectroscopy: Novel Variations of an Established Technique. *Annual Review of Biophysics and Biomolecular Structure* **2007,** *36* (1), 151-169.
147. Eggeling, C.; Fries, J. R.; Brand, L.; Gunther, R.; Seidel, C. A. M., Monitoring Conformational Dynamics of a Single Molecule by Selective Fluorescence Spectroscopy. *Proceedings of the National Academy of Sciences of the United States of America* **1998,** *95* (4), 1556-1561.
148. Osborne, M. A.; Balasubramanian, S.; Furey, W. S.; Klenerman, D., Optically Biased Diffusion of Single Molecules Studied by Confocal Fluorescence Microscopy. *J. Phys. Chem. B FIELD Full Journal Title:Journal of Physical Chemistry B* **1998,** *102* (17), 3160-3167.
149. Schmidt, T.; Schuetz, G. J.; Baumgartner, W.; Gruber, H. J.; Schindler, H., Characterization of Photophysics and Mobility of Single Molecules in a Fluid Lipid Membrane. *J. Phys. Chem.* **1995,** *99* (49), 17662-17668.
150. Wennmalm, S.; Edman, L.; Rigler, R., Conformational Fluctuations in Single DNA Molecules. *Proceedings of the National Academy of Sciences of the United States of America* **1997,** *94* (20), 10641-10646.
151. Wennmalm, S.; Edman, L.; Rigler, R., Non-ergodic behaviour in conformational

transitions of single DNA molecules. *Chemical Physics* **1999,** *247* (1), 61-67.
152. Morel, F.; Hering, J., *Principles and Applications of Aquatic Chemistry*. John Wiley and Sons: New York, 1993; p 588.
153. Stumm, W.; Morgan, J. J., *Aquatic Chemistry: Chemical Equilibria and Rates in Natural Waters*. 3rd ed.; John Wiley and Sons: New York, 1993; p 1022.
154. Helt, J. M.; Batteas, J. D., Wear of Mica under Aqueous Environments:Direct Observation of Defect Nucleation by AFM. *Langmuir* **2005,** *21* (2), 633-639.
155. Suni, T.; Henttinen, K.; Suni, I.; Maekinen, J., Effects of plasma activation on hydrophilic bonding of Si and SiO2. *Proc. - Electrochem. Soc. FIELD Full Journal Title:Proceedings - Electrochemical Society* **2002,** *2001-27* (Semiconductor Wafer Bonding), 22-30.
156. Feng, J.; Wong, K.-Y.; Dyer, K.; Pettitt, B. M., Transport properties of water at functionalized molecular interfaces. *J. Chem. Phys.* **2009,** *131* (12), 125102/1-125102/8.
157. Hopkins, A. J.; McFearin, C. L.; Richmond, G. L., Investigations of the solid-aqueous interface with vibrational sum-frequency spectroscopy. *Curr. Opin. Solid State Mater. Sci. FIELD Full Journal Title:Current Opinion in Solid State & Materials Science* **2006,** *9* (1-2), 19-27.
158. Harpham, M. R.; Ladanyi, B. M.; Levinger, N. E.; Herwig, K. W., Water motion in reverse micelles studied by quasielastic neutron scattering and molecular dynamics simulations. *J. Chem. Phys. FIELD Full Journal Title:Journal of Chemical Physics* **2004,** *121* (16), 7855-7868.
159. Scodinu, A.; Fourkas, J. T., Comparison of the orientational dynamics of water confined in hydrophobic and hydrophilic nanopores. *J. Phys. Chem. B* **2002,** *106* (40), 10292-10295.
160. Ha, T.; Enderle, T.; Chemla, D. S.; Selvin, P. R.; Weiss, S., Single molecular dynamics studied by polarization modulation. *Phys. Rev. Lett. FIELD Full Journal Title:Physical Review Letters* **1996,** *77* (19), 3979-3982.
161. Ha, T.; Glass, J.; Enderle, T.; Chemla, D. S.; Weiss, S., Hindered Rotational Diffusion and Rotational Jumps of Single Molecules. *Physical Review Letters* **1998,** *80* (10), 2093-2096.
162. Osborne, M. A.; Barnes, C. L.; Balasubramanian, S.; Klenerman, D., Probing DNA Surface Attachment and Local Environment Using Single Molecule Spectroscopy. *J. Phys. Chem. B* **2001,** *105* (15), 3120-3126.
163. Southern, E. M., K.; Shchepinov, M., Molecular Interactions on Microarrays. *Nature Genetics* **1999,** *21* (1s), 5.
164. Bacia, K.; Schwille, P., Practical guidelines for dual-color fluorescence cross-correlation spectroscopy. *Nat. Protoc. FIELD Full Journal Title:Nature Protocols* **2007,** *2* (11), 2842-2856.
165. Bacia, K.; Schwille, P., Fluorescence correlation spectroscopy. *Methods Mol. Biol. (Totowa, NJ, U. S.) FIELD Full Journal Title:Methods in Molecular Biology (Totowa, NJ, United States)* **2007,** *398* (Lipid Rafts), 73-84.
166. Dertinger, T.; Pacheco, V.; von der Hocht, I.; Hartmann, R.; Gregor, I.; Enderlein, J., Two-focus fluorescence correlation spectroscopy: a new tool for accurate and absolute diffusion measurements. *ChemPhysChem FIELD Full Journal Title:ChemPhysChem* **2007,** *8* (3), 433-443.

167. Loman, A.; Dertinger, T.; Koberling, F.; Enderlein, J., Comparison of optical saturation effects in conventional and dual-focus fluorescence correlation spectroscopy. *Chem. Phys. Lett. FIELD Full Journal Title:Chemical Physics Letters* **2008,** *459* (1-6), 18-21.
168. Petrasek, Z.; Schwille, P., Precise measurement of diffusion coefficients using scanning fluorescence correlation spectroscopy. *Biophys. J. FIELD Full Journal Title:Biophysical Journal* **2008,** *94* (4), 1437-1448.
169. Petrov, E. P.; Schwille, P., State of the art and novel trends in fluorescence correlation spectroscopy. *Springer Ser. Fluoresc. FIELD Full Journal Title:Springer Series on Fluorescence* **2008,** *6* (Standardization and Quality Assurance in Fluorescence Measurements II), 145-197.
170. Reznik, C.; Darugar, Q.; Wheat, A.; Fulghum, T.; Advincula, R. C.; Landes, C. F., Single Ion Diffusive Transport within a Poly(styrene sulfonate) Polymer Brush Matrix Probed by Fluorescence Correlation Spectroscopy. *J. Phys. Chem. B FIELD Full Journal Title:Journal of Physical Chemistry B* **2008,** *112* (35), 10890-10897.
171. Haustein, E.; Schwille, P., Fluorescence correlation spectrosocpy in vitro and in vivo. *Single-Mol. Tech. FIELD Full Journal Title:Single-Molecule Techniques* **2008**, 259-278.
172. Kim, S. A.; Heinze, K. G.; Schwille, P., Fluorescence correlation spectroscopy in living cells. *Nat. Methods FIELD Full Journal Title:Nature Methods* **2007,** *4* (11), 963-973.
173. Petrasek, Z.; Schwille, P., Photobleaching in two-photon scanning fluorescence correlation spectroscopy. *ChemPhysChem FIELD Full Journal Title:ChemPhysChem* **2008,** *9* (1), 147-158.
174. Reznik, C. R.; Estillore, N.; Advincula, R. C.; Landes, C. F., Single Molecule Spectroscopy Reveals Heterogeneous Transport Mechanisms for Molecular Ions in a Polyelectrolyte Polymer Brush. *in press* **2009**.
175. Ries, J.; Klose, C.; Walch-Solimena, C.; Schwille, P., How to measure slow diffusion in yeast cell membranes. *Proc. SPIE FIELD Full Journal Title:Proceedings of SPIE* **2008,** *6991* (Biophotonics: Photonic Solutions for Better Health Care), 69910W/1-69910W/8.
176. Sanabria, H.; Kubota, Y.; Waxham, M. N., Multiple diffusion mechanisms due to nanostructuring in crowded environments. *Biophys. J. FIELD Full Journal Title:Biophysical Journal* **2007,** *92* (1), 313-322.
177. Ye, F.; Higgins, D. A.; Collinson, M. M., Probing Chemical Interactions at the Single-Molecule Level in Mesoporous Silica Thin Films. *Journal of Physical Chemistry C* **2007,** *111* (18), 6772-6780.
178. Enderlein, J., Gregor, I., Patra, D., Dertinger, T., Kaupp, U. B., Performance of Fluorescence Correlation Spectroscopy for Measuring Diffusion and Concentration. *ChemPhysChem* **2005,** *6* (11), 2324-2336.
179. Enderlein, J.; Gregor, I.; Patra, D.; Fitter, J., Art and artefacts of fluorescence correlation spectroscopy. *Curr. Pharm. Biotechnol. FIELD Full Journal Title:Current Pharmaceutical Biotechnology* **2004,** *5* (2), 155-161.
180. Avnir, D.; Levy, D.; Reisfeld, R., The nature of the silica cage as reflected by spectral changes and enhanced photostability of trapped Rhodamine 6G. *J. Phys. Chem. FIELD Full Journal Title:Journal of Physical Chemistry* **1984,** *88* (24), 5956-9.
181. Boutin, C.; Plain, J.; Jaffiol, R.; Deturche, R.; Royer, P., Dye-substrate interactions evidenced by fluorescence correlation spectroscopy. *Annales de Physique (Paris, France)* **2007,** *32* (2-3), 143-145.

182. Chen, Z.; Tang, Y.; Xie, T.; Chen, Y.; Li, Y., Fluorescence Spectral Properties of Rhodamine 6G at the Silica/Water Interface. *Journal of Fluorescence* **2008,** *18* (1), 93-100.
183. Schuster, J.; Cichos, F.; Wrachtrup, J.; von Borczyskowski, C., Diffusion of Single Molecules Close to Interfaces. *Single Molecules* **2000,** *1* (4), 299-305.
184. Weber, M. A.; Stracke, F.; Meixner, A. J., Dynamics of Single Dye Molecules Observed by Confocal Imaging and Spectroscopy. *Cytometry* **1999,** *36* (3), 217-223.
185. Zheng, X.; Harata, A.; Ogawa, T., Study of the Adsorptive Behavior of Water-Soluble Dye Molecules (Rhodamine 6G) at the Air-Water Interface using Confocal Fluorescence Microscope. *Spectrochimica Acta* **2001,** *57A* (2), 315-322.
186. Zheng, X.; Wachi, M.; Harata, A.; Hatano, Y., Acidity Effects on the Fluorescence Properties and Adsorptive Behaviorof Rhodamine 6G Molecules at the Air-Water Interface Studied with Confocal Fluorescence Microscopy. *Spectrochimica Acta* **2004,** *60A* (5), 1085-1090.
187. Nie, S.; Chiu, D. T.; Zare, R. N., Probing individual molecules with confocal fluorescence microscopy. *Science (Washington, D. C.) FIELD Full Journal Title:Science (Washington, D. C.)* **1994,** *266* (5187), 1018-21.
188. Gell, C.; Brockwell, D. J.; Beddard, G. S.; Radford, S. E.; Kalverda, A. P.; Smith, D. A., Accurate use of single molecule fluorescence correlation spectroscopy to determine molecular diffusion times. *Single Mol. FIELD Full Journal Title:Single Molecules* **2001,** *2* (3), 177-181.
189. Meseth, U.; Wohland, T.; Rigler, R.; Vogel, H., Resolution of fluorescence correlation measurements. *Biophys. J. FIELD Full Journal Title:Biophysical Journal* **1999,** *76* (3), 1619-1631.
190. Parks, G. A., The isoelectric points of solid oxides, solid hydroxides, and aqueous hydroxo complex systems. *Chem. Rev. FIELD Full Journal Title:* **1965,** *65* (2), 177-98.
191. Bedzyk, M. J.; Bommarito, G. M.; Caffrey, M.; Penner, T. L., Diffuse-double layer at a membrane-aqueous interface measured with x-ray standing waves. *Science (Washington, D. C., 1883-) FIELD Full Journal Title:Science (Washington, DC, United States)* **1990,** *248* (4951), 52-6.
192. Hansen, R. L.; Harris, J. M., Total internal reflection fluorescence correlation spectroscopy for counting molecules at solid/liquid interfaces. *Anal. Chem. FIELD Full Journal Title:Analytical Chemistry* **1998,** *70* (13), 2565-2575.
193. Wirth, M. J.; Swinton, D. J., Single-molecule spectroscopy and fluorescence correlation spectroscopy of the lateral transport of the T3 promoter primer at a chemical interface. *Applied Spectroscopy* **2001,** *55* (8), 1013-1017.
194. Aguilar, G. A.; Hiza, R. J. Extreme-pressure additives for lubricating greases containing thiadiazoles, polyoxyalkylenes, and metal dithiophosphates. 2008-332891

2009156444, 20081211., 2009.
195. Hoffman, A. S., Non-Fouling Surface Technologies. *Journal of Biomaterial Science: Polymer Edition* **1999,** *10* (10), 1011-1014.
196. Brash, J. L.; Horbett, T. A., Proteins at interfaces. An overview. *ACS Symp. Ser. FIELD Full Journal Title:ACS Symposium Series* **1995,** *602* (Proteins at Interfaces 2), 1-23.
197. Ostuni, E.; Chapman, R. G.; Holmlin, R. E.; Takayama, S.; Whitesides, G. M., A Survey of Structure-Property Relationships of Surfaces that Resist the Adsorption of Protein. *Langmuir FIELD Full Journal Title:Langmuir* **2001,** *17* (18), 5605-5620.

198. Jeon, S. I.; Andrade, J. D., Protein-surface interactions in the presence of polyethylene oxide. II. Effect of protein size. *J. Colloid Interface Sci.* **1991,** *142* (1), 159-66.
199. Jeon, S. I.; Lee, J. H.; Andrade, J. D.; De Gennes, P. G., Protein-surface interactions in the presence of polyethylene oxide. I. Simplified theory. *J. Colloid Interface Sci.* **1991,** *142* (1), 149-58.
200. Feldman, K.; Haehner, G.; Spencer, N. D.; Harder, P.; Grunze, M., Probing Resistance to Protein Adsorption of Oligo(ethylene glycol)-Terminated Self-Assembled Monolayers by Scanning Force Microscopy. *J. Am. Chem. Soc.* **1999,** *121* (43), 10134-10141.
201. Ramsden, J. J.; Roush, D. J.; Gill, D. S.; Kurrat, R.; Willson, R. C., Protein Adsorption Kinetics Drastically Altered by Repositioning a Single Charge. *J. Am. Chem. Soc.* **1995,** *117* (Copyright (C) 2011 American Chemical Society (ACS). All Rights Reserved.), 8511-16.
202. Brooks, D. E.; Haynes, C. A.; Hritcu, D.; Steels, B. M.; Muller, W., Size exclusion chromatography does not require pores. *Proc. Natl. Acad. Sci. U. S. A.* **2000,** *97* (Copyright (C) 2011 American Chemical Society (ACS). All Rights Reserved.), 7064-7067.
203. Knotts, T. A. I. V.; Rathore, N.; de Pablo, J. J., An entropic perspective of protein stability on surfaces. *Biophys. J.* **2008,** *94* (11), 4473-4483.
204. Hamilton-Brown, P.; Gengenbach, T.; Griesser, H. J.; Meagher, L., End Terminal, Poly(ethylene oxide) Graft Layers: Surface Forces and Protein Adsorption. *Langmuir* **2009,** *25* (16), 9149-9156.
205. Prime, K. L.; Whitesides, G. M., Adsorption of proteins onto surfaces containing end-attached oligo(ethylene oxide): a model system using self-assembled monolayers. *J. Am. Chem. Soc.* **1993,** *115* (23), 10714-21.
206. Sharma, S.; Johnson, R. W.; Desai, T. A., XPS and AFM analysis of antifouling PEG interfaces for microfabricated silicon biosensors. *Biosensors & Bioelectronics* **2004,** *20* (2), 227-239.
207. Wach, J.-Y.; Malisova, B.; Bonazzi, S.; Tosatti, S.; Textor, M.; Zurcher, S.; Gademann, K., Protein-resistant surfaces through mild dopamine surface functionalization. *Chemistry--A European Journal* **2008,** *14* (34), 10579-10584.
208. Benhabbour, S. R.; Liu, L.; Sheardown, H.; Adronov, A., Protein Resistance of Surfaces Prepared by Chemisorption of Monothiolated Poly(ethylene glycol) to Gold and Dendronization with Aliphatic Polyester Dendrons: Effect of Hydrophilic Dendrons. *Macromolecules (Washington, DC, U. S.)* **2008,** *41* (7), 2567-2576.
209. Inoue, Y.; Ishihara, K., Reduction of protein adsorption on well-characterized polymer brush layers with varying chemical structures. *Colloids and Surfaces, B: Biointerfaces* **2010,** *81* (1), 350-357.
210. Yang, H.; Shin, K.; Tae, G.; Satija, S. K., Structure of a monolayer of poly(ethylene glycol) end-capped with a fluoroalkyl group and its relationship with protein adsorption at the aqueous interface. *Soft Matter* **2009,** *5* (14), 2731-2737.
211. Advincula, R. C.; Brittain, W. J.; Baster, K. C.; Ruhe, J., *Polymer Brushes: Synthesis, Characterization, Applications*. 2004; p 483 pp.
212. Harbers, G. M.; Emoto, K.; Greef, C.; Metzger, S. W.; Woodward, H. N.; Mascali, J. J.; Grainger, D. W.; Lochhead, M. J., Functionalized Polyethylene Glycol-Based Bioassay Surface Chemistry that Facilitates Bio-Immobilization and Inhibits Nonspecific Protein, Bacterial, and Mammalian Cell Adhesion. *Chemistry of Materials* **2007,** *19* (18), 4405-4414.
213. Ju, H.; McCloskey, B. D.; Sagle, A. C.; Kusuma, V. A.; Freeman, B. D., Preparation and

characterization of crosslinked poly(ethylene glycol) diacrylate hydrogels as fouling-resistant membrane coating materials. *Journal of Membrane Science* **2009,** *330* (1+2), 180-188.
214. Liu, S. X.; Kim, J.-T.; Kim, S.; Singh, M., The effect of polymer surface modification via interfacial polymerization on polymer-protein interaction. *Journal of Applied Polymer Science* **2009,** *112* (3), 1704-1715.
215. Zhu, B.; Eurell, T.; Gunawan, R.; Leckband, D., Chain-length dependence of the protein and cell resistance of oligo(ethylene glycol)-terminated self-assembled monolayers on gold. *Journal of Biomedical Materials Research* **2001,** *56* (3), 406-416.
216. Vanderah, D. J.; Vierling, R. J.; Walker, M. L., Oligo(ethylene oxide) Self-Assembled Monolayers with Self-Limiting Packing Densities for the Inhibition of Nonspecific Protein Adsorption. *Langmuir* **2009,** *25* (Copyright (C) 2011 American Chemical Society (ACS). All Rights Reserved.), 5026-5030.
217. Vanderah, D. J.; La, H.; Naff, J.; Silin, V.; Rubinson, K. A., Control of Protein Adsorption: Molecular Level Structural and Spatial Variables. *J. Am. Chem. Soc.* **2004,** *126* (42), 13639-13641.
218. Li, L.; Chen, S.; Zheng, J.; Ratner, B. D.; Jiang, S., Protein Adsorption on Oligo(ethylene glycol)-Terminated Alkanethiolate Self-Assembled Monolayers: The Molecular Basis for Nonfouling Behavior. *J. Phys. Chem. B* **2005,** *109* (7), 2934-2941.
219. Yeh, P.-Y.; Kainthan, R. K.; Zou, Y.; Chiao, M.; Kizhakkedathu, J. N., Self-Assembled Monothiol-Terminated Hyperbranched Polyglycerols on a Gold Surface: A Comparative Study on the Structure, Morphology, and Protein Adsorption Characteristics with Linear Poly(ethylene glycol)s. *Langmuir* **2008,** *24* (9), 4907-4916.
220. Heyes Colin, D.; Groll, J.; Moller, M.; Nienhaus, G. U., Synthesis, patterning and applications of star-shaped poly(ethylene glycol) biofunctionalized surfaces. *Mol Biosyst* **2007,** *3* (6), 419-30.
221. Daniels, C. R.; Reznik, C.; Landes, C. F., Dye Diffusion at Surfaces: Charge Matters. *Langmuir* **2010,** *26* (7), 4807-4812.
222. Wang, S.; Zhu, Y., Molecular diffusion on surface tethered polymer layers: coupling of molecular thermal fluctuation and polymer chain dynamics. *Soft Matter* **2010,** *6* (19), 4661-4665.
223. Felipe, M. J.; Ponnapati, R.; Pernites, R.; Dutta, P.; Advincula, R., Synthesis and Electrografting of Dendron Anchored OEGylated Surfaces and their Protein Adsorption Resistance. *ACS Applied Materials and Interfaces* **2010,** *2* (12), 3401-3405.
224. Kaewtong, C.; Jiang, G.; Felipe, M. J.; Pulpoka, B.; Advincula, R., Self-Assembly and Electrochemical Oxidation of Polyamidoamine-Carbazole Dendron Surfmer Complexes: Nanoring Formation. *ACS Nano* **2008,** *2* (8), 1533-1542.
225. Taranekar, P.; Fulghum, T.; Patton, D.; Ponnapati, R.; Clyde, G.; Advincula, R., Investigating Carbazole Jacketed Precursor Dendrimers: Sonochemical Synthesis, Characterization, and Electrochemical Crosslinking Properties. *J. Am. Chem. Soc.* **2007,** *129* (41), 12537-12548.
226. Felipe, M. J.; Ponnapati, R.; Pernites, R.; Dutta, P.; Advincula, R., Synthesis and Electrografting of Dendron Anchored OEGylated Surfaces and their Protein Adsorption Resistance. *ACS Applied Materials and Interfaces* **2010**, submitted.
227. Kreuzer, H. J.; Wang, R. L. C.; Grunze, M., Hydroxide Ion Adsorption on Self-

Assembled Monolayers. *J. Am. Chem. Soc.* **2003,** *125* (Copyright (C) 2011 American Chemical Society (ACS). All Rights Reserved.), 8384-8389.
228. Rubinson, K. A.; Krueger, S., Poly(ethylene glycol)s 2000-8000 in water may be planar: A small-angle neutron scattering (SANS) structure study. *Polymer* **2009,** *50* (20), 4852-4858.
229. Capuano, F.; Vergara, A.; Paduano, L.; Annunziata, O.; Sartorio, R., Electrostatic and Excluded Volume Effects on the Transport of Electrolytes in Poly(ethylene glycol)−Water "Mixed Solvents". *The Journal of Physical Chemistry B* **2003,** *107* (44), 12363-12369.
230. Tan, C.; Albright, J. G.; Annunziata, O., Determination of Preferential Interaction Parameters by Multicomponent Diffusion. Applications to Poly(ethylene glycol)−Salt−Water Ternary Mixtures. *The Journal of Physical Chemistry B* **2008,** *112* (16), 4967-4974.
231. Misra, V.; Mishra, H.; Joshi, H. C.; Pant, T. C., Excitation energy transfer between acriflavine and rhodamine 6G as a pH sensor. *Sensors and Actuators B: Chemical* **2000,** *63* (1-2), 18-23.
232. Panchuk-Voloshina, N.; Haugland, R. P.; Bishop-Stewart, J.; Bhalgat, M. K.; Millard, P. J.; Mao, F.; Leung, W.; Haugland, R. P., Alexa Dyes, a Series of New Fluorescent Dyes that Yield Exceptionally Bright, Photostable Conjugates. *The Journal of Histochemistry & Cytochemistry* **1999,** *47* (9), 1179-1188.
233. Ustinov, A. N.; Afanas'ev, V. N., Quantitative characteristics of hydration in solutions of sodium sulfate and sodium chloride at 278.15-323.15 K. *Zhurnal Neorganicheskoi Khimii* **2008,** *53* (5), 882-889.
234. Azam, S. S.; Zaheer-ul-Haq; Fatmi, M. Q., Classical and QM/MM MD Simulations of Sodium(I) and Potassium(I) Ions in Aqueous Solution. *Journal of Molecular Liquids* **2010,** *153* (2-3), 95-100.
235. Balasubramanian, D.; Chandani, B., Poly(ethylene glycol): a poor chemist's crown. *Journal of Chemical Education* **1983,** *60* (Copyright (C) 2011 American Chemical Society (ACS). All Rights Reserved.), 77-8.
236. Ono, K.; Konami, H.; Murakami, K., Conductometric studies of ion binding to poly(oxyethylene) in methanol. *J. Phys. Chem.* **1979,** *83* (Copyright (C) 2011 American Chemical Society (ACS). All Rights Reserved.), 2665-9.
237. Hakem, I. F.; Lal, J.; Bockstaller, M. R., Binding of Monovalent Ions to PEO in Solution: Relevant Parameters and Structural Transitions. *Macromolecules* **2004,** *37* (22), 8431-8440.
238. Schlapak, R.; Armitage, D.; Saucedo-Zeni, N.; Hohage, M.; Howorka, S., Dense Passivating Poly(ethylene glycol) Films on Indium Tin Oxide Substrates. *Langmuir* **2007,** *23* (20), 10244-10253.
239. Blom, H.; Chmyrov, A.; Hassler, K.; Davis, L. M.; Widengren, J., Triplet-state investigations of fluorescent dyes at dielectric interfaces using total internal reflection fluorescence correlation spectroscopy. *Journal of Physical Chemistry A* **2009,** *113* (19), 5554-5566.
240. Blom, H.; Hassler, K.; Chmyrov, A.; Widengren, J., Electrostatic interactions of fluorescent molecules with dielectric interfaces studied by Total Internal Reflection Fluorescence Correlation Spectroscopy. *International Journal of Molecular Sciences* **2010,** *11*, 386-406.

241. Zhang, Z.; Ma, H.; Hausner, D. B.; Chilkoti, A.; Beebe, T. P., Jr., Pretreatment of Amphiphilic Comb Polymer Surfaces Dramatically Affects Protein Adsorption. *Biomacromolecules* **2005,** *6* (6), 3388-3396.
242. Kubota, N.; Miura, S.; Saito, K.; Sugita, K.; Watanabe, K.; Sugo, T., Comparison of protein adsorption by anion-exchange interaction onto porous hollow-fiber membrane and gel bead-packed bed. *Journal of Membrane Science* **1996,** *117* (Copyright (C) 2011 American Chemical Society (ACS). All Rights Reserved.), 135-142.
243. Mueller, W., New ion exchangers for the chromatography of biopolymers. *J. Chromatogr.* **1990,** *510* (Copyright (C) 2011 American Chemical Society (ACS). All Rights Reserved.), 133-40.
244. Chen, W.-h.; Fu, J. Y.; Kourentzi, K.; Willson, R. C., Nucleic acid affinity of clustered-charge anion exchange adsorbents: Effects of ionic strength and ligand density. *J. Chromatogr., A* **2011,** *1218* (Copyright (C) 2012 American Chemical Society (ACS). All Rights Reserved.), 258-262.
245. Cano, T.; Offringa, N. D.; Willson, R. C., Competitive ion-exchange adsorption of proteins: Competitive isotherms with controlled competitor concentration. *J. Chromatogr., A* **2005,** *1079* (Copyright (C) 2012 American Chemical Society (ACS). All Rights Reserved.), 116-126.
246. Jennissen, H. P.; Heilmeyer, L. M. G., Jr., General aspects of hydrophobic chromatography. Adsorption and elution characteristics of some skeletal muscle enzymes. *Biochemistry* **1975,** *14* (Copyright (C) 2011 American Chemical Society (ACS). All Rights Reserved.), 754-60.
247. Gon, S.; Santore, M. M., Single Component and Selective Competitive Protein Adsorption in a Patchy Polymer Brush: Opposition between Steric Repulsions and Electrostatic Attractions. *Langmuir* **2011,** *27* (Copyright (C) 2011 American Chemical Society (ACS). All Rights Reserved.), 1487-1493.
248. Reichert, U.; Linden, T.; Belfort, G.; Kula, M.-R.; Thommes, J., Visualizing protein adsorption to ion-exchange membranes by confocal microscopy. *Journal of Membrane Science* **2002,** *199* (Copyright (C) 2011 American Chemical Society (ACS). All Rights Reserved.), 161-166.
249. Wang, Z.; Yang, S., Adsorption Behaviors of DPPC/MO Aggregates on SiO2 Surfaces. *Langmuir FIELD Full Journal Title:Langmuir* **2008,** *24* (20), 11616-11624.
250. Yang, K.; Shi, Q.-H.; Sun, Y., Modeling and simulation of protein uptake in cation exchanger visualized by confocal laser scanning microscopy. *J. Chromatogr., A* **2006,** *1136* (Copyright (C) 2011 American Chemical Society (ACS). All Rights Reserved.), 19-28.
251. Harinarayan, C.; Mueller, J.; Ljunglof, A.; Fahrner, R.; Van, A. J.; van, R. R., An exclusion mechanism in ion exchange chromatography. *Biotechnol. Bioeng.* **2006,** *95* (Copyright (C) 2011 American Chemical Society (ACS). All Rights Reserved.), 775-787.
252. Wirth, M. J.; Swinton, D. J.; Ludes, M. D., Adsorption and Diffusion of Single Molecules at Chromatographic Interfaces. *J. Phys. Chem. B* **2003,** *107* (Copyright (C) 2011 American Chemical Society (ACS). All Rights Reserved.), 6258-6268.
253. Schirmer, E. B.; Carta, G., Protein adsorption kinetics in charged agarose gels: effect of agarose content and modeling. *AIChE J.* **2008,** *55* (Copyright (C) 2011 American Chemical Society (ACS). All Rights Reserved.), 331-341.
254. Boyd, G. E.; Adamson, A. W.; Myers, L. S., Jr., The exchange adsorption of ions from

aqueous solutions by organic zeolites. II. Kinetics. *J. Am. Chem. Soc.* **1947,** *69* (Copyright (C) 2011 American Chemical Society (ACS). All Rights Reserved.), 2836-48.
255. Isailovic, S.; Li, H.-W.; Yeung, E. S., Adsorption of single DNA molecules at the water/fused-silica interface. *J. Chromatogr., A* **2007,** *1150* (Copyright (C) 2012 American Chemical Society (ACS). All Rights Reserved.), 259-266.
256. Kang, S. H.; Shortreed, M. R.; Yeung, E. S., Real-Time dynamics of single-DNA molecules undergoing adsorption and desorption at liquid-solid interfaces. *Anal. Chem.* **2001,** *73* (Copyright (C) 2012 American Chemical Society (ACS). All Rights Reserved.), 1091-1099.
257. Kang, S. H.; Yeung, E. S., Dynamics of single-protein molecules at a liquid/solid interface: Implications in capillary electrophoresis and chromatography. *Anal. Chem.* **2002,** *74* (Copyright (C) 2012 American Chemical Society (ACS). All Rights Reserved.), 6334-6339.
258. Xu, X.-H. N.; Yeung, E. S., Long-range electrostatic trapping of single-protein molecules at a liquid-solid interface. *Science (Washington, D. C.)* **1998,** *281* (Copyright (C) 2012 American Chemical Society (ACS). All Rights Reserved.), 1650-1653.
259. Daniels, C. R.; Reznik, C. G.; Landes, C. F., Permeability of anti-fouling PEGylated surfaces probed by fluorescence correlation spectroscopy. *Colloids and Surfaces B: Biointerfaces* **2011,** *88* (1), 33-38.
260. Afanassiev, V.; Hanemann, V.; Wolfl, S., Preparation of DNA and protein micro arrays on glass slides coated with an agarose film. *Nucleic Acids Research* **2000,** *28* (Copyright (C) 2011 American Chemical Society (ACS). All Rights Reserved.), e66, ii-v.
261. Berland, K. M.; So, P. T. C.; Chen, Y.; Mantulin, W. W.; Gratton, E., Scanning two-photon fluctuation correlation spectroscopy: particle counting measurements for detection of molecular aggregation. *Biophys. J.* **1996,** *71* (Copyright (C) 2011 American Chemical Society (ACS). All Rights Reserved.), 410-420.
262. Ajikumar, P. K.; Ng, J. K.; Tang, Y. C.; Lee, J. Y.; Stephanopoulos, G.; Too, H.-P., Carboxyl-Terminated Dendrimer-Coated Bioactive Interface for Protein Microarray: High-Sensitivity Detection of Antigen in Complex Biological Samples. *Langmuir* **2007,** *23* (Copyright (C) 2010 American Chemical Society (ACS). All Rights Reserved.), 5670-5677.
263. Xavier, K. A.; Shick, K. A.; Smith-Gill, S. J.; Willson, R. C., Involvement of water molecules in the association of monoclonal antibody HyHEL-5 with bobwhite quail lysozyme. *Biophys. J.* **1997,** *73* (Copyright (C) 2012 American Chemical Society (ACS). All Rights Reserved.), 2116-2125.
264. Berk, D. A.; Yuan, F.; Leunig, M.; Jain, R. K., Fluorescence photobleaching with spatial Fourier analysis: measurement of diffusion in light-scattering media. *Biophys. J.* **1993,** *65* (Copyright (C) 2011 American Chemical Society (ACS). All Rights Reserved.), 2428-36.
265. Langford, J. F.; Schure, M. R.; Yao, Y.; Maloney, S. F.; Lenhoff, A. M., Effects of pore structure and molecular size on diffusion in chromatographic adsorbents. *J Chromatogr A* **2006,** *1126* (Copyright (C) 2011 U.S. National Library of Medicine.), 95-106.
266. Yao, Y.; Czymmek, K. J.; Pazhianur, R.; Lenhoff, A. M., Three-Dimensional Pore Structure of Chromatographic Adsorbents from Electron Tomography. *Langmuir* **2006,** *22* (Copyright (C) 2011 American Chemical Society (ACS). All Rights Reserved.), 11148-11157.
267. Fernandez-Sousa, J. M.; Perez-Castells, R.; Rodriguez, R., A simple, one-step chromatographic procedure for the purification of lysozyme. *Biochim. Biophys. Acta,*

Enzymol. **1978,** *523* (Copyright (C) 2011 American Chemical Society (ACS). All Rights Reserved.), 430-4.
268. Fernandez-Sousa, J. M.; Rodriguez, R., Lysozyme-agarose interaction. *Biochem. Biophys. Res. Commun.* **1977,** *74* (Copyright (C) 2011 American Chemical Society (ACS). All Rights Reserved.), 1426-31.
269. Qasba, P. K.; Kumar, S., Molecular divergence of lysozymes and α-lactalbumin. *Crit. Rev. Biochem. Mol. Biol.* **1997,** *32* (Copyright (C) 2011 American Chemical Society (ACS). All Rights Reserved.), 255-306, 5 plates.
270. Acharya, K. R.; Stuart, D. I.; Walker, N. P. C.; Lewis, M.; Phillips, D. C., Refined structure of baboon α-lactalbumin at 1.7 Å resolution. Comparison with C-type lysozyme. *Journal of Molecular Biology* **1989,** *208* (Copyright (C) 2011 American Chemical Society (ACS). All Rights Reserved.), 99-127.
271. Pluen, A.; Netti, P. A.; Jain, R. K.; Berk, D. A., Diffusion of macromolecules in agarose gels: Comparison of linear and globular configurations. *Biophys. J.* **1999,** *77* (Copyright (C) 2011 American Chemical Society (ACS). All Rights Reserved.), 542-552.
272. Layman, J. M.; Hirani, A. A.; Hunley, M. T.; Lee, Y. W.; Lepene, B.; Thatcher, C. D.; Long, T. E., Macromolecules with tailored non-covalent interactions for biomedical applications. *PMSE Prepr.* **2007,** *96* (Copyright (C) 2012 American Chemical Society (ACS). All Rights Reserved.), 325-326.
273. Luo, Y.; Yao, X.; Yuan, J.; Ding, T.; Gao, Q., Preparation and drug controlled-release of polyion complex micelles as drug delivery systems. *Colloids and Surfaces, B: Biointerfaces* **2009,** *68* (Copyright (C) 2012 American Chemical Society (ACS). All Rights Reserved.), 218-224.
274. Robbens, J.; Vanparys, C.; Nobels, I.; Blust, R.; Van, H. K.; Janssen, C.; De, S. K.; Roland, K.; Blanchard, G.; Silvestre, F.; Gillardin, V.; Kestemont, P.; Anthonissen, R.; Toussaint, O.; Vankoningsloo, S.; Saout, C.; Alfaro-Moreno, E.; Hoet, P.; Gonzalez, L.; Dubruel, P.; Troisfontaines, P., Eco-, geno- and human toxicology of bio-active nanoparticles for biomedical applications. *Toxicology* **2010,** *269* (Copyright (C) 2012 American Chemical Society (ACS). All Rights Reserved.), 170-181.
275. Shiratori, S. S.; Rubner, M. F., pH-Dependent Thickness Behavior of Sequentially Adsorbed Layers of Weak Polyelectrolytes. *Macromolecules* **2000,** *33* (Copyright (C) 2011 American Chemical Society (ACS). All Rights Reserved.), 4213-4219.
276. Yoo, D.; Shiratori, S. S.; Rubner, M. F., Controlling Bilayer Composition and Surface Wettability of Sequentially Adsorbed Multilayers of Weak Polyelectrolytes. *Macromolecules* **1998,** *31* (Copyright (C) 2011 American Chemical Society (ACS). All Rights Reserved.), 4309-4318.
277. Wang, S.; Zhu, Y., Conformation transition and electric potential of single weak polyelectrolyte: molecular weight dependence. *Soft Matter* **2011,** *7* (Copyright (C) 2011 American Chemical Society (ACS). All Rights Reserved.), 7410-7415.
278. Gabriel, S.; Dubruel, P.; Schacht, E.; Jonas, A. M.; Gilbert, B.; Jerome, R.; Jerome, C., Electrografting of poly(ethylene glycol) acrylate: A one-step strategy for the synthesis of protein-repellent surfaces. *Angewandte Chemie, International Edition* **2005,** *44* (34), 5505-5509.
279. Wood, G. A.; Iroh, J. O., Efficiency of electropolymerization of pyrrole onto carbon fibers. *Synthetic Metals* **1996,** *80* (1), 73-82.

280. Yavuz, O.; Berlouis, L. E. A.; Hitchman, M. L.; Sarac, A. S., The optical, thermal and electrochemical properties of co-electropolymerized films of acrylamide and carbazole. *Synthetic Metals* **2000,** *110* (2), 165-174.
281. Ambrose, J. F.; Carpenter, L. L.; Nelson, R. F., Electrochemical and spectroscopic properties of cation radicals. III. Reaction pathways of carbazolium radical ions. *Journal of the Electrochemical Society* **1975,** *122* (7), 876-94.
282. Ambrose, J. F.; Nelson, R. F., Anodic oxidation pathways of carbazoles. I. Carbazole and N-substituted derivatives. *Journal of the Electrochemical Society* **1968,** *115* (11), 1159-64.
283. Inzelt, G., Formation and redox behaviour of polycarbazole prepared by electropolymerization of solid carbazole crystals immobilized on an electrode surface. *Journal of Solid State Electrochemistry* **2003,** *7* (8), 503-510.
284. Macit, H.; Sen, S.; Sacak, M., Electrochemical synthesis and characterization of polycarbazole. *Journal of Applied Polymer Science* **2005,** *96* (3), 894-898.
285. Mengoli, G.; Musiani, M. M.; Schreck, B.; Zecchin, S., Electrochemical synthesis and properties of polycarbazole films in protic acid media. *Journal of Electroanalytical Chemistry and Interfacial Electrochemistry* **1988,** *246* (1), 73-86.
286. Benda, A.; Benes, M.; Marecek, V.; Lhotsky, A.; Hermens, W. T.; Hof, M., How To Determine Diffusion Coefficients in Planar Phospholipid Systems by Confocal Fluorescence Correlation Spectrocopy. *Langmuir* **2003,** *19* (10), 4120-4126.

Appendix A

I. AUTOCORRELATION CURVES:

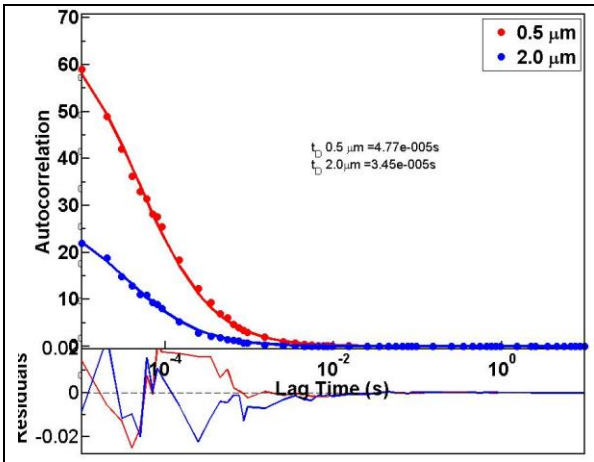

Figure A1: Representative autocorrelation curves for R6G. Both 0.5 and 2.0 µm data sets are pictured, as well as the residuals below the curves.

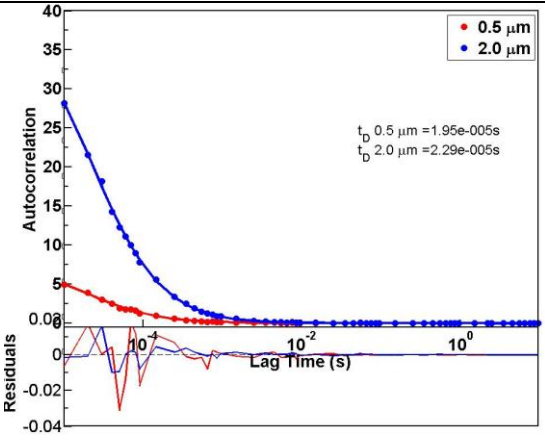

Figure A2: Representative autocorrelation curves for Alexa. Both 0.5 and 2.0 µm data sets are pictured, as well as the residuals below the curves.

It is important to note that, although there is an inverse relationship between the concentration and the autocorrelation amplitude, other factors such as dye photophysics, brightness, and scattering as a function of depth within the sample complicate the observed relationship, as shown in Figures S1 and S2.

II. SINGLE MOLECULE BLIP FREQUENCY ANALYSIS:

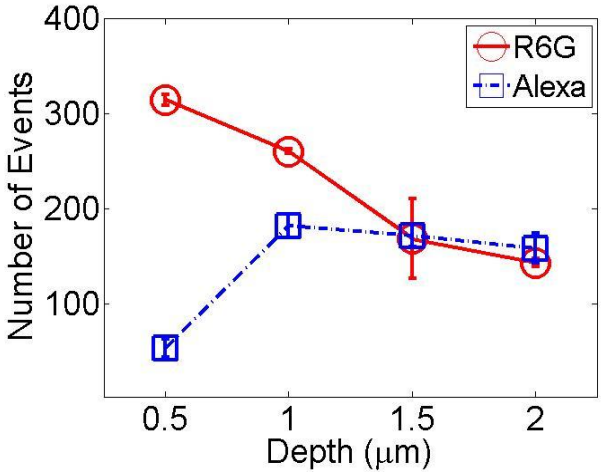

Figure A3: Mean events for R6G and Alexa in acidic conditions. The spread in intensity values at each depth reflect reproducibility from multiple experiments. Lines are drawn as a guide for the eye.

Appendix B

Contents **Page**

Characterization of the Linear PEG Brush Surface

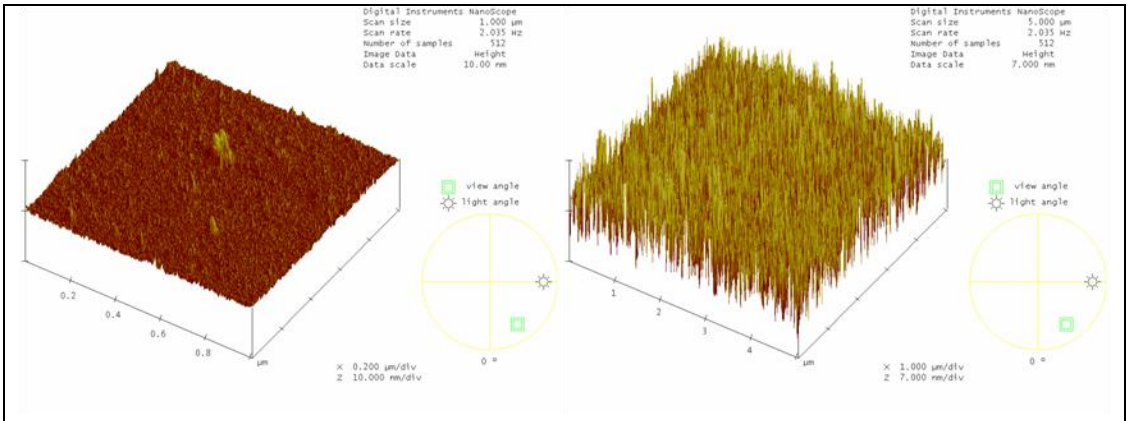

Figure B1: 5.0 μm^2AFM images of bare (l) and PEGylated (r) surfaces.

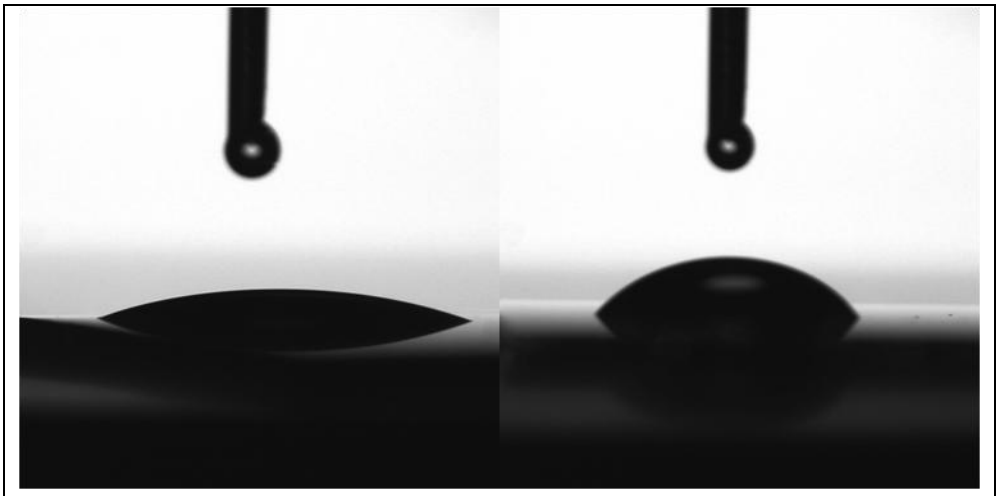

Figure B2: Visualization of contact angle measurement of bare (l) and PEGylated (r) surfaces. Contact angles: 20.82 ± 0.68° for bare substrate and 51.42 ± 1.23° for PEGylated surface.

The PEGylated surface was characterized by atomic force microscopy (AFM), ellipsometry, and

contact angle measurements. Figure S1 shows the AFM imaging of a 5.0 x 5.0 μm^2 section of the surfaces. Figure S2 depicts the contact angle measurement. The water contact angle measurement of a bare surface was found to be 20.82 ± 0.68°; the contact angle measurement of the polymerized surface was found to be 51.42 ± 1.23°. These contact angles show that the surface was hydrophilic, which is consistent with the properties of the surfaces.

Scheme and Characterization of the PEG Dendrons & Surface [223]

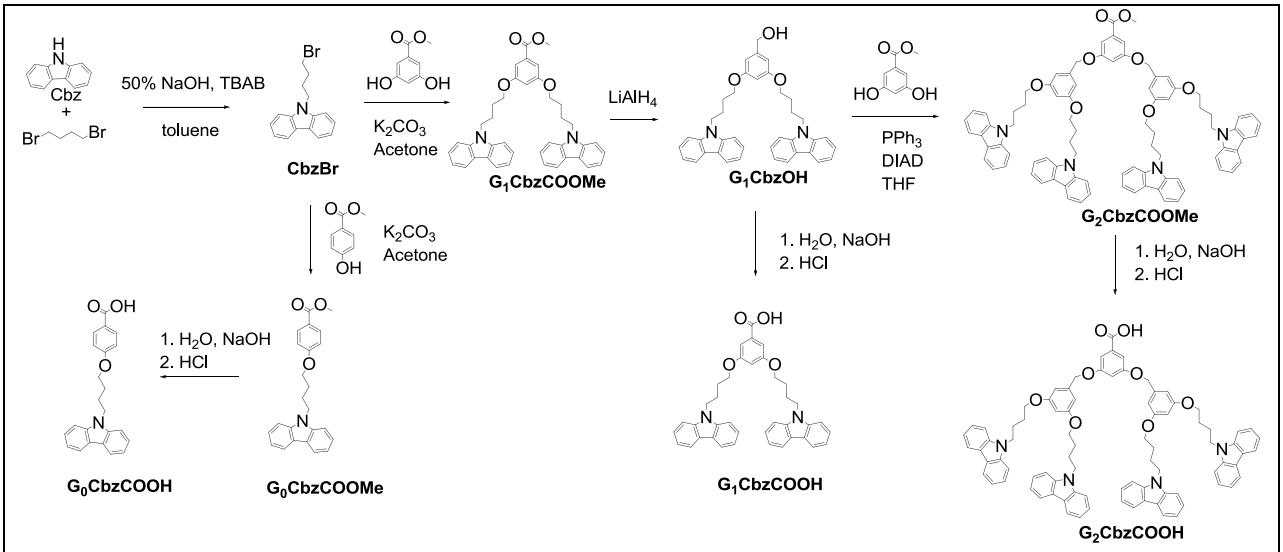

Scheme B1: Synthesis of the GnCbztEG linear dendrons.

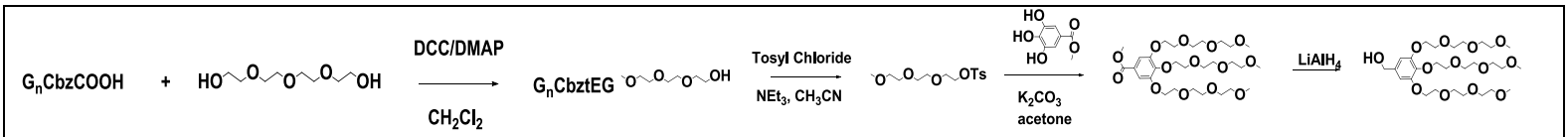

Scheme B2: Reactions that resulted in the linear (top) and branched (bottom) dendrons.

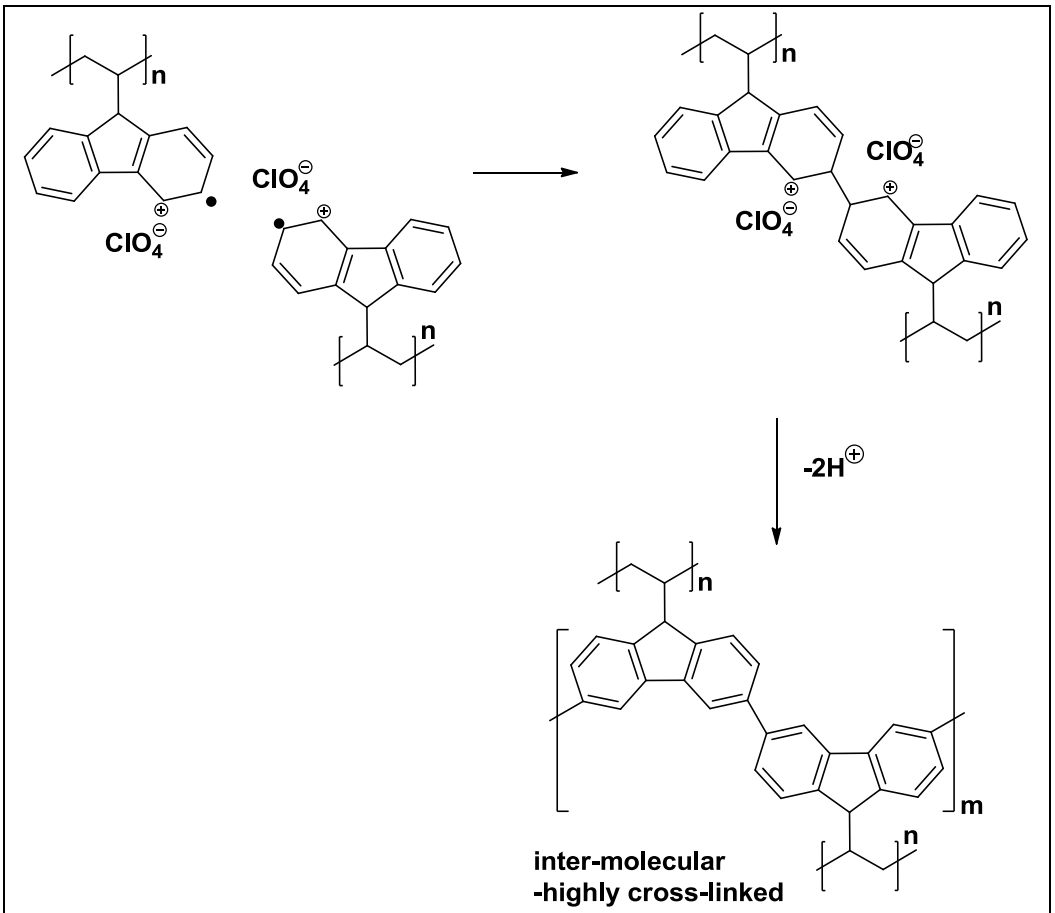

Scheme B3: Radical cation mechanism for carbazole electropolymerization.

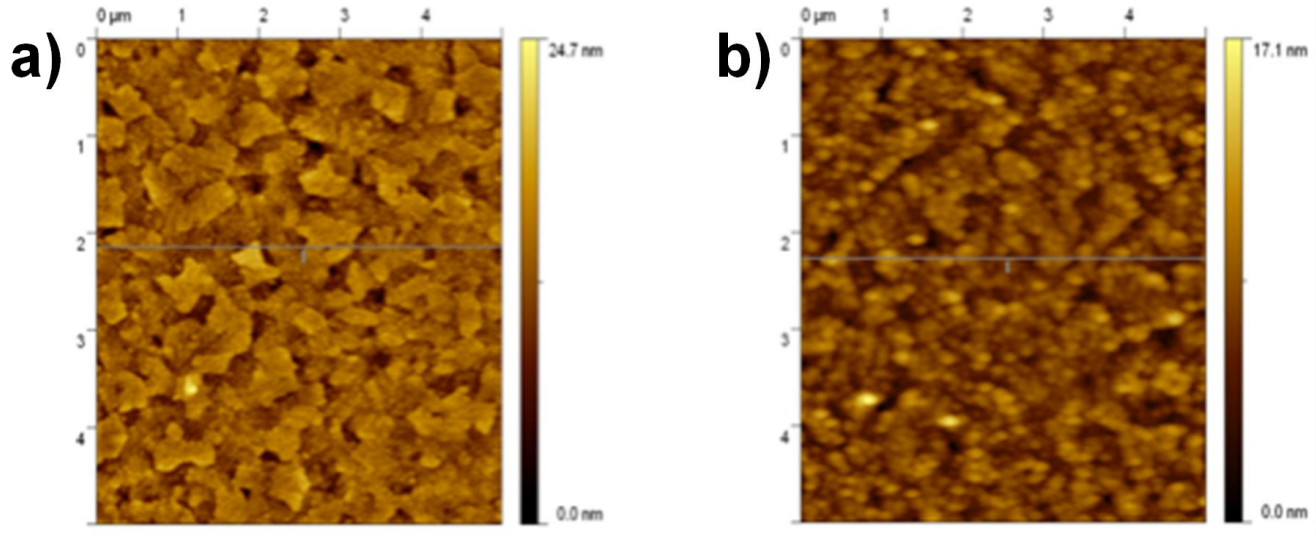

Figure B3: AFM phase images of (a) bare ITO, and (b) topographic image of G_2CbztEG after cyclic voltammetry deposition

The electrochemical deposition of PEGylated materials onto solid substrates offers the advantages of obtaining a uniform coating in a fast and economical process, control of thickness, the analytical application of potentiostatic and potentiodynamic methods, and the feasibility of deposition onto a wide variety of substrates including metals and alloys, semiconductors, ITO–coated glass, Au, and carbon [278-280]. The electrochemical oxidation and polymerization of carbazole have been reported previously [281-282]. Ambrose, et. al. suggested that the formation of the dicarbazyl dication at the 3- and 3'- positions (Scheme S3) is the predominant pathway during anodic oxidation while other groups reported the electrodeposition of films with longer polycarbazole chains under suitable conditions [283-285].

In this study, 20 µM each of the PEGylated carbazole linear dendrons dissolved in acetonitrile was electrochemically deposited by cyclic voltammetry (CV) on ITO-coated cover slips. Electrochemical grafting of these linear-dendrons onto conducting surfaces from a very dilute

solution should allow for a very thin film of PEGylated molecules, provided that both the solvent and the potential (scan rate) are properly selected [278]. Figure S4 shows the 1st and 20th cycles of the cyclic voltammograms of 20 µM solutions of each PEGylated carbazole dendron.

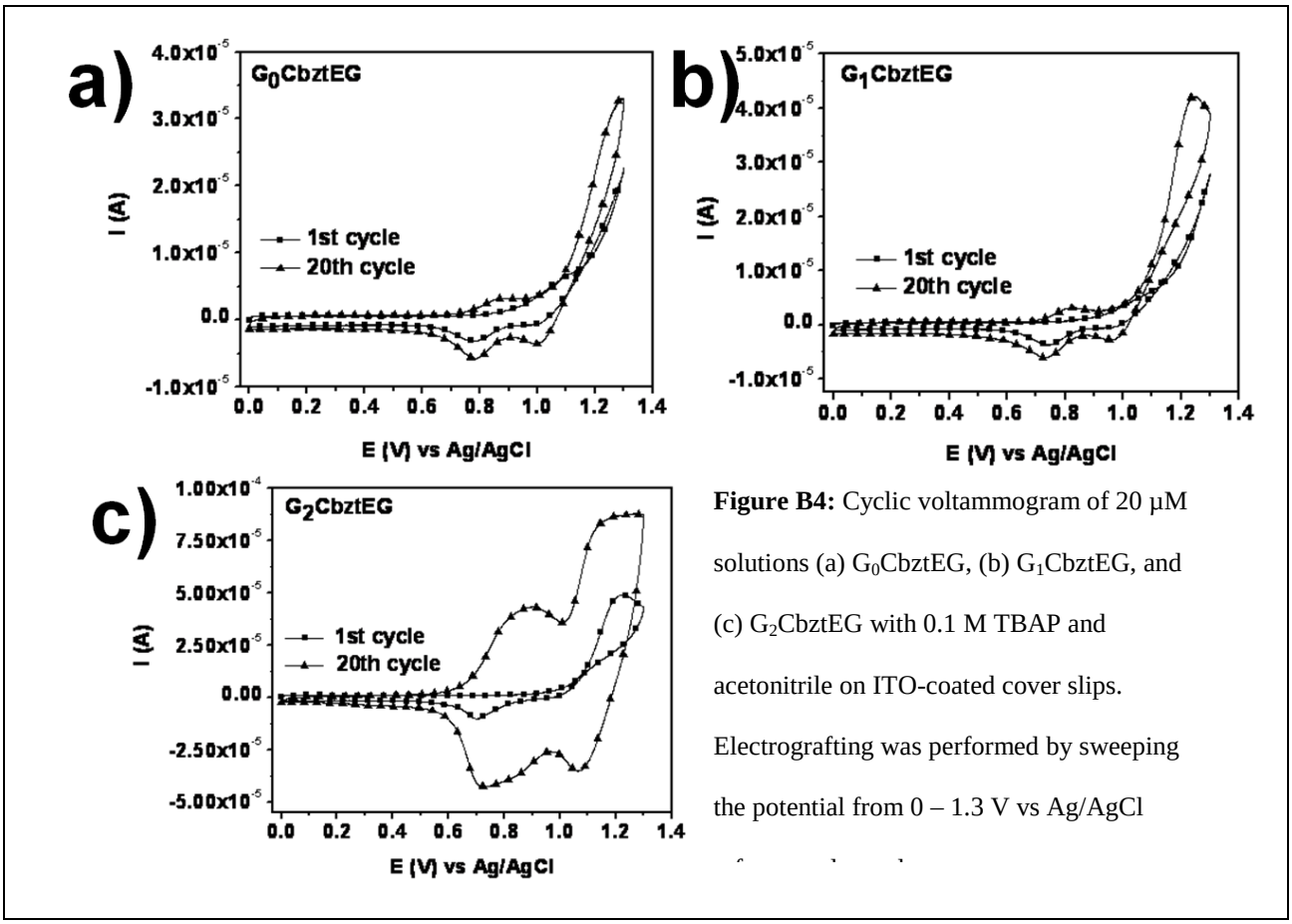

Figure B4: Cyclic voltammogram of 20 µM solutions (a) G_0CbztEG, (b) G_1CbztEG, and (c) G_2CbztEG with 0.1 M TBAP and acetonitrile on ITO-coated cover slips. Electrografting was performed by sweeping the potential from 0 – 1.3 V vs Ag/AgCl

From the cyclic voltammograms, the strong peaks observed for these films at 0.86 V – 1.24 V for all the generations are due to the oxidation of the carbazole units [281-282]. Further, the redox process is quasi-reversible for all the generations, giving a corresponding reduction peak at 0.77 – 1.01 V (vs Ag/AgCl). It can also be observed that as the polymerization proceeds for each of the generations, the peak current increases in the successive cycles for all the three G_nCbztEG molecules indicating the growth of the polymer film on the ITO electrode.

To further characterize the deposition onto ITO-coated substrates, 5 mM of G_1CbztEG dissolved in acetonitrile was electrodeposited using the same conditions. The formation of a green colored film on the surface of the working electrode and the change from a pale yellow/colorless (reduced) into a green color (oxidized) solution was detected accompanying the redox processes. These observations were in good agreement with earlier reports [281, 283]. Further analysis of the electrografted films using UV-visible spectroscopy revealed an absorption maximum at about 396 nm corresponding to the π-π* transitions attributed to the 3,3′-dicarbazyl radical cation (polaronic band or doped state). In addition, the appearance of a broad peak in the 600-800 nm region confirms the highly conjugated nature of the materials deposited on the ITO substrates [224]. AFM phase images (Figure S3) showed the deposition of globular shaped domain features of G_2CbztEG on ITO compared to the rough-edged surface of the native ITO substrate. (The dendrons are abbreviated as Gn in the remainder of the discussion, with the branched dendron as GnB)

Surface Characterization of the Bottle Brush Surface [22]

Static contact angle goniometry was conducted using a KSV CAM 200 instrument (KSV Ltd.) using the bubble drop method with water.

All atomic force microscopy (AFM) images were recorded in air under ambient conditions on PicoScan 2500 (Agilent Technologies formerly Molecular Imaging, Corp.) equipped with an 8 × 8 μm scanner. Intermittent contact mode was used for all phase imaging. The AFM tip used was a silicon-nitride AFM probe from Ted Pella Inc.

A PHI 5700 X-ray photoelectron spectrometer (XPS) was equipped with a monochromatic Al

Kα X-ray source ($h\nu$=1486.7 eV) incident at 90° relative to the axis of a hemispherical energy analyzer. The spectrometer was operated both at high and low resolutions with pass energies of 23.5 eV and 187.85 eV, respectively, a photoelectron take off angle of 45° from the surface, and an analyzer spot diameter of 1.1 mm. The survey spectra were collected from 0 to 1400 eV, and the high-resolution spectra were obtained for photoelectrons emitted from C 1s, O 1s, S 2p, and N 1s. All spectra were collected at room temperature with a base pressure of 1 x10 $^{-8}$. Electron binding energies were calibrated with respect to the C1s line at 284.8 eV.

A PHI Multipak software (version 5.0A) was used for all XPS data processing. The high-resolution data were analyzed first by background subtraction using the Shirley routine and a subsequent non-linear fitting to mixed Gaussian-Lorentzian functions. Atomic compositions were derived from the high-resolution scans. Peak areas were obtained after subtraction of the integrated baseline and corrected for sensitivity factors.

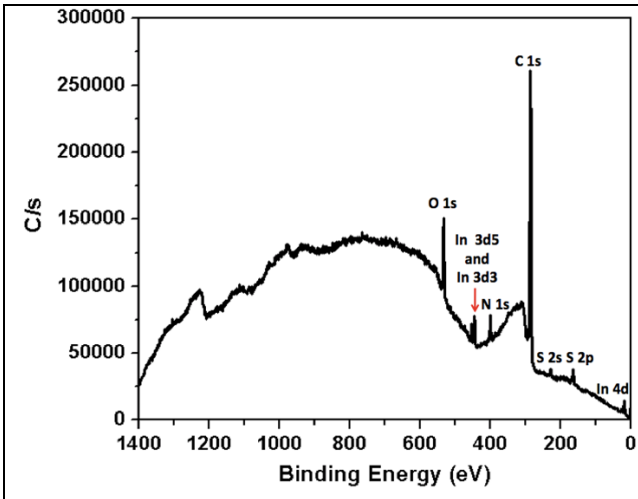

Figure B5. XPS survey spectrum of the electrodeposited CTA on the ITO cover slip.

The ability of the electro-active CTA (CBz-CTA) to mediate surface-initiated RAFT (SI-RAFT) polymerization on conducting surfaces was demonstrated by Tria *et al.* [22]. The CTA necessary for surface-initiated RAFT polymerization of the PEGMEMA on ITO cover slips was deposited through potentiostatic techniques. A higher voltage than the oxidation peak of the carbazole monomer of the CTA (~1.15 V), in this case 1.4 V, was used to ensure the electrodeposition of the CTA on the surface [22]. Successful electrodeposition of the CTA on the surface was confirmed by surface characterization. The static contact angle of

the surface increased from 39.28 ± 1.85° (bare ITO cover slip) to 71.44 ± 2.80° (CTA-modified slide), signifying the introduction of a relatively hydrophobic material on the surface. An XPS survey scan (Figure S5) of the CTA film showed all the expected elemental peaks of C, N, O, and S coming from the electro-generated CTA. Indium signals also showed up due to the indium tin oxide (ITO) surface. AFM images of the bare ITO cover slip and CTA-modified slip (Figure S6) also displayed a large difference in morphology where the appearance of globular domains of the CTA on the slide was prominent relative to the very flat surface of the bare slide.

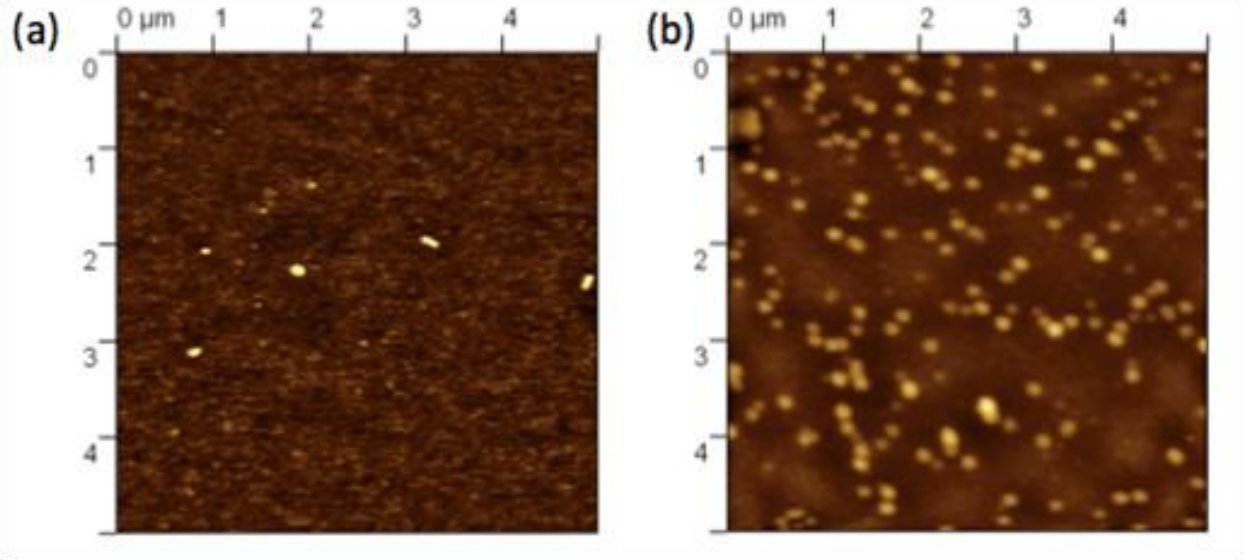

Figure B6. AFM topography images of (a) bare ITO cover slip and (b) CTA-modified slide.

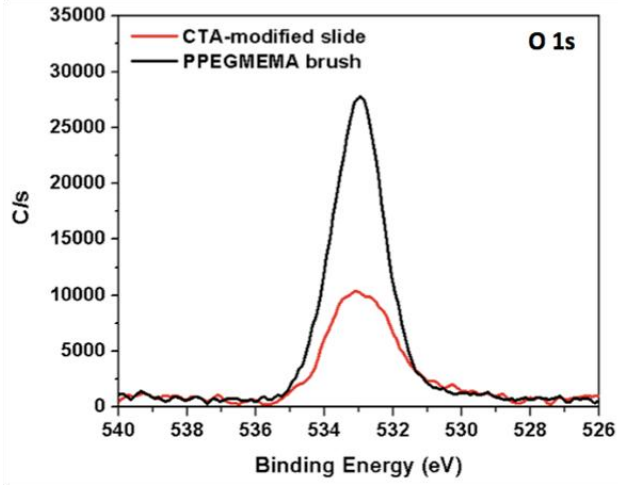

Figure B7. High-resolution scan of O 1s peak before and after growing the PPEGMEMA brush.

SI-RAFT polymerization of PEGMEMA was then performed on the CTA-modified ITO cover slips after the confirmation of the electrodeposition of the CTA on the surface. The contact angle decreased from 71.44 ± 2.80 (CTA-modified slide) to 54.78 ± 0.20 (poly-PEGMEMA (PPEGMEMA) brush), which supports the incorporation of the surface-grafted hydrophilic PEG chains. This observation was further proven by the XPS analysis of the films, which showed an increase in O 1s signal after the SI-RAFT polymerization of PEGMEMA due to the oxygen-rich polymer chain (Figure S7). Furthermore, deconvolution of the C 1s peak of the PPEGMEMA brush (Figure S8) exhibited an increase in the C-O area as compared to the electrodeposited CTA, assigned to the growth of the PEG methacrylate on the surface. The AFM topography image of the brush also showed a change after the growth of the brush (Figure S9).

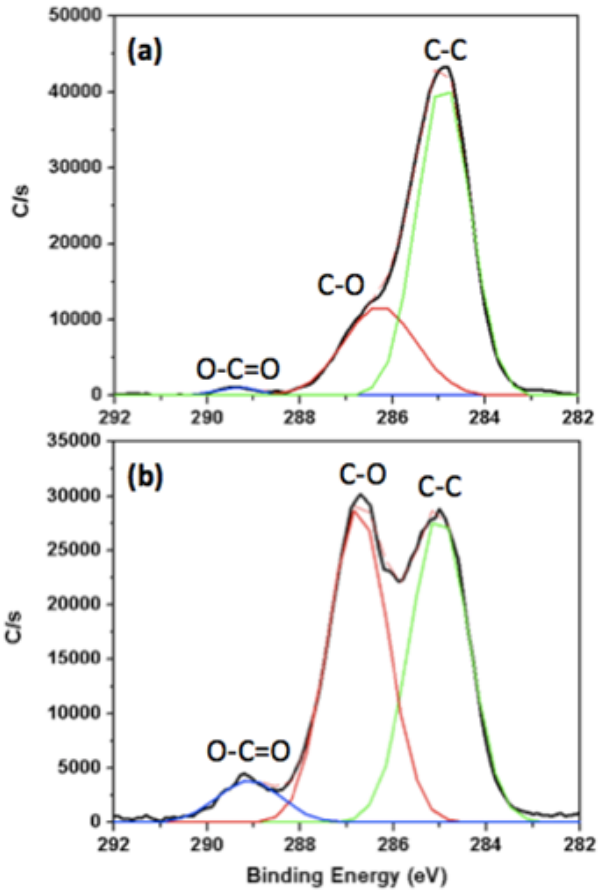

Figure B8. Deconvoluted high-resolution scans of C 1s peak for (a) CTA-modified slide and (b) PPEGMEMA brush.

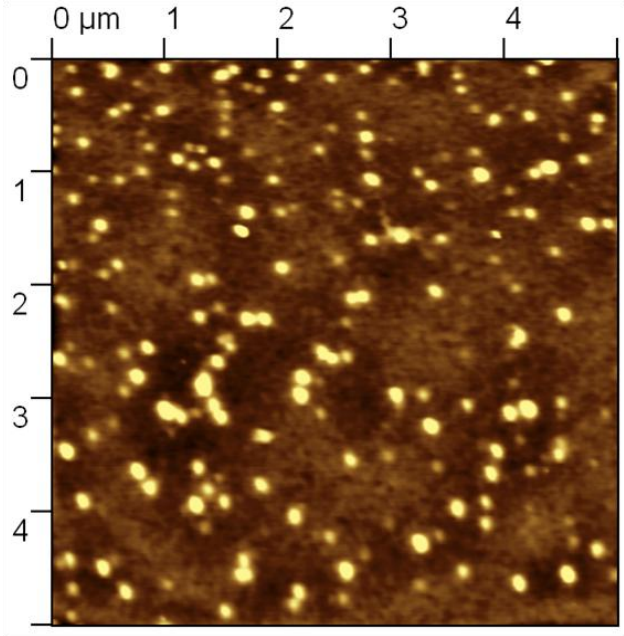

Figure B9. AFM topography image after SI-RAFT of PPEGMEMA.

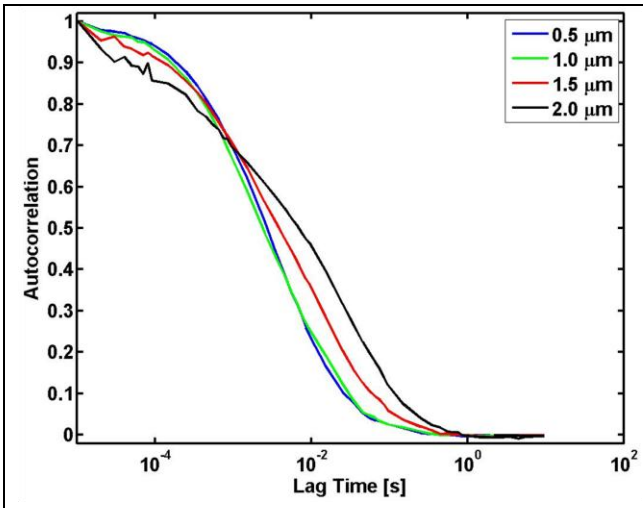

Figure B10: A comparison of the normalized autocorrelation curves of the negatively charged Alexa probe on the bare ITO surface. The probe is shown to have strong interactions with the surface, as the characteristic diffusion time seemingly increases with the increase in distance from the surface.

Interaction of the Probe with Functionalized Surfaces

When probing the bare ITO surface, we find that AlexaFluor® 555 (Alexa) exhibits strong attraction to the surface (Figure S10). This is evident from the extremely uncharacteristic behavior of the solvated probe over the bare substrate. In solution over a glass surface, Alexa has a

characteristic diffusion time of 22 ± 2 μs. Near the ITO surface, the characteristic diffusion time slowed to 272 ± 33 μs. This is even more pronounced as we explore higher depths and observe what appears to be longer diffusion times. This is consistent with the finding that as a slow event is recorded over a widening focal volume space (Figure 7 in the main text), the diffusion time appears to increase [286]. It is apparent that the probe is heavily interacting with the surface in the absence of modification. This effect is eliminated with the addition of the soft surfaces. Below are the normalized autocorrelation curves depicting the probe interacting with the dendronized surfaces (Figure S11).

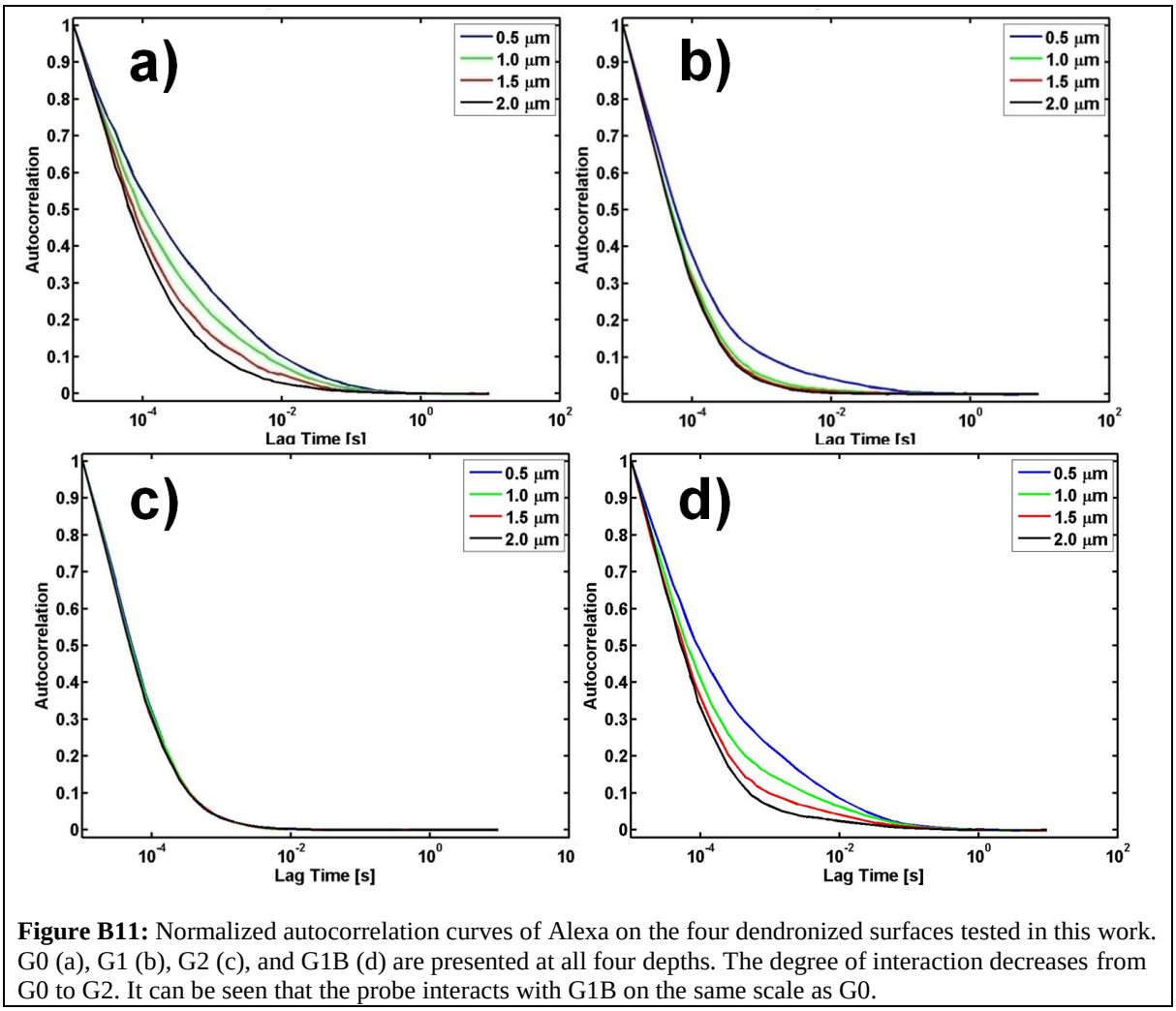

Figure B11: Normalized autocorrelation curves of Alexa on the four dendronized surfaces tested in this work. G0 (a), G1 (b), G2 (c), and G1B (d) are presented at all four depths. The degree of interaction decreases from G0 to G2. It can be seen that the probe interacts with G1B on the same scale as G0.

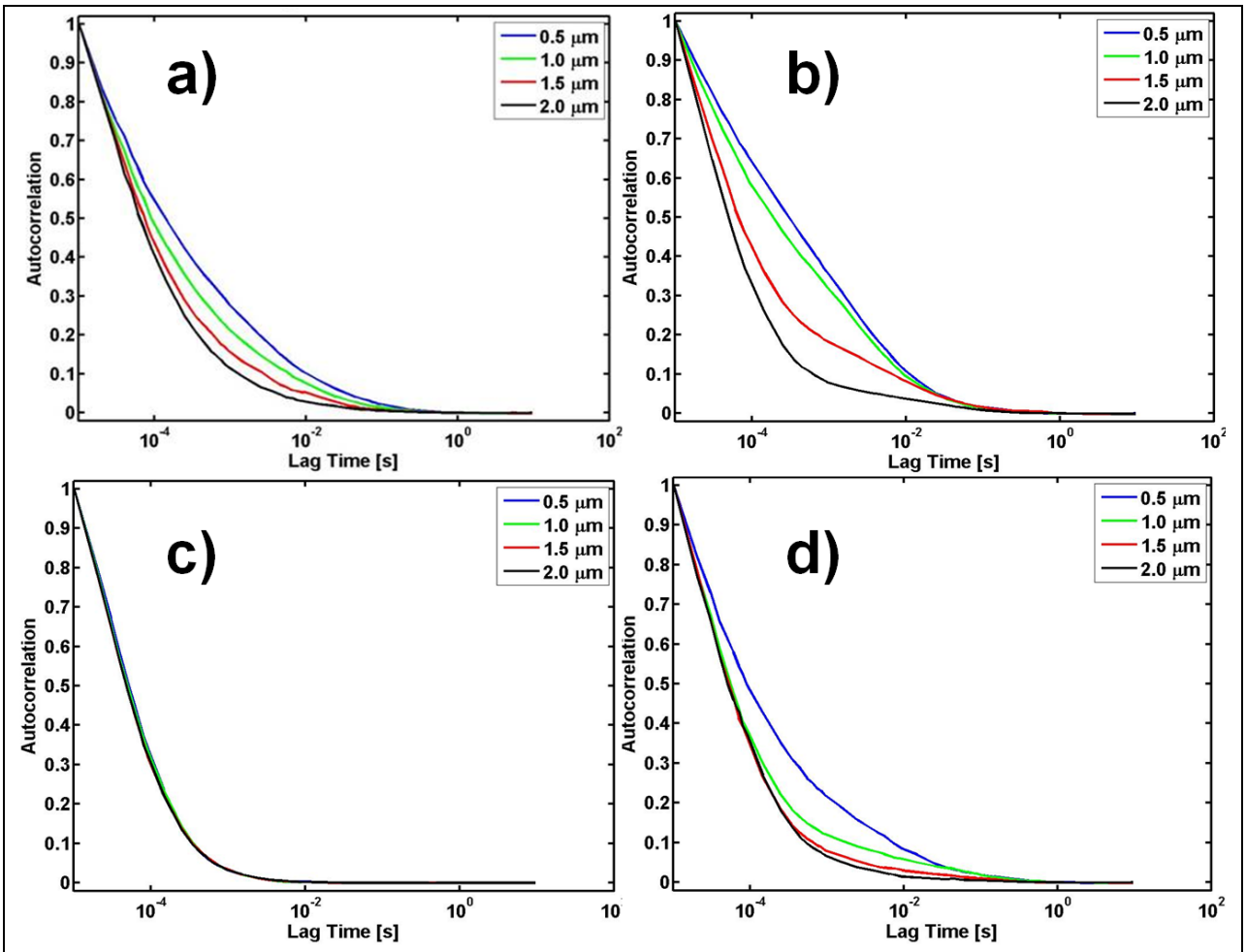

Figure B12: Normalized autocorrelation curves of Alexa (a,c) and R6G (b,d) on the G0 (a,b) and G2(c,d) dendronized surfaces tested in this work, presented at all four depths. The degree of interaction is similar for both dyes on the G0 surface. There is an increase in interaction with R6G on the G2 surface at the closest depth measured. However, due to the length of the π-systems of the dyes and the carbazoles on the surface of the dendrons, the trend observed is unexpected for the case of strong π-π interactions between the dyes and the carbazole portion of the dendron.

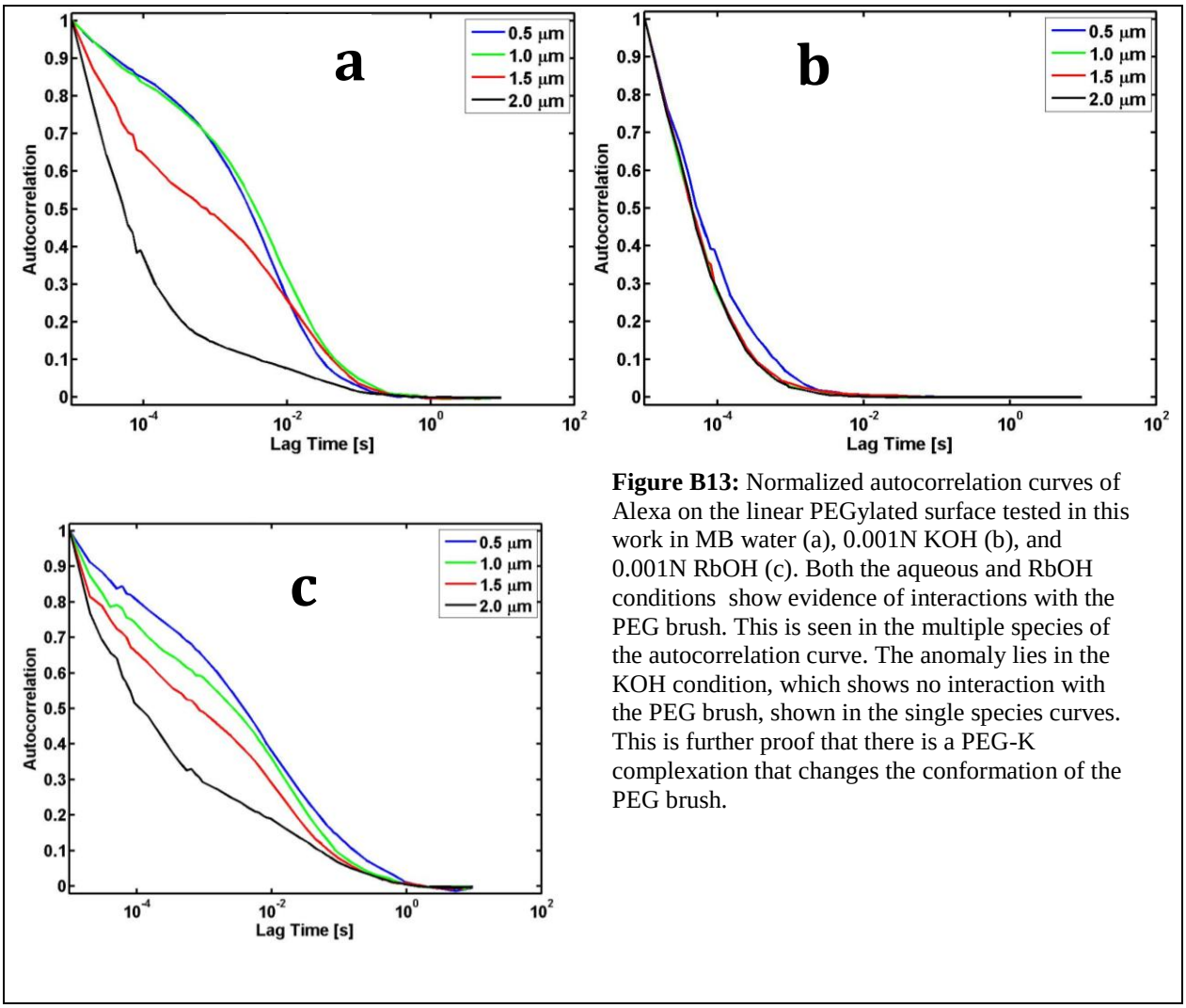

Figure B13: Normalized autocorrelation curves of Alexa on the linear PEGylated surface tested in this work in MB water (a), 0.001N KOH (b), and 0.001N RbOH (c). Both the aqueous and RbOH conditions show evidence of interactions with the PEG brush. This is seen in the multiple species of the autocorrelation curve. The anomaly lies in the KOH condition, which shows no interaction with the PEG brush, shown in the single species curves. This is further proof that there is a PEG-K complexation that changes the conformation of the PEG brush.